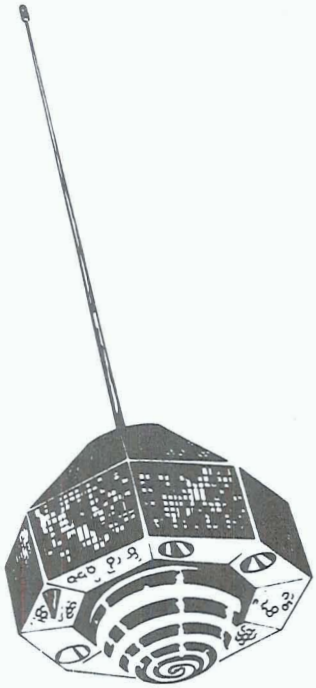

NOVEMBER 1970

PROCEEDINGS OF THE GEOS-2 PROGRAM REVIEW MEETING 22-24 JUNE 1970

VOLUME III

LASER AND RADAR INVESTIGATIONS

EDITED BY:
CSC
COMPUTER SCIENCES CORPORATION
6565 ARLINGTON BOULEVARD POST OFFICE BOX 530 FALLS CHURCH VA 22046

NATIONAL AERONAUTICS AND SPACE ADMINISTRATION

NASA

PROCEEDINGS OF THE GEOS-2 PROGRAM REVIEW MEETING

22-24 June 1970
NASA Goddard Space Flight Center
Greenbelt, Maryland

Volume III

LASER AND RADAR INVESTIGATIONS

Edited by Computer Sciences Corporation
6565 Arlington Boulevard, Falls Church, Virginia

November 1970

VOLUME III

TABLE OF CONTENTS

FUTURE USES OF LASER TRACKING

E. M. Gaposchkin

To be presented at the Geos 2 Review Meeting
Goddard Space Flight Center, Greenbelt, Maryland

June 1970

Smithsonian Institution
Astrophysical Observatory
Cambridge, Massachusetts 02138

FUTURE USES OF LASER TRACKING

E. M. Gaposchkin

1. INTRODUCTION

Laser technology has advanced to the extent that specific plans for its use can be made. Satellite tracking with lasers has become routine and the limits of accuracy are known, though only approximately realized. There are three different types of laser tracking units; the data are compatible and can be satisfactorily combined.

Satellite tracking by laser is a very precise method of range measurement. The energy requirements are such that satellites must be equipped with corner-cube reflectors, which are passive devices and have an indefinite lifetime; there is no limit to the number of observations that can be made.

Precise satellite tracking has evolved through many stages. Laser tracking is the most promising of the many ground-based techniques under development and in use today. The ultimate accuracy limit of laser tracking is set by the indeterminacy of the tropospheric refraction correction, a problem common to all ground-based observing systems.

It seems, therefore, that we are at the final stage of ground-based tracking, and further advances will very likely come from satellite-based tracking systems. This discussion is limited to ground-based precision tracking and its viability. However, satellite-based tracking will need to be related to the earth's surface. Precision tracking has been most commonly

*This work was supported in part by grant NGR 09-015-002 from the National Aeronautics and Space Administration.

used in geodetic studies. The first question is, thus, what impact will laser tracking have on determining the gravity field of the earth and the locations of observing stations.

The present accuracy of laser ranges is 50 cm (see Section 5). Not all the systems in use have this capability, but even the primitive systems have an accuracy of 1.5 m. This can be compared with the 20-m accuracy of Baker-Nunn camera observations and the 15-m accuracy of the Goddard Range and Range Rate (GRARR) data. The ultimate accuracy of laser measurements will be 6 to 8 cm. To obtain this precision, we require very detailed meteorological data, which are not yet available.

There are many other uses for precision tracking of 50-cm accuracy. For example, ranging to the moon has been successful, and there is no doubt that uses other than those mentioned here will be found for laser satellite tracking.

2. SATELLITE GRAVITY-FIELD DETERMINATION BY CLASSICAL METHODS

The methods discussed here are now classical (Kaula, 1966; Lundquist and Veis, 1966). The new data can be treated in the traditional framework, and alternative methods will be discussed in Section 7.

2.1 The method used to determine the earth's gravity field is the inverse of the classical celestial mechanics problem, which is to determine the trajectory of a body, given a set of forces. Observations are used to check the theory. The geodetic problem is to determine the forces, i.e., the gravity field of the earth, given an orbital theory and observations of the trajectory. At the same time, one can and must determine the locations of the observing stations.

2.2 The representation of the geopotential in spherical harmonics, i.e., in harmonic functions, is a spectral decomposition of the field. Specific features in the gravity field are not related to specific harmonic terms. Conversely, specific harmonics cannot be related to particular features. The situation is completely analogous to Fourier decomposition in one dimension. In general, the harmonic functions that arise in the solution of the equations of motion are similarly not related to specific features in the motion, in this case a spectral decomposition in time. There are some pronounced spectral features in the motion, as we shall see, and hence to some extent the satellite acts as a filter, amplifying some spectral components.

2.3 We can determine the trajectory directly by numerical integration of the equations of motion. Alternatively, we can seek an analytical solution. In this case, we are forced to use approximate solutions, which appear to be satisfactory. This discussion is based on one such analytical theory.

The zonal harmonics have the largest effects, and rather elaborate analysis is required. The equations of motion for a satellite under the influence of tesseral harmonics of the gravity field are approximated by expansions in harmonic functions. These expressions can be integrated directly to first order, which is satisfactory.

2.4 The equations of motion are solved by successive approximation. The expressions are for small changes, called perturbations, with respect to some reference, called a mean orbit. There are two classes of changes: 1) nonperiodic ($\delta \varepsilon_s$), which increases indefinitely with time, and 2) periodic ($\delta \varepsilon_p$).

Periodic perturbations result from the spectral decomposition of the solution and are defined to have an average value of zero:

$$\int_{t_a}^{t_b} \delta \varepsilon_p \, dt = 0 \quad . \tag{1}$$

The remaining motion is generally defined as the secular part. Terms in t^2, t^3, etc. are not excluded in principle and apparently arise in practice. It is an open theoretical question if such terms can arise. They can also appear from very long-periodic terms that have not been included. In addition, some analytical theories have so-called mixed secular terms, e.g., t(sin αt). For our purposes, we can ignore these questions and rely on equation (1) to define periodic perturbations, where t_a and t_b are the first and last times of the trajectory. Hence, if $\delta\mathcal{E}$ is the total perturbation,

$$\delta\mathcal{E} = \delta\mathcal{E}_s + \delta\mathcal{E}_p \cong \delta\mathcal{E}'^{t}_{s} + \delta\mathcal{E}_p \quad ,$$

then

$$\delta\mathcal{E}'_s = \frac{1}{t_b - t_a} \int_{t_a}^{t_b} \delta\mathcal{E}\, dt \quad . \tag{2}$$

The $\delta\mathcal{E}_s$ are integrated effects and become very large. Thus, the coefficients controlling $\delta\mathcal{E}_s$, the zonal harmonics of even degree, can be determined very precisely. These are integrated effects (in time) of specific harmonics (i.e., averaged in space). For $\delta\mathcal{E}_p$, we can rely on integration in time only for long-period terms. The latter fall into two categories: 1) zonal harmonics of odd degree, and 2) harmonics that are resonant with the satellite orbit. For the remaining terms in the harmonic decomposition of the trajectory, we cannot use integrated effects and must use the large spatial averaging of the harmonics, another kind of integrated effect.

In summary, the gravity field is expressed in a spatial spectral decomposition, and the orbital theory in a temporal spectral decomposition. The satellite is sensitive to certain spatial components of the gravity field through certain temporal components arising in the orbital theory.

2.5 The development of perturbations, now classical, is given in many papers (Kaula, 1966; Lundquist and Veis, 1966). The choice of dependent variables is arbitrary. The most common are ω (perigee), Ω (argument of the node), I (inclination), e (eccentricity), M (mean anomaly), and a (semimajor axis). These elements ε_i can be combined into any other set. For descriptive purposes we use M and the shift in position $dr = (\overline{dr} \cdot \overline{dr})^2 = \hat{dr} \cdot \overline{dr}$.

The expression of a periodic perturbation (say in M) due to harmonic $C_{\ell m}$ is given in the form

$$\delta M_{\ell m} = C_{\ell m} \sum_{p=0}^{\ell} \sum_{q=-\infty}^{\infty} A(\ell, m, p, q, a, e, I) \mathcal{S}[(\ell - 2p)\omega + (\ell - 2p + q) M + m(\Omega - \theta)] \tag{3}$$

or

$$\delta M_{\ell mpq} = C_{\ell m} \delta M^{*}_{\ell mpq} \mathcal{S}[(\ell - 2p)\omega + (\ell - 2p + q)M + m(\Omega - \theta)] \quad , \tag{4}$$

where $\mathcal{S}$ is either sin or cos and θ is the sidereal angle.

A few well-known remarks follow:

1. $A(\ell, m, p, q, a, e, I) \propto e^{|q|}$; hence the largest terms generally come with $q = 0$.

2. The q summation, though formally from $-\infty$ to $+\infty$, only needs to go from -10 to +10.

3. $n \cong \dot{M} > \dot{\theta} \approx 1 \gg \dot{\omega}, \dot{\Omega}$; therefore, the frequency

$$f = \frac{(\ell - 2p)\dot{\omega} + (\ell - 2p + q)n + m(\dot{\Omega} - \dot{\theta})}{2\pi}$$

of any term is mainly controlled by $\dot{M}$ and $m\dot{\theta}$.

4. Since $A(\ell, m, p, q, a, e, I)$ depends on elements that have virtually no change, A is constant for any particular satellite. The $\mathcal{S}$ term contains all the temporal variations.

2.6 For any given value of order m, all perturbations of degree ℓ (even) will have the same frequency. Since $0 \leq \ell \leq m$ and $0 \leq p \leq 1$, arguments with $\ell - 2p = r$ exist. This can be seen by examining the dominant term for each ℓ, i.e., $q = 0$. The frequency becomes

$$f = \frac{(\ell - 2p)(\dot{\omega} + n) + m(\dot{\Omega} - \dot{\theta})}{2\pi} \quad .$$

With $\ell = 12$, $p = 6$, $m = 12$, we have the same frequency as with $\ell = 14$, $p = 7$, $m = 12$; $\ell = 16$, $p = 6$, $m = 12$; etc. Similarly for ℓ (odd). In addition, we cannot have the same period for both ℓ odd and ℓ even.

For example, the perturbations in M for D1D (6701401) are given in expression (5) for only the principal terms with $m = 1, 2$ and $\ell = 3, 4, 5, 6, 7, 8$. For this satellite, a = 7614 km, e = 0.0843, and I = 39°.455.

$$\begin{aligned}
\delta M = {} & C_{31}[-7.1 \sin(\omega + \Omega - \theta) + 0.8 \sin(\omega + 2M + \Omega - \theta) - 63.3 \sin(-\omega + \Omega - \theta) + \ldots] \\
& + C_{32}\{-42.5 \cos[\omega + 2(\Omega - \theta)] + 10.5 \cos[\omega + 2M + 2(\Omega - \theta)] - 13.6 \cos[-\omega + 2(\Omega - \theta)] + \ldots\} \\
& + C_{41}[7.0 \cos(-M + \Omega - \theta) - 8.2 \cos(M + \Omega - \theta) + 5.1 \cos(-2\omega + \Omega - \theta) + \ldots] \\
& + C_{42}\{-10.3 \sin[-M + 2(\Omega - \theta)] + 14.2 \sin[M + 2(\Omega - \theta)] + \ldots\} \\
& + C_{51}[-87.4 \sin(\omega + \Omega - \theta) + 6.9 \sin(\omega + 2M + \Omega - \theta) + 87.9 \sin(-\omega + \Omega - \theta) + \ldots] \\
& + C_{52}\{8.6 \cos[\omega + 2(\Omega - \theta)] - 1.4 \cos[\omega + 2M + 2(\Omega - \theta)] + 43.9 \cos[-\omega + 2(\Omega - \theta)] + \ldots\} \\
& + C_{61}[5.1 \cos(-M + \Omega - \theta) - 6.0 \cos(M + \Omega - \theta) - 16.2 \cos(-2\omega + \Omega - \theta) + \ldots] \\
& + C_{62}\{5.4 \sin[-M + 2(\Omega - \theta)] - 7.4 \sin[M + 2(\Omega - \theta)] + \ldots\} \\
& + C_{71}[33.1 \sin(\omega + \Omega - \theta) + 0.0 \sin(\omega + 2M + \Omega - \theta) + 1.4 \sin(-\omega + \Omega - \theta) + \ldots] \\
& + C_{72}\{40.0 \cos[\omega + 2(\Omega - \theta)] - 5.5 \cos[\omega + 2M + 2(\Omega - \theta)] - 40.3 \cos[-\omega + 2(\Omega - \theta)] + \ldots\} \\
& + C_{81}[-6.8 \cos(-M + \Omega - \theta) + 7.9 \cos(M + \Omega - \theta) + 19.1 \cos(-2\omega + \Omega - \theta) + \ldots] \\
& + C_{82}\{4.1 \sin[-M + 2(\Omega - \theta)] - 5.7 \sin[M + 2(\Omega - \theta)] + \ldots\} \\
& + \ldots \quad . \qquad (5)
\end{aligned}$$

We can rearrange this expression in terms of the same frequency (the period of each term, in days, is given in parentheses):

$$\begin{aligned}
\delta M = {} & (-7.1\, C_{31} - 87.4\, C_{51} + 33.1\, C_{71} + \ldots) \sin(\omega + \Omega - \theta) && (-1.001) \\
& + (0.8\, C_{31} + 6.9\, C_{51} + 0.0\, C_{71} + \ldots) \sin(\omega + 2M + \Omega - \theta) && (0.040) \\
& + (-63.3\, C_{31} + 87.9\, C_{51} + 1.4\, C_{71} + \ldots) \sin(-\omega + \Omega - \theta) && (-0.971) \\
& + (7.0\, C_{41} + 5.1\, C_{61} - 6.8\, C_{81} + \ldots) \cos(-M + \Omega - \theta) && (-0.071) \\
& + (-8.2\, C_{41} - 6.0\, C_{61} + 7.9\, C_{81} + \ldots) \cos(M + \Omega - \theta) && (0.083) \\
& + (5.1\, C_{41} - 16.2\, C_{61} + 19.1\, C_{81} + \ldots) \cos(-2\omega + \Omega - \theta) && (-0.958) \\
& + (-42.5\, C_{32} + 8.6\, C_{52} + 40.0\, C_{72} + \ldots) \cos[\omega + 2(\Omega - \theta)] && (-0.497) \\
& + (10.5\, C_{32} - 1.4\, C_{52} - 5.5\, C_{72} + \ldots) \cos[\omega + 2M + 2(\Omega - \theta)] && (0.041) \\
& + (-13.6\, C_{32} + 43.9\, C_{52} - 40.3\, C_{72} + \ldots) \cos[-\omega + 2(\Omega - \theta)] && (-0.327) \\
& + (-10.3\, C_{42} + 5.4\, C_{62} + 4.1\, C_{82} + \ldots) \sin[-M + 2(\Omega - \theta)] && (-0.066) \\
& + (14.2\, C_{42} - 7.4\, C_{62} - 5.7\, C_{82} + \ldots) \sin[M + 2(\Omega - \theta)] && (0.091) \\
& + \ldots \quad . && (6)
\end{aligned}$$

As a second example, we give in expression (7) the perturbations in M for the satellite PEOLE, to be launched by Centre National d'Études Spatiales (CNES), for which a = 7173 km, e = 0.009, and I = 15.°0. In this case, we give the terms for m = 1, 2 and ℓ = 3, 4, 5, 6.

$$\delta M = C_{31}\,[-1493 \sin(\omega + \Omega - \theta) + 160 \sin(\omega + 2M + \Omega - \theta) - 164 \sin(-\omega + \Omega - \theta) + \ldots]$$

$$+ C_{32}\,\{-341 \cos[\omega + 2(\Omega - \theta)] + 77 \cos[\omega + 2M + 2(\Omega - \theta)] + \ldots\}$$

$$+ C_{41}\,[126 \cos(-M + \Omega - \theta) - 146 \cos(M + \Omega - \theta) + \ldots]$$

$$+ C_{42}\,\{135 \sin[2\omega + 3M + 2(\Omega - \theta)] - 35 \sin[-M + 2(\Omega - \theta)] + 47 \sin[M + 2(\Omega - \theta)]$$
$$+ 50 \sin[2\omega + M + 2(\Omega - \theta)] + \ldots\}$$

$$+ C_{51}\,[1600 \sin(\omega + \Omega - \theta) - 114 \sin(\omega + 2M + \Omega - \theta) + 579 \sin(-\omega + \Omega - \theta) + \ldots]$$

$$+ C_{52}\,\{761 \cos[\omega + 2(\Omega - \theta)] - 115 \cos[\omega + 2M + 2(\Omega - \theta)] + \ldots\}$$

$$+ C_{61}\,[-165 \cos(-M + \Omega - \theta) + 190 \cos(M + \Omega - \theta) + \ldots]$$

$$+ C_{62}\,\{-76 \sin[2 + 3M + 2(\Omega - \theta)] + 73 \sin[-M + 2(\Omega - \theta)] - 99 \sin[M + 2(\Omega - \theta)]$$
$$- 69 \sin[2\omega + M + 2(\Omega - \theta)] + \ldots\}$$

$$+ \ldots \quad . \tag{7}$$

We can rearrange this expression in terms of the same frequency (the period of each term, in days, is given in parentheses):

$$\delta M = (-1493\, C_{31} + 1600\, C_{51} + \ldots) \sin(\omega + \Omega - \theta) \qquad (-1.013)$$

$$+ (160\, C_{31} - 114\, C_{51} + \ldots) \sin(\omega + 2M + \Omega - \theta) \qquad (0.036)$$

$$+ (-164\, C_{31} + 579\, C_{51} + \ldots) \sin(-\omega + \Omega - \theta) \qquad (-0.949)$$

$$+ (126\, C_{41} - 165\, C_{61} + \ldots) \cos(-M + \Omega - \theta) \qquad (-0.065)$$

$$+ (-146\, C_{41} + 190\, C_{61} + \ldots) \cos(M + \Omega - \theta) \qquad (0.075)$$

$$+ (-341\, C_{32} + 761\, C_{52} + \ldots) \cos[\omega + 2(\Omega - \theta)] \qquad (-0.498)$$

$$+ (77\, C_{32} - 115\, C_{52} + \ldots) \cos[\omega + 2M + 2(\Omega - \theta)] \qquad (0.038)$$

$$+ (135\, C_{42} - 76\, C_{62} + \ldots) \sin[2\omega + 3M + 2(\Omega - \theta)] \qquad (0.024)$$

$$+ (-35\, C_{42} + 73\, C_{62} + \ldots) \sin[-M + 2(\Omega - \theta)] \qquad (-0.061)$$

$$+ (47\, C_{42} - 99\, C_{62} + \ldots) \sin[M + 2(\Omega - \theta)] \qquad (0.082)$$

$$+ (50\, C_{42} - 69\, C_{62} + \ldots) \sin[2\omega + M + 2(\Omega - \theta)] \qquad (0.081)$$

$$+ \ldots \quad . \qquad (8)$$

Even if we assume the satellite to be a perfect filter, uncontaminated by other model errors, and the tracking data and analysis process to be perfect, we see that with one satellite we can only determine spectral components that are linear combinations of the gravity field ($C_{\ell m}$) and functions of orbital elements [$A(\ell, m, p, q, a, e, I)$]. From each satellite we obtain one or two linear combinations of harmonics for ℓ odd and for ℓ even. By using additional data we can only refine the numerical value of these linear combinations. The coefficients of the relations will depend on the orbital elements so that other linear combinations can be determined only from additional distinct orbits. Generally, this is achieved by selecting satellites with different inclination, but independent linear relations can also be obtained with changes in eccentricity e or semimajor axis a.

As the degree increases, the perturbations become negligible, and so the linear relation does not involve an infinite number of parameters. The number of parameters required is determined from this study.

From equation (6) (for DID) we see that a linear combination of C_{31}, C_{51}, C_{71}, ... can be determined from the -1.001-day-period term and another of equal size from the -0.971-day term. The third term (and there are many similar smaller terms) is a factor of 10 smaller and will not contribute significantly as an observation equation. The linear combination of C_{32}, C_{52}, C_{72}, ... has only one significant spectral component for the -0.327-day period.

From equation (8) (for PEOLE) the linear combination will be determined from the -1.013-day period. There are two other components at periods of 0.036 and -0.949 day. The effects are a factor of 2 to 10 smaller. A second linear relation of lower weight can be determined. These additional terms arise in satellites with nonzero eccentricity; e.g., for D1D the terms of $q \neq 0$ are significant, as illustrated by equation (6).

Therefore, one or two finite linear relations are determined for ℓ (odd) and one or two for ℓ (even). In addition, weaker relations can be established. Each satellite can contribute to the unique determination of 1 or 2 odd and 1 or 2 even degree harmonic coefficients in each order; i.e., if there are 24 sets of unique gravity-field coefficients affecting the orbits for a given order, then 12 distinct satellites would be sufficient to determine them.

For a nonhomogeneous set of satellites, i.e., where they are not all equally sensitive to the gravity field, subsets of coefficients are determined. In the case where insufficient satellites are available, the linear relations are generally solved by constraining the higher degree and order coefficients to zero.

The linear relations are not determined with equal accuracy; for example, the resonant harmonics have a very large effect and the spectral component is strongly determined. However, the resonant period is commensurate with the arc length, which will cover only a small number of cycles. This makes separating nearly commensurate periods difficult. For spectral components bunched between P = 0.02 and P = 0.04 day, i.e., between 50 and 60 min, the effects are small and the spectral decomposition is also difficult.

3. GRAVITY-FIELD DETERMINATION BY TERRESTRIAL MEASUREMENTS

3.1 The gravity field of the earth is measured with gravimeters. These measurements have been made on part of the surface only — 25% of the 1° × 1°

elements of the earth's surface. By combining these into 5° × 5° elements, 56% of the surface is covered. These measurements can be used to determine the spherical harmonic expansion representing the gravity field.

3.2 Rigorous analysis of surface-gravity measurements can lead to the determination of these spherical harmonic coefficients. This requires 1) knowledge of gravity everywhere on the surface (e.g., with 5° × 5° averages), 2) reduction of gravity values to a common reference, and 3) knowledge of the correlation function (now generally approximated) (Heiskanen and Moritz, 1967).

3.3 The above three conditions are not met today, so the usefulness of surface-gravity measurements is reduced. For example, one cannot determine spherical harmonics, from the data available, without some assumptions such as model anomalies. Used in combination with other techniques, surface-gravity measurements provide additional observation equations and comparisons.

3.4 Local gravity cannot give much information about very long-wavelength properties of the gravity field. The lower degrees $\ell = 2, 3, 4, 5$ are poorly determined; they are, however, particularly well determined by satellite techniques. Apart from this consideration, there is no preferential set of harmonics determined by surface gravity, unless there is a "topographic" selection. The satellite effects for degrees $\ell = 10, 11, \ldots, 25$ are dominated by resonances, and there is virtually no information for $C/S\ (\ell, 5)$, $C/S\ (\ell, 6)$, and $C/S\ (\ell, 7)$ for $\ell = 10, 11, \ldots, 25$.

3.5 The combination and comparison of surface-gravity anomalies δg and geopotential anomalies $\delta\psi$ involve the gradient of $\delta\psi$:

$$\delta g = \gamma(\ell + 1)\, \delta\psi \quad . \tag{9}$$

Hence, the variance of $\delta\psi$, determined from δg, increases more slowly than the variance of δg by the factor $1/(\ell + 1)$. The effects of $\delta\psi$ from satellite perturbations become very small as ℓ increases. Therefore, the lower

harmonics will be determined from satellite studies, and the higher harmonics from surface gravity (Section 3.4).

3.6 Rapp (1968) has pointed out that in surface-gravity analysis the amplitude of the spherical harmonic coefficient decreases with increasing ℓ, the variance increases with increasing ℓ, and they cross at approximately $\ell = 18$. If one adopts the position that the coefficients cease to be meaningful when they are smaller than their variances, then $\ell = 18$ seems to be the limit of usefulness of surface-gravity measurements.

3.7 The rule of thumb for decrease of coefficient size is

$$C_{\ell,m} \approx \frac{10^{-5}}{\ell^2} \quad . \tag{10}$$

Hence, $C_{18,m} = 3 \times 10^{-8}$, which is equivalent to $980 \times (18+1) \times 3 \times 10^{-8} = 0.56$ mgal (from equation (9)). If we consider the result for the variance of a $5° \times 5°$ square,

$$\sigma_g^2 = \frac{1000}{n} \text{ mgal}^2 \quad ,$$

where n is the number of anomalies given in the $5° \times 5°$ square, then for $n = 25$, we have

$$\sigma_g = \sqrt{1000/25} = 6.3 \text{ mgal} \quad .$$

Even if we take the optimistic value of $6.3/4 = 1.6$ mgal, it hardly approaches the 0.56 mgal required.

4. 1969 SMITHSONIAN STANDARD EARTH (SEII)

4.1 The SEII (Gaposchkin and Lambeck, 1970) was determined primarily from optical tracking data, combined with significant but not dominating amounts of laser data. The number of optical data used in the form of simultaneous observations was comparable to that used in a dynamical solution. The former give information about relative station positions, and the analysis is relatively free of assumptions.

4.2 The determination of station coordinates is significantly improved by the use of both geometrical and dynamical methods for two reasons. First, a completely different analysis for simultaneous observations was not contaminated by assumptions made in the dynamical solution. For example, some orbits were chosen because of large gravity-field effects. These effects degraded the solution for coordinates during early iterations and the simultaneous observations canceled out these biases. Second, the validation of the results is critical and was made possible by the two methods.

4.3 A further geometrical data set was included — the relative longitudes and distances to the axis of rotation of the JPL DSN stations — which strengthened the solution and provided an additional check on the results.

4.4 Twenty-one satellites were used in the dynamical analysis. Only six of these had any laser data. In addition, there were only five laser stations. The 21 satellites ranged from 28° to 95° inclination. The variation in orbital elements was sufficient for the separation of the harmonics. The complexity of the field determined was fixed by the accuracy of the data (15 to 20 m). The gravity field could be completely determined through $\ell = 10$, $m = 10$ from satellite data. For the 11th- and 12th-degree terms only C/S (11,7), C/S (12,6), and C/S (12,9) were not determined. Higher order terms selected were C/S $(\ell, 1)$, $13 \leq \ell \leq 16$; C/S $(\ell, 2)$, $13 \leq \ell \leq 15$; C/S (14,3); C/S $(\ell, 12)$, $13 \leq \ell \leq 19$; C/S $(\ell, 13)$, $13 \leq \ell \leq 21$; and C/S $(\ell, 14)$, $14 \leq \ell \leq 22$. The 12th-, 13th-, and 14th-order terms are, of course, the resonant harmonics.

4.5 The remaining harmonics through $\ell = 16$, $m = 16$ are determined in a combination with the available surface-gravity data: 935 300 × 300 n mi squares out of the 1654 possible squares. Of these, only 136 had more than 20 1° × 1° anomalies. The 16th degree and order were chosen to be the point where the data did not significantly contribute to an extended field; i.e., the residuals were not reduced by adding unknowns. In addition, some surface-gravity anomalies were rejected on a 3σ criterion. Generally, these rejected anomalies were in regions of significant tectonic activity, such as the Puerto Rico trench. Hence, the rejected data are probably good, but not characteristic of the long-wavelength features of the gravity field that we are determining.

4.6 Figure 1 shows the degree variance and the standard error of the coefficients for SEII. The coefficients for $\ell > 16$ are determined by the resonant effects. The standard error of the solution for the harmonics will apparently cross the degree variance line between $\ell = 18$ and $\ell = 20$, confirming Section 3.6. Since the harmonics from $\ell = 12$ to $\ell = 16$ were mostly determined by surface gravity, this result is not independent of Section 3.6.

5. LASER TRACKING

5.1 The precise measurement of range gives one component of the satellite position. For zenith passes this will be a radial component dr that is less affected by the earth's gravity field. Observing at lower elevation angles measures part of the along-tracking component du, which is generally the largest effect, and the across-track component dw, which is the same size as dr. For the following discussion, we assume that we measure a general component of the position and are not restricted to the radial component. If we observe at an elevation of 30°, we get $\sqrt{3}/2 = 0.87$ of the along-track component.

5.2 Laser systems differ in three principal ways:

A. Accuracy. The first systems were limited to an accuracy of 1.5 m, and some are still at that level. Newer systems have achieved an accuracy

of 50 cm (Lehr, Pearlman, and Scott, 1970; Pearlman, Lehr, Mendes, and Wolf, 1970). The limitation on accuracy arises from two sources. The first is the resolution of the equipment itself and is discussed in Lehr et al. (1970) and Pearlman et al. (1970). The second, and ultimately limiting, source of error is the determination of refraction for the atmosphere. The current accuracy (Lehr et al., 1970; Pearlman et al., 1970; Lehr, Pearlman, Salisbury, and Butler, 1969) of the refraction correction is sufficient. For future observations where system accuracy is improved to between 1 and 5 cm, the atmospheric correction will have to be treated with greater precision, perhaps along the lines described in Hopfield (1970).

B. Repetition rate. The number of observations per pass run from 5 to 200. The passes with 200 observations have been analyzed statistically, and the observation errors (residuals) have a white noise spectrum.

C. Acquisition method. The SAO and Goddard Space Flight Center (GSFC) systems have automatic-pointing capability and can observe 24 hours a day. Other systems, e.g., those operated by CNES and the National Technical University (NTU), Athens, acquire the satellite visually and can observe only during twilight.

Some of these differences are related. For example, the number of observations is related to the cooling system, as is the power output. The latter determines the efficacy of daylight observations and accuracy.

5.3 The minimum elevation for successful observations could be as low as 15° or as high as 30°. The ability to make the atmospheric correction is the controlling factor.

5.4 In order to use laser tracking data to determine the geopotential, we must sample the gravity field everywhere. We can find out how many stations are necessary for complete coverage. Table 1 lists for a variety of heights (h) the geocentric angle subtended (θ), the fraction of the earth's surface sampled by one station (ζ), and the number of stations necessary for an almost complete sampling of the whole earth (N_{sta}). Each quantity is given

for zenith distances of 60° and 75°, corresponding to elevations of 30° and 15°, respectively. Also computed is the subsatellite height at minimum elevation (h'). The satellite must reach this height to be observed everywhere at minimum elevation. Therefore, h' would correspond to a minimum apogee height.

5.5 Table 1 is computed for a polar satellite, and Figure 2 represents the computation graphically. For a satellite of arbitrary inclination the amount of the earth covered will be less. These figures can be appropriately modified by multiplying $[\zeta \sin (I + \theta)]$ by $[N_{sta}/\sin (I + \theta)]$.

5.6 It is quite apparent that to obtain reasonable coverage with a modest number of stations (say, < 50) for satellites with low apogee heights (say, < 1 Mm), we must make observations at the minimum elevation of 15°.

5.7 This analysis holds for any ground-based tracking system.

6. FUTURE GRAVITY-FIELD DETERMINATIONS WITH LASER SATELLITES

6.1 In Section 2.4 the decomposition of a satellite perturbation into a sum of products was described. Each term in the sum is of the form

$$\delta \varepsilon_{\ell mpq} = S_{\ell m}\, \delta \varepsilon^{*}_{\ell m}\, \mathcal{S}[\alpha\omega + \beta m + \gamma(\Omega - \theta)] \quad ,$$

where $S_{\ell m}$ is the gravity-field coefficient; $\delta \varepsilon^{*}_{\ell mpq}$ is a function of a, e, and I and is virtually constant for any satellite; and $\mathcal{S}[\alpha\omega + \beta m + \gamma(\Omega - \theta)]$ is a trigonometric sine or cosine function of the angular variables, α, β, γ being integers. Since $-1 \leq \mathcal{S} \geq 1$ and the amplitude of $S_{\ell m}$ can be roughly estimated as

$$S_{\ell m} \propto 10^{-5}/\ell^{2} \quad ,$$

we can estimate which terms $\delta\varepsilon_{\ell mpq}$ are significant by calculating $\delta\varepsilon^{*}_{\ell mpq}$. Any C/S (ℓ, m) may be much smaller than the estimate, and the perturbation will not, in fact, be necessary. Conversely, there could be very large C/S (ℓ, m), which would be ignored by use of the rule $(10^{-5}/\ell^{2})$. These two possibilities must be reinvestigated after the coefficients are determined by examining the numerical values or by looking for unmodeled effects in the orbital residuals.

The term $\delta\varepsilon_{\ell mpq}$ is a generic element, and it is more meaningful to collect the perturbations of the elements into the perturbation of the position vector with components du, dw, and dr. The total change is computed as $(du^2 + dw^2 + dr^2)^{1/2} = d\rho$. Values of $d\rho \times 10^{-5}/\ell^{1.7} > 0.01 \times 10^{-5}$ are kept as significant. The value of $\ell^{1.7}$ is used as a conservative estimate of the decrease in the size of C/S (ℓ, m). We therefore tend to keep more coefficients than necessary. For future reference, we give in Table 2 the estimated size of C/S (ℓ, m).

In Tables 3 to 7 and 9 to 12 the $\delta\varepsilon_{\ell mpq}$ are collected into $d\rho$ and summed over p and q for any ℓ, m. The units are given so that the product of the numerical and gravity-field coefficients multiplied by 10^{6} yields the perturbation in meters. For example, in Table 3 (PEOLE satellite) for $\ell = 3$, $m = 1$, $d\rho = 271$, and $C_{31} = 1.9 \times 10^{-6}$, the total perturbation due to C_{31} is $1.9 \times 271 = 515$ m. From one aspect, the coefficients are sensitivity coefficients.

6.2 Table 3 gives the complete list of sensitivity coefficients for the proposed PEOLE satellite through $\ell = 20$, $m = 20$. We note two characteristics of PEOLE: 1) for any degree ℓ the size of the perturbation decreases with the order, and 2) there are no effects for $m \geq 7$ for any degree, but all $m > 6$ are important through $\ell = 20$.

Table 4 lists sensitivity coefficients for satellite 6508101 (OGO 2) for $11 \leq \ell \leq 20$. The main differences between OGO and PEOLE are shown as follows:

	PEOLE	OGO
I	15°	87°
a	7.173 Mm	7.343 Mm
perigee	730 km	424 km
apogee	860 km	1504 km

Note that for OGO all but a few coefficients are significant, although it has a larger semimajor axis. This is essentially due to the high inclination, because OGO samples the field everywhere. However, the size of the lower order terms is smaller. Therefore, PEOLE will be stronger in determining coefficients $m \leq 6$. Also, OGO has resonant harmonics of the 14th order. OGO is not a laser satellite and is given here for illustrative purposes only.

Higher inclination satellites sample more gravity-field coefficients, and lower inclinations help to separate the coefficients.

6.3 Table 5 gives the sensitivity coefficients for satellite 6701401 (D1D), a laser satellite of moderate height at I = 39°. Note that 1) it does not sample the complete field even to $\ell = 10$, $m = 10$; 2) most of the coefficients to $\ell = 15$, $m = 15$ are sampled; and 3) between $\ell = 17$ and $\ell = 20$ a little more than half the coefficients are sampled, and even for $\ell = 20$, $m = 5$ the effect is $0.025 \times 18 = 0.45$ m.

Table 6 gives the coefficients for satellite 6503201 (BE-C). We can determine the complete field with laser data only to perhaps $\ell = 15$, $m = 15$.

6.4 Table 7 gives the sensitivity coefficients for the seven laser satellites for $\ell = 20$. As we previously noted, not all the coefficients are sampled: $m = 7, 9, 16, 17, 18, 19, 20$ are not determined at all; $m = 6, 8, 10$ are very weakly determined. Apart from the resonant harmonics for $\ell > 20$, a reasonable field to $\ell = 20$, $m = 20$ would allow orbit calculation to an accuracy of the data.

6.5 The seven satellites can determine $7 \times 2 = 14$ degrees of gravity-field coefficients. It is clear that the satellites at different inclinations are distinct (see Section 2.5). We will show that the three satellites at 40° are also distinct. This can be seen by examining the ratio of the perturbation for each order. The analogy of spectrum analysis shows that each order provides a linear equation relating the coefficients of all degrees. If two satellites are identical, these two equations will be the same; i.e., the coefficients of $C_{\ell m}$ will be in the same ratio. We then investigate the ratio of $\delta\rho^*_{\ell,m}$ (D1D)/$\delta\rho^*_{\ell,m}$ (BE-C) in Table 8. We see for the odd degrees that the ratios are significantly different, as they are for the even degrees. Hence, the seven satellites do indeed constitute seven unique objects.

6.6 This selection of satellites will allow us to determine the field approximately to $\ell = 18$, $m = 18$. However, there are significant effects for higher order harmonics that are at best weakly determined. We would suggest one or more additional satellites to aid this analysis. A polar satellite would be the best choice since it samples the field everywhere.

Tables 9 and 10 give the effects for the 18th-degree harmonics for an inclination of 85° and a variety of apogee and perigee heights. It is clear that the 450- by 500-km orbit has the largest sensitivity to the geopotential.

Perigee was arbitrarily chosen at 450 km. The air drag for a geodetic satellite at that height can be adequately treated theoretically. For example, the change in semimajor axis for satellite 6701401 is less that 1 m per revolution, and an analytical theory can be used to compute that perturbation. The general "secular or logarithmic" terms are satisfactorily computed with empirical polynomials.

For a complete sampling of the gravity field directly by use of geodetic satellites such as 6701401 to 18th degree and order, the apogee height must be 550 km. From Figure 2, if $\phi_{max} = 75°$, we would need about 120 stations, clearly an unreasonable number.

6.7 Determination of spherical harmonics to $\ell = 18$, $m = 18$ describes the gravity field to a linear resolution of

$$\frac{2\pi}{18} \times 6378 = 2220 \text{ km} \quad ,$$

which is equivalent to a central angle $\theta = 19^{\circ}.5$. Referring to Table 1, if $\phi_{max} = 75^{\circ}$, we need roughly 30 stations and satellites with apogee heights (corresponding to h') of at least 1.3 Mm.

7. ALTERNATIVE METHODS OF GRAVITY-FIELD DETERMINATION BY SATELLITE TECHNIQUES

7.1 Satellite altimetry to determine the sea surface to an accuracy of 1 m and satellite-to-satellite tracking promise to provide significant improvements in our knowledge of the geopotential. Neither method yields information about site coordinates. Both methods have other uses, such as routine orbit maintenance. The satellite-to-satellite tracking used to improve the gravity field will need low satellites for the same reason that classical methods require lower satellites. The principal advantages of these methods are complete coverage and reduction of some refraction errors.

7.2 These two methods of gravity determination will apparently become useful operational systems within the next 5 years. They will never improve knowledge of the long-wavelength phenomenon that is determined from long integration effects in the classical method. Therefore, the three methods should be combined.

7.3 These two new methods require precise tracking from the ground, which, presumably, will be provided by laser and very long baseline interferometry (VLBI) tracking. It is apparent that laser tracking will become a vital component in these future methods.

8. FURTHER USES FOR LASER TRACKING

8.1 Any program that uses precise positional information on a global scale will ultimately use laser tracking in some form. The GEOLE project (Husson, 1969) is one such program. Laser ranging, perhaps to the moon or to synchronous satellites, can measure the polar motion and rotation of the earth. Of course, laser tracking is ideal for routine orbit maintenance. The satellite system is completely passive. It provides day and night operation with reasonably simple equipment.

8.2 We now turn to the discussion of high satellites, which are very stable orbiting objects with minimal perturbations from the gravity field, air drag, and radiation pressure. Such satellites of intermediate height can be used for determining polar motion, variations in the rotation of the earth, station location, and ultimately the temporal motion of observing stations, which will measure crustal motion and earth tides.

Our present knowledge of the gravity field limits the usefulness of such a satellite. Tables 11 and 12 list the sensitivity coefficients for two satellites of this type. As expected, the low-order terms are the largest. There are modest and manageable resonances. Table 13 lists the formal uncertainties for the first four degrees resulting from the SEII solution. If we conservatively take 0.01×10^{-6} as the uncertainty in any $C_{\ell m}/S_{\ell m}$, then for SAO1 we would make an error of 1.7 m for C_{22} or 1.4 m for C_{41}; for SAO2 this error reduces to 0.8 m for C_{22}. It is apparent that improvements in the gravity field of the earth in the next year or two will easily reduce this uncertainty by a factor of 10, which allows an accurate enough determination of the gravitational perturbations to calculate the position of the satellite to 20 cm.

The principal problem with a high satellite will be the radiation pressure. Even with extreme mass-to-area ratios, the long-term effect cannot be eliminated. However, with suitable satellite design this perturbation can be computed with sufficient accuracy. For example, for a satellite with

$M/A = 3300\ kg/m^2$, $I = 80°$, $e = 0.05$, perigee = 2500 km, and $a = 9.345$ Mm, the short-period effects will be 6.5 cm in one revolution. The maximum perturbation, which is really a very long-period effect, will be 40 cm after one revolution. The short-period perturbation in the radius vector in one revolution will be less than 1 cm. This satellite would be ideal for studying the vertical component of the earth tide, which is 50 cm.

Laser tracking of synchronous satellites would have the advantage of reducing the effects of the uncertainties in the earth's gravity field. The radiation-pressure effects are greater since they are proportional to a. However, the geometry of ranging is significantly degraded. For geometrical programs the heights of SAO1 and SAO2 are preferable.

9. CONCLUSIONS

A. Even with 10-cm laser observations the gravity field cannot be determined complete to $\ell = 20$, $m = 20$.

B. By use of optical data on lower satellites, in conjunction with laser data, the gravity field can be determined accurately enough to utilize fully 10-cm laser data. With higher satellites the gravity field would be accurate enough to compute 15-cm orbits.

C. In addition to the resonant harmonics, many higher harmonics will have to be determined. This can be done by combining surface-gravity data, optical data from lower satellites, and laser data.

D. Kinematic properties such as earth tides, polar motion, and crustal motion can be studied by means of these accurate laser data, relatively unaffected by lack of knowledge of the gravity field.

E. Without large quantities of laser data the goals of the National Geodetic Satellite Program (NGSP) for a $\ell = 15$, $m = 15$ gravity field cannot be reached without the use of surface-gravity data.

F. Currently available surface-gravity data (classified or not) used in combination with satellite data will not permit determination complete to $\ell = 20$, $m = 20$.

G. The NGSP goal of 10 m for station-coordinate accuracy has been reached for some stations. The ultimate accuracy of laser sites can be 20 to 30 cm. For this accuracy to be achieved, an amount of data comparable to that used in the SEII must be acquired.

H. To attain the $\ell = 20$, $m = 20$ gravity field, we must determine 420 coefficients, requiring a computer memory of 90,000 words. In addition, to determine station coordinates and higher harmonics, say 30 stations and 60 additional harmonics, we require $(420 + 30 \times 3 + 60)^2/2 = 163,000$ words of computer memory.

I. If we use satellites with apogee heights of 1.3 Mm, we require 30 stations to obtain complete global coverage of the gravity field, assuming no observations below 15° elevation angle.

J. The station selection should be such as to distribute the area covered globally; the Southern Hemisphere in particular has been inadequately covered in the past. In addition, as many as possible of the original Baker-Nunn sites should be retained to allow better initial starting values and a tie to an inertial reference system.

K. Assuming that the seven satellites described in Table 7 are distinct for purposes of gravity-field analysis, we can separate 14 harmonics. By use of optical observations on other satellites, the lower harmonics are separated. An advisable approach is to add three laser satellites at distinct inclinations, say at 30°, 50°, and 90°. These could be retrograde or prograde. Retrograde satellites provide additional information on the odd zonal harmonics and a consistency check on timekeeping, both clock time and UT1.

L. For orbital maintenance, such as GEOLE, ATS-F, or ATS-G, fewer laser stations would be needed. Indeed, it seems that the geodetic program is making the greatest demands on laser satellite tracking.

10. REFERENCES

GAPOSCHKIN, E. M., and LAMBECK, K.

1970. 1969 Smithsonian Standard Earth (II). Smithsonian Astrophys. Obs. Spec. Rep. No. 315, 93 pp.

HEISKANEN, M., and MORITZ, H.

1967. Physical Geodesy. W. H. Freeman and Co., San Francisco.

HOPFIELD, H. S.

1970. Tropospheric effect on electromagnetically measured range: Prediction from surface weather data. Presented at 51st Annual Meeting of the American Geophysical Union, Washington, April.

HUSSON, J. C.

1969. Le Projet GEOLE. Centre National d'Études Spatiales, Document no. CNES/PR/PS-SY/69-T-42, June.

KAULA, W. M.

1966. Theory of Satellite Geodesy. Blaisdell Publ. Co., Waltham, Massachusetts.

LEHR, C. G., PEARLMAN, M. R., SALISBURY, M. H., and BUTLER, T. F.

1969. The laser system at the Mount Hopkins Observatory. Presented at the International Symposium on Electromagnetic Distance Measurement and Atmospheric Refraction, Boulder, Colorado, June.

LEHR, C. G., PEARLMAN, M. R., and SCOTT, J. L.

1970. A photographic technique for improved laser-ranging accuracy. This conference.

LUNDQUIST, C. A., and VEIS, G., Eds.

1966. Geodetic Parameters for a 1966 Smithsonian Institution Standard Earth. Smithsonian Astrophys. Obs. Spec. Rep. No. 200, vol. 1, 231 pp.

PEARLMAN, M. R., LEHR, C. G., MENDES, G. M., and WOLF, M. R.

1970. A two-laser collocation experiment. This conference.

RAPP, R. H.

1968. A global 5° × 5° anomaly field. Presented at the 49th Annual Meeting of the American Geophysical Union, Washington, April.

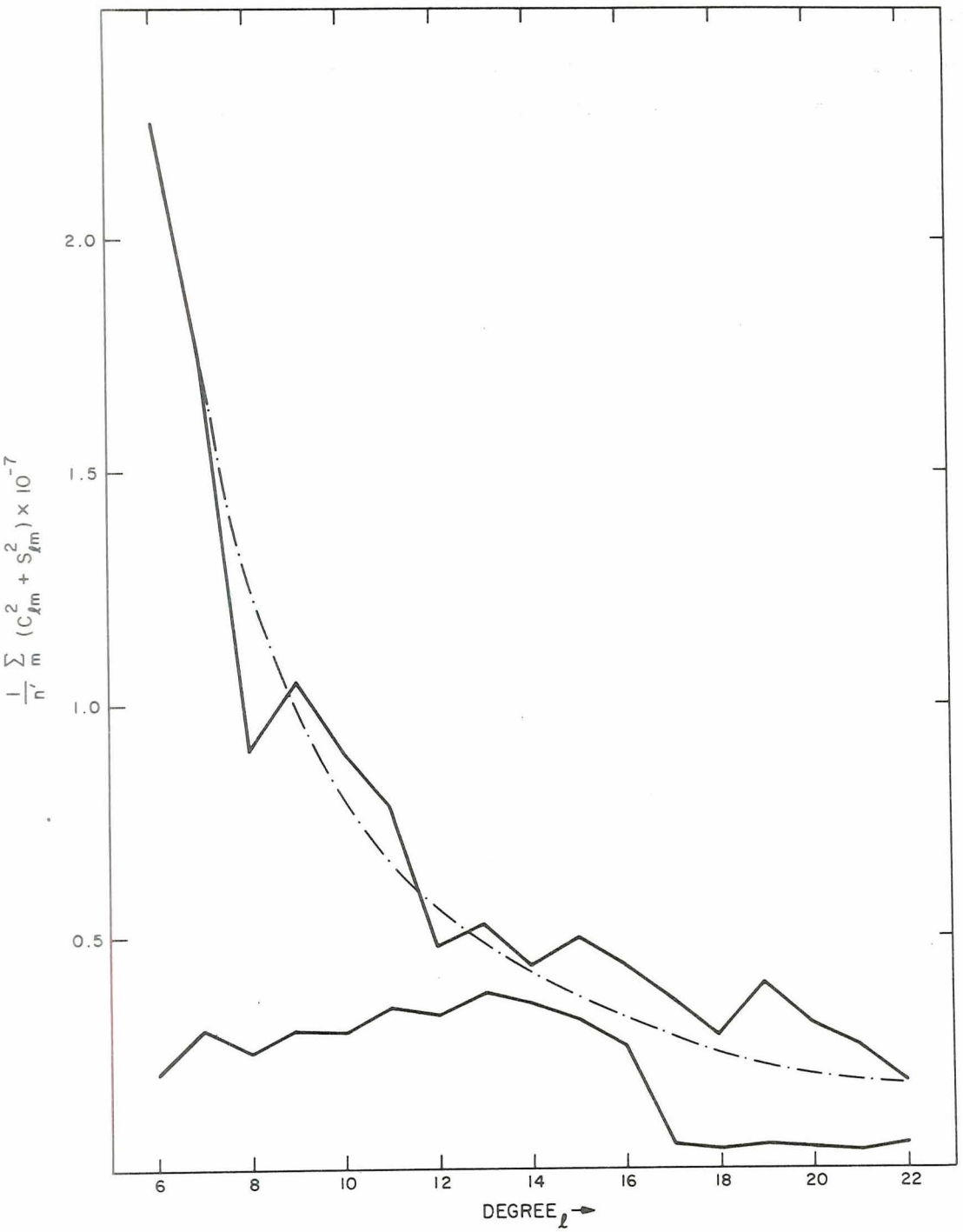

Figure 1. Degree variances for $6 < \ell < 22$ for the combination solution. Kaula's rule of thumb is indicated by the dashed line. For $2 < \ell < 6$ the degree variances are in complete agreement with this rule. The lower curve gives the degree variances corresponding to the precision estimates of the harmonics, i.e., $1/n' \sum_m \left(\sigma^2_{C_{\ell m}} + \sigma^2_{S_{\ell m}}\right)$.

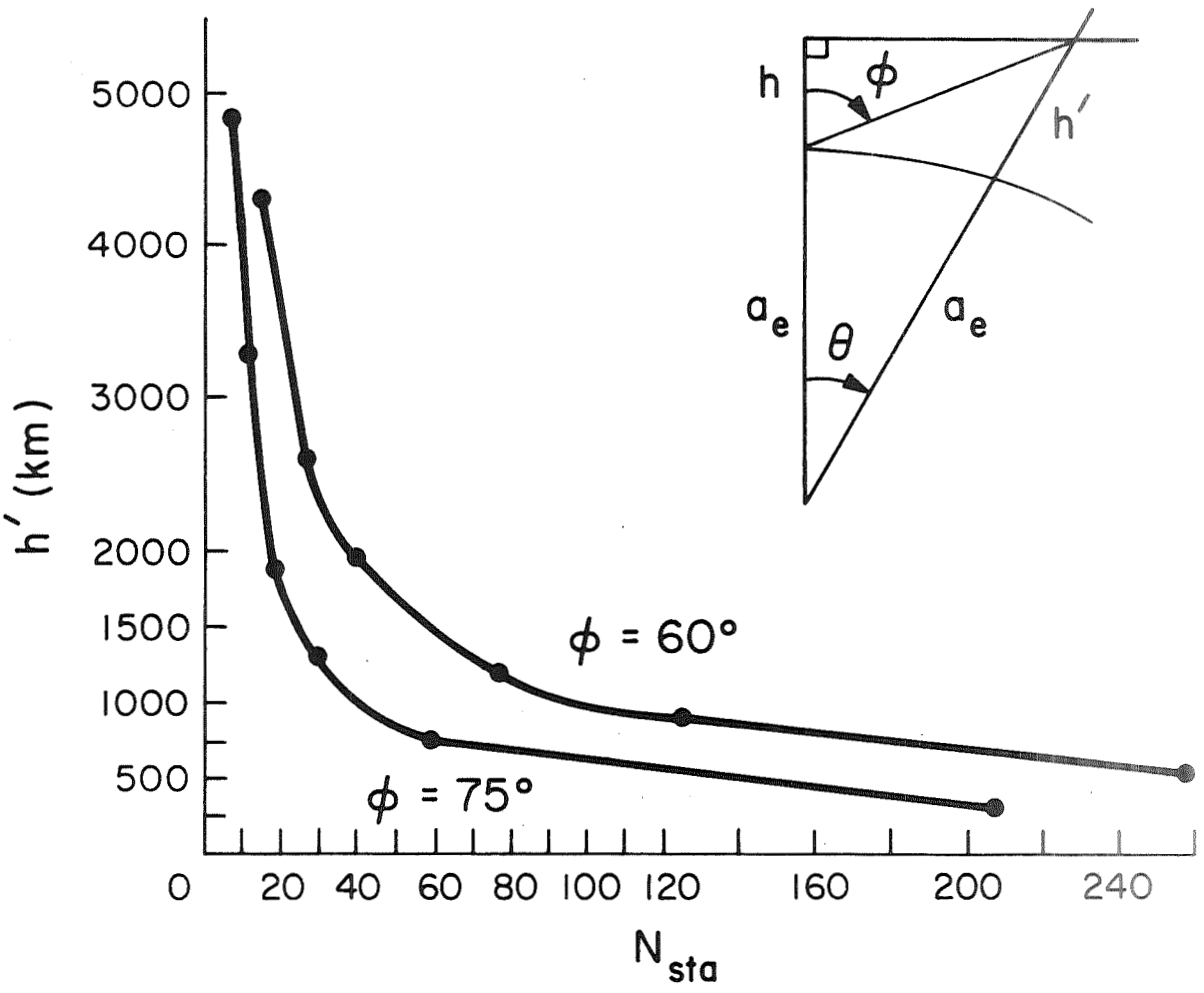

Figure 2. Relation between maximum height and minimum number of stations for global coverage.

Table 1. Dependence of station visibility on satellite height.

h (Mm)	$\theta°$		h′ (Mm)		ζ		N_{sta}	
	$\phi = 60°$	$\phi = 75°$	$\phi = 60°$	$\phi = 75°$	$\phi = 60°$	$\phi = 75°$	$\phi = 60°$	$\phi = 75°$
3.0	29.1	50.0	4.36	8.21	0.063	0.178	16	6
2.0	22.4	41.6	2.68	4.86	0.038	0.126	27	8
1.5	18.2	35.2	1.92	3.26	0.025	0.092	40	11
1.0	13.2	26.6	1.20	1.85	0.013	0.053	77	19
0.75	10.3	21.3	0.867	1.27	0.008	0.034	125	30
0.50	7.2	15.2	0.560	0.749	0.0039	0.017	256	59
0.25	3.8	8.05	0.265	0.315	0.0011	0.0048	910	208

Table 2. Estimated size of $C_{\ell m}/S_{\ell m} = 10^{-5}/\ell^2$ or $10^{-5}/\ell^{1.7}$, in units of 10^{-6}.

ℓ	$10/\ell^2$	$10/\ell^{1.7}$
2	2.50	3.08
3	1.11	1.54
4	0.625	0.947
5	0.400	0.648
6	0.278	0.476
7	0.204	0.366
8	0.156	0.291
9	0.123	0.239
10	0.100	0.199
11	0.083	0.169
12	0.069	0.146
13	0.059	0.128
14	0.051	0.113
15	0.044	0.100
16	0.039	0.090
17	0.035	0.081
18	0.031	0.074
19	0.028	0.067
20	0.025	0.061
21	0.023	0.057
22	0.021	0.052

Table 3. Sensitivity coefficients for satellite PEOLE.

e = 0.0090616		a = 7.173158 Mm	
I = 15°0		perigee = 730 km	
n = 14.281930 rev/day		apogee = 860 km	

m \ ℓ	2	3	4	5	6	7	8	9	10
1		271	621	311	738	229	696	148	526
2	64	71	118	128	201	164	263	165	294
3		58	62	66	107	95	145	116	152
4			50	52	39	56	47	48	61
5				46	28	23	30	17	27
6					13	12	7	7	0
7						0	0	0	0
8							0	0	0
9								0	0
10									0

m \ ℓ	11	12	13	14	15	16	17	18	19	20
1	253	317	295	191	253	220	160	242	58	226
2	150	292	131	233	121	157	125	81	102	52
3	137	165	131	156	100	128	68	98	29	64
4	57	75	53	74	52	70	31	74	31	70
5	25	40	46	45	45	52	52	44	29	47
6	10	0	11	9	28	11	23	14	26	18
7	0	0	0	0	0	0	0	0	0	0
8	0	0	0	0	0	0	0	0	0	0
9	0	0	0	0	0	0	0	0	0	0
10	0	0	0	0	0	0	0	0	0	0
11	0	0	0	0	0	0	0	0	0	0
12		0	0	0	0	0	0	0	0	0
13			0	0	0	0	0	0	0	0
14				0	0	0	0	0	0	0
15					0	0	0	0	0	0
16						0	0	0	0	0
17							0	0	0	0
18								0	0	0
19									0	0
20										0

Table 4. Sensitivity coefficients for satellite 6508101 (OGO 2).

e	= 0.0735840	a	= 7.342592 Mm
I	= 87.°37123	perigee	= 424 km
n	= 13.8026480 rev/day	apogee	= 1504 km

m \ ℓ	11	12	13	14	15	16	17	18	19
1	144	162	142	158	134	155	134	150	131
2	116	101	107	80	77	64	68	52	41
3	68	52	61	43	60	41	47	38	45
4	75	51	69	40	41	32	27	26	22
5	60	37	49	25	40	24	37	22	18
6	62	38	57	32	23	22	20	18	25
7	52	32	46	30	41	16	20	16	19
8	58	33	47	27	34	23	0	0	0
9	80	44	56	29	33	19	29	0	0
10	76	67	49	27	26	22	22	8	19
11	162	56	81	51	53	34	46	35	40
12		198	83	104	65	61	61	38	37
13			708	182	313	144	198	121	138
14				7381	2022	4098	1855	2926	1544
15					663	174	341	167	10
16						250	61	122	52
17							149	41	79
18								133	0
19									77

Table 5. Sensitivity coefficients for satellite 6701401 (D1D).

e = 0.0843130		a = 7.613973 Mm	
I = 39.°45459		perigee = 594 km	
n = 13.064356 rev/day		apogee = 1878 km	

m \ ℓ	11	12	13	14	15	16	17	18	19	20
1	154	229	121	75	139	160	66	69	118	67
2	113	43	61	94	58	35	59	46	0	33
3	52	78	65	25	54	43	12	18	39	26
4	66	34	19	39	38	14	10	27	0	0
5	38	28	51	29	0	23	10	0	0	18
6	65	48	42	14	27	19	0	17	0	0
7	68	62	61	45	10	0	18	16	0	0
8	46	62	45	37	18	12	0	0	18	0
9	21	30	46	64	55	53	23	0	0	0
10	0	0	29	44	43	58	37	32	0	0
11	0	0	8	16	27	48	47	57	48	44
12		0	0	21	44	64	89	101	75	99
13			425	1203	2987	4758	8014	9531	12277	11613
14				0	0	20	47	77	111	145
15					0	0	0	0	16	20
16						0	0	0	0	0
17							0	0	0	0
18								0	0	0
19									0	0
20										0

Table 6. Sensitivity coefficients for satellite 6503201 (BE-C).

e = 0.025143		a = 7.50385 Mm	
I = 41°.18464		perigee = 936 km	
n = 13.35329 rev/day		apogee = 1314 km	

m \ ℓ	11	12	13	14	15	16	17	18	19	20
1	65	182	99	77	57	115	48	38	41	59
2	89	60	27	73	47	25	18	39	25	15
3	36	59	48	37	23	36	24	14	16	21
4	54	52	33	39	32	20	6	23	19	
5	42	26	45	41	11	17	23	13		
6	56	56	40	24	20	20	16	13		
7	60	59	40	37	21	15	14	20		
8	50	50	51	33	30	29	17			
9	26	42	49	46	43	20	20			
10	15	24	36	43	48	39	27	15		14
11			13	28	30	44	36	43	31	25
12		0		22	37	52	51	64	36	38
13			99	113	626	423	1537	793	2142	882
14				0	16	21	65	61	138	93
15					0	0			21	18
16						0	0	0		0
17							0	0	0	0
18								0	0	0
19									0	0
20										0

Table 7. Sensitivity coefficients for seven laser satellites for 20th-degree harmonics.

	6701101	6701401	6503201	6508901	6406401	6800201	PEOLE
perigee (km)	572	594	936	1007	882	1079	730
apogee (km)	1347	1878	1314	2284	1086	1582	860
a (Mm)	7.337318	7.613973	7.50385	8.073824	7.362215	7.708513	7.173158
e	0.052792	0.084313	0.025143	0.072874	0.013901	0.032589	0.0090616
I	39°.98397	39°.45459	41°.18464	59°.37892	79°.69292	105°.79157	15°.0
n (rev/day)	13.810053	13.064356	13.35329	11.967651	13.74706	12.830433	14.281930
m							
1	106	67	59	19	46	21	226
2	40	33	15	0	31	0	52
3	39	26	21	0	0	0	64
4	0	0	0	0	16	0	70
5	25	18	0	0	0	0	47
6	0	0	0	0	0	0	18
7	0	0	0	0	0	0	0
8	17	0	0	0	0	0	0
9	0	0	0	0	0	0	0
10	0	0	14	0	0	0	0
11	43	44	25	0	0	0	0
12	20	99	38	955	0	0	0
13	191	11613	882	25	27	622	0
14	897	145	93	0	156	0	0
15	64	20	18	0	0	0	0
16	0	0	0	0	0	0	0
17	0	0	0	0	0	0	0
18	0	0	0	0	0	0	0

Table 8. $\delta\rho^{*}_{\ell,m}$(D1D)/$\delta\rho^{*}_{\ell,m}$(BE-C).

m \ ℓ	11	12	13	14	15	16	17	18	19	20
1	2.4	1.3	1.2	0.98	2.4	1.4	1.4	1.8	2.9	1.1
2	1.3	0.71	2.3	1.3	1.2	1.4	3.3	1.2	0	2.2

Table 9. Sensitivity coefficients for three hypothetical satellites of 85° inclination for 18th degree.

perigee (km)	650	650	750
apogee (km)	850	950	850
a (Mm)	7.128156	7.178155	7.178156
e	0.0140289	0.020897	0.0069656
n (rev/day)	14.430302	14.279730	14.279728
m			
1	159	143	138
2	39	35	34
3	53	48	46
4	19	17	17
5	33	29	28
6	12	0	0
7	24	21	21
8	0	0	0
9	19	17	16
10	0	0	0
11	42	14	14
12	32	32	29
13	79	71	68
14	268	911	396
15	218	180	124
16	87	84	67
17	38	35	0
18	88	80	75

Table 10. Sensitivity coefficients for six hypothetical satellites of 85° inclination for 18th degree.

perigee (km)	450	450	450	450	450	450
apogee (km)	950	850	750	650	550	500
a (Mm)	7.078155	7.028155	6.978155	6.928155	6.878155	6.853155
e	0.035320	0.028457	0.021496	0.014434	0.007269	0.003648
n (rev/day)	14.583547	14.7395154	14.898284	15.0599248	15.2245111	15.307932
m						
1	199	218	241	269	303	323
2	48	53	59	65	74	79
3	67	74	81	91	102	108
4	24	26	29	32	36	39
5	41	45	50	55	62	66
6	15	17	19	21	24	25
7	30	33	36	40	45	48
8	0	12	14	15	17	18
9	24	26	29	32	58	60
10	0	0	0	0	13	28
11	57	59	61	64	67	68
12	43	43	54	55	56	57
13	104	104	105	108	111	114
14	311	209	191	180	184	184
15	728	1260	3404	16991 + L.P.*	1462	812
16	196	225	242	256	302	348
17	65	82	90	99	108	114
18	148	150	151	162	186	201

*L. P. indicates a very long-period term.

Table 11. Sensitivity coefficients for satellite SAO1.

e = 0.01		a	= 8.8656 Mm
I = 80.°0		perigee	= 2399 km
n = 10.402 rev/day		apogee	= 2576 km

m \ ℓ	2	3	4	5	6	7	8	9	10	11	12
1		96	144	78	88	45	52	22	29	0	15
2	170	82	90	41	29	10	12	0	8	0	0
3		74	66	45	35	22	18	0	10	0	0
4			80	38	28	13	6	0	0	0	0
5				48	32	10	11	5	7	0	0
6					40	9	5	0	0	0	0
7						23	14	8	0	0	0
8							30	4	0	0	0
9								22	14	0	0
10									75	110	22
11										176	21
12											0

Table 12. Sensitivity coefficients for satellite SAO2.

e = 0.01							a = 9.867 Mm				
I = 81.°0							perigee = 3390 km				
n = 8.859 rev/day							apogee = 3588 km				
m \ ℓ	2	3	4	5	6	7	8	9	10	11	12
1		68	87	39	39	16	21	0	10	0	0
2	136	63	58	26	14	0	5	0	0	0	0
3		54	42	20	13	4	7	0	0	0	0
4			51	19	9	0	0	0	0	0	0
5				31	7	6	0	0	0	0	0
6					21	4	0	0	0	0	0
7						12	0	0	0	0	0
8							19	5	0	0	0
9								1141	50	306	25
10									0	0	0
11										8	0
12											0

Table 13. Formal statistics for SEII gravity field.

Degree	$\sigma_\ell \times 10^{-6}$
2	0. 006
3	0. 010
4	0. 007
5	0. 015

AFCRL LASER-SATELLITE GEODESY AND FUTURE PLANS

by

Robert L. Iliff

Terrestrial Sciences Laboratory
Air Force Cambridge Research Laboratories
L. G. Hanscom Field, Bedford, Massachusetts 01730

Presented at

The GEOS-II Review Conference

Goddard Space Flight Center
Greenbelt, Maryland

22-24 June 1970

Abstract

AFCRL has been actively engaged in the instrumentation of a system for laser-satellite geodesy. The system is a dual laser concept to obtain range using a Q switched laser and to obtain angular information by photographic reflected high energy normal mode laser pulses against stellar fields. The Q switched laser system is capable of obtaining up to ten range measurements in a single pumping period which increases the confidence in returns, especially in the presence of high noise. Satellite range measurements have been made using only satellite position predictions.

AFCRL has been engaged in the development of a geodetic laser system in which the approach has expanded into a dual laser concept. One laser, operating in the Q switched mode, is used for satellite ranging. Another laser is operated in the normal mode for satellite illumination - sufficient for photographing the reflections in star fields. One advantage of such an approach is that fewer stations need to make observations for geodetic reductions. This means that for a given number of stations the time required for geodetic positioning is reduced, mainly because of weather restrictions, i.e. a higher percentage of stations can be "weathered in" without seriously affecting the time scale.

Other aspects of the system differ from "normal" in other ways also. The ranging laser is capable of obtaining up to ten pulses in a single pumping period allowing ten range measurements to be made in 300 microseconds. The Haute Provence dual laser system operates alternately - a range measurement is made and 4 seconds later a normal mode laser is fired for a photograph; 4 seconds later a range measurement, etc. - so as to avoid return echo ambiguity. It is felt that the AFCRL system will avoid ambiguity by virtue of the ten range measurements made by the multipulse laser. Therefore, the range and angle measurements can be made nearly simultaneously.

The range laser is Q switched with a Pockels cell ten times per pumping period, normally at a repetition rate of once per 30 microseconds (the rate can be varied). The output is about one joule per

pulse with half power points of 30 ns. The output is presently collimated to two milliradians. When the cooling system is completed the laser can be pulsed once every three seconds.

Start pulses are generated when the laser is fired. The pulses are picked off the rear of the ruby, sent to a photodiode through fiber optics. The return is collected by a 22 cm telescope and then directed to an EMI 9558B photomultiplier after passing through a 10 Å filter. The PMT high voltage is normally off and is gated on for five ms during the time the return is expected. A mechanical shutter is also used if the normal mode laser is operated immediately before or after the range laser but before the return is expected. It has been found that, even with the high voltage off during the time of firing a high energy laser, the PMT is extremely noisy when the high voltage is gated on up to 20 ms later.

The elapsed transit times are measured by a counter system with one ns resolution. Since there are 10 expected returns at specific intervals the counter system must be range-gated 10 times. Range-gating is accomplished by timing delays referred to the Q restoration pulses. The counter system accepts a stop pulse only during a specified duration for each of the ten gates. These open-times must be smaller than the interval between Q switched pulses. If the range uncertainty is large, then as well as opening the range gate, the rate at which the Q is restored must also be lengthened. The method of setting the range gates is optional, depending on the mode of operation; the minimum time delay

can be preset for discrete times by setting the values by thumb wheel switches or the delay can be set in via punched paper tape at a rate of once or twice per second as programmed, the latter being used when tracking visually and firing the laser at will. For the case when only large uncertainty of the expected range is available, the system can be operated as a single pulse system with an infinite-time range-gate; i.e. it is opened and remains open until a stop pulse is generated or until it is reset in the "no range" condition. The counter system is started and stopped when the signal reaches preset threshold levels - the level is set according to prevailing noise conditions.

The "photographic laser", operating in the normal mode, is capable of about 500 joules output but can be pulsed at a faster rate with less input. The flash lamps are water cooled and the 330 mm by 19 mm ruby is cooled to liquid nitrogen temperature. The 2 ms beam is collimated to 2 mrad. When the output is about 200 joules the laser can be pumped at a rate of once every three seconds for a limited time. The PC 1000 camera used to photograph the returns has a 10 degree field. The approach used is to obtain 5 returns spaced 3 seconds apart in the same star field, swing the camera and obtain another set of 5 data points in the same pass. Of course, range data are taken during the entire pass without interruption. Depending on the pass, up to three plates can be exposed.

Several groups have succeeded in photographing Q switched laser pulses; it has been our experience that this present Q switched system

is somewhat marginal. Although photographs of the return have been succesful with the Q switched laser under favorable conditions, it is felt that with the relatively large divergence and small camera aperture (200 mm) that much more reliability can be achieved by using a laser designed specifically for the purpose.

The two lasers, power supply and pulser for the Pockels cell, and the receiver are mounted in the tracking pedestal. (Modifications are also being made to mount a CCTV camera in the pedestal.) The PC 1000 camera is located a few meters away and is operated in a non-tracking mode. The mount can be operated by joy stick or in a programmed mode. In the programmed mode, five sets of azimuth and elevation angles are dialed into the programmer using thumb wheel switches with a resolution of 0.001 degree. The pedestal automatically positions to the first set and upon receipt of a slew command pulse proceeds to the next position. As soon as the pedestal goes to position 2, the first set can be changed to the sixth set and so on. This allows continuous stepping of the mount for an entire pass.

The accuracy with which the pedestal points the lasers and receiver is about 4 arc seconds. A print-out of the angles can also be made; this is especially useful when the system is operated in the joy stick mode. When the laser is fired a pulse is generated which is used to obtain a print-out of time of firing and position of the pedestal at that time.

To operate the system it is necessary to set thumb wheel switches on the clock for the time a sequence is to start. (The cesium controlled clock

is accurate to one microsecond as compared to Loran C and several traveling clocks.) Using thumb wheel switches on the "sequence controller", the following functions are programmed: the number of laser firings, up to 7; the interval between laser firings; the interval between range laser and photographic laser firings; the range gate (the length of time between firing the range laser and application of the PMT high voltage); the interval between Q restoration pulses; the minimum expected transit time delays; and the time delay to slew the pedestal to the next position-delay with respect to laser firing. Then, the width of the gate is set on the time interval measurement system (TIM). The width is the uncertainty of the range in microseconds and noise or signal pulses during this time interval will stop the counter. Start and stop thresholds are also set on the TIM unit. Five sets of look angles are programmed in the tracking pedestal control rack by means of thumb wheel switches.

All data thus far collected were taken using a hand-cranked mount and is, therefore, limited in volume. The mount was incapable of housing both laser units and each has had to take its turn for testing. The most immediate future plans include gathering a sufficient amount of data to evaluate the system. Using the multipulse approach, the difference in range within the 300 microseconds between the first and last pulses in a single firing have been observed. This is another area which will be pursued in the near future. In order to attain more consistent accuracy in both range and range rate measurements, the pulse length will be

shortened. Some equipment modifications are also in our future plans; they include: (1) modification of the tracking pedestal programming method. It is intended to program the mount with punched paper tape with provisions to manually offset from the program in order to "update" at the last minute, and, possibly, provide for a search mode in which the pointing will deviate around the program in an orderly fashion. (2) Cooling the range laser is in the immediate future. (3) Provide temperature control for the narrow band filter. (4) In addition, complete many small modifications to improve the system.

A PHOTOGRAPHIC TECHNIQUE FOR IMPROVED LASER-RANGING ACCURACY

C. G. Lehr, M. R. Pearlman, and J. L. Scott

To be presented at the Geos 2 Review Meeting
Goddard Space Flight Center, Greenbelt, Maryland

June 1970

Smithsonian Institution
Astrophysical Observatory
Cambridge, Massachusetts 02138

A PHOTOGRAPHIC TECHNIQUE FOR IMPROVED LASER-RANGING ACCURACY

C. G. Lehr, M. R. Pearlman, and J. L. Scott

ABSTRACT

The instrumental errors of the ruby-laser systems of Smithsonian Astrophysical Observatory (SAO) can be reduced from 1 to 2 m to 20 to 50 cm by applying corrections to the readings of the time-interval counters. These corrections are obtained from oscilloscope photographs of the return pulses. The correction is the time between the intersection of the counter's "stop" threshold and the centroid of the pulse. The accuracy of the correction depends on how well the threshold and the centroid can be located on the photograph. It also depends on the accuracy with which the system's electrical delay can be measured. The statistical procedures that were used for accurate determinations of the threshold, the centroid, and the delay are described.

The returns from the ruby-laser system at SAO's Mt. Hopkins Observatory (Lehr, Pearlman, Scott, and Wohn, 1970) exhibit a variation in signal strength that is typical of laser systems. The variation is due in part to the fact that the signal varies inversely with the fourth power of the satellite range. It is also due to an observed "scintillation," or random variation in returns from the same satellite range. The situation is illustrated in Figure 1. The range measurements are affected by this variation in signal

This work was supported in part by grant NGR 09-015-002 from the National Aeronautics and Space Administration.

strength when they are obtained directly from a time-interval counter that is started by the transmitted pulse and stopped by the received pulse. The resolution of the counter is 1 nsec, which corresponds to 15 cm. But the duration of the pulse is 18 nsec (full width between half-power points). Consequently, counter readings corresponding to a given range can vary significantly if the counter stops at different points on the pulse's leading edge. The point at which the counter stops is the threshold level of the counter. Under customary operating procedures, an attempt is made to set this threshold at about half the amplitude of an average pulse. The laser system is calibrated for such a pulse and such a setting, but errors will be introduced when the return signal differs from its average strength. Figure 2 shows how the measured range varies for a fixed theshold setting and a 100:1 variation in signal strength. Such variations can be expected in actual operation. The rms error in such range measurements is probably a little less than half the total 5-m variation shown in the figure. In principle, this error can be reduced by adjusting the threshold voltage for predictions of the signal strength. Such predictions are based on an inverse fourth-power variation with range. In practice, as Figure 1 shows, the scintillation is so large that such a procedure is not particularly effective.

Even if all returning signals were of the same strength, there would still be errors related to the intersection of the threshold and the pulse's leading edge. These errors come from pulse-shape irregularities that are due to the random emission of electrons in the photomultiplier tube. The fewer the number of electrons per pulse, the more irregular the pulse becomes. The details of this effect have been described by Lehr, Pearlman, and Scott (1970). Figure 3 shows sketches of typical transmitted and received pulses. Since the transmitted pulse retains a fixed shape and size, the time T_1 between threshold crossing and centroid remains constant. It is the corresponding time T_2 for the received pulse that changes considerably from one satellite return to another. However, the pulse-to-pulse variations in T_c, the counter reading, should have signs opposite to those in T_2, and one should tend to compensate for the other. The compensation is not perfect because there are independent errors of the order of 1 nsec in the counter readings and in the determinations of T_2.

The measurement of T_2 is based on a knowledge of V_2, the effective threshold voltage. Since V_2 depends somewhat on the slope of the pulse's leading edge, its effective value was determined experimentally. The method involved finding the centroid of an irregular pulse. It also yielded an accurate value of the electrical delay of the system. The effective threshold, the centroid, and the delay are treated together in the experiment described below.

The experiment consisted of 48 range measurements to a ground-based reflector at the Mt. Hopkins Observatory. The reflector was 776.329 m from the intersection of the laser system's azimuth and altitude axes. Twelve returns were obtained at each of four settings of the threshold voltage. Neutral-density filters reduced the return from the target to a strength of 30 electrons, the level of a typical satellite return. The calculated two-way travel time over the 776.329-m distance is 5180.4 nsec. This is the time between the peaks of the transmitted and received pulses. The system delay is the value that the laser system gives for K in Figure 3, less 5180.4 nsec. This delay is subtracted from satellite ranges that are measured to the centroid of the returned pulse.

Let us consider ground-reflector returns that were obtained for a given setting of the threshold voltage. Since the effective threshold voltage V_2 is unknown, its value has to be determined. The determination is performed by assuming a number of values of threshold voltage. If we let V designate these assumed values, we obtain results corresponding to those sketched in Figure 4. For simplicity, this figure is drawn for only 5 laser returns, but 12 returns were obtained in practice. Seven assumed values of V are shown in the figure. Thus, for each of the five returns we have seven values of T_2 and one value of T_c, the counter reading. Figure 4 shows 35 values of $T_c + T_2$ plotted against the 7 assumed values of V. According to Figure 3, $T_c + T_2$ equals K when $V = V_2$. When $V = V_2$, T_c and T_2 should have the greatest correlation, so the variation in $T_c + T_2$ should be smallest. This fact is used to find the unknown value of V_2. It is that value of V that gives a minimum dispersion of $T_c + T_2$. In other words, it is the abscissa in

Figure 4 where the curve "necks down." The corresponding ordinate is K, the quantity from which the system delay is determined. Figure 4 is just an illustration. In practice, V_2 is found by computing the correlation coefficient of the measured values of T_c and T_2 and looking for the point where the correlation, which is negative, has its greatest absolute value.

The measurement of T_2 values from the photographs of the return pulses requires that the centroid of the irregular pulse be located. Figure 5 shows a triangular-shaped overlay used for this purpose. The sides of the triangle are separated at their midpoints by 18 nsec, the duration of the transmitted pulse. The absolute values of the slopes of the two sides are equal to each other and to the maximum slope of the pulse's leading edge. The overlay is moved horizontally until the sides of the triangle and the sides of the pulse are in best alignment, as judged by eye. Other methods of centroid determination were tried, but this one, although simple, turned out to be quite accurate.

Figure 6 shows experimental results for a threshold setting of 1.5 v. The correlation coefficient of T_c and T_2 and also the average of $T_c + T_2$ are plotted against the assumed voltage V. The statistical sample consisted of 12 returns. The effective voltage came out to be 1.0 v, and the corresponding K value was 5268.4 nsec. The standard deviation of $T_c + T_2$ at V_2 was 2.2 nsec, which when multiplied by 15 cm/nsec gives a range error for a 1.5-v threshold setting of 33 cm. The same procedure was repeated for threshold settings of 0.5, 1.0, and 2.0 v. In each case, V_2, K, and the standard deviation of $T_c + T_2$ were determined. The four values of K were within an interval of 0.3 nsec. Their average, 5268.4 nsec, was then used to correct the V_2 values slightly. The corrected value, rather than the one corresponding to the actual minimum of the correlation coefficient, is shown in Figure 6.

Figure 7 shows how the error in $T_1 + T_2$ varies with threshold setting. This error lies between about 1 and 4 nsec or about 20 to 50 cm. It provides

an estimate of the instrumental accuracy that can be obtained from photographed pulses. As might be expected, it is largest at low threshold values, where the slope of the pulse's leading edge is smallest.

This method was used to determine several satellite ranges from photographed returns. In Table 1, the values are compared with the corresponding ones obtained from the counter readings alone. The threshold was set at 1.0 v. The standard delay, which is used when photographs are not available, corresponds to a typical point on the leading edge of an average pulse. Its value was 60 nsec for the returns under consideration. The system delay that came from the tests described above is 88.0 nsec. Since it corresponds to the pulse's centroid, rather than to a point on its leading edge, it is larger than the standard delay. Table 1 indicates that centroid detection can appreciably reduce the error in the range measurement.

Table 1. Comparative range measurements on satellite 6503201.

Date and time [UT]		Range [nsec] Determined from photographed returns	Range [nsec] Teletyped from Mt. Hopkins	Difference between range values [nsec]	Difference between range values [m]
8 April 1970	$6^h25^m30^s$	9594256	9594279	23	3.4
8 April 1970	6 26 00	10498082	10498100	18	2.7
8 April 1970	12 09 00	9345429	9345446	17	2.6
9 April 1970	9 33 30	10385879	10385896	17	2.6
15 April 1970	3 33 30	8528719	8528728	9	1.4

REFERENCES

LEHR, C. G, PEARLMAN, M. R., and SCOTT, J. L.

1970. Range corrections from oscilloscopic displays of laser returns. SAO Laser Report No. 4 (to be published).

LEHR, C. G., PEARLMAN, M. R., SCOTT, J. L., and WOHN, J.

1970. Laser satellite ranging. In Laser Applications in the Geosciences, Western Periodicals Company, pp. 111-130.

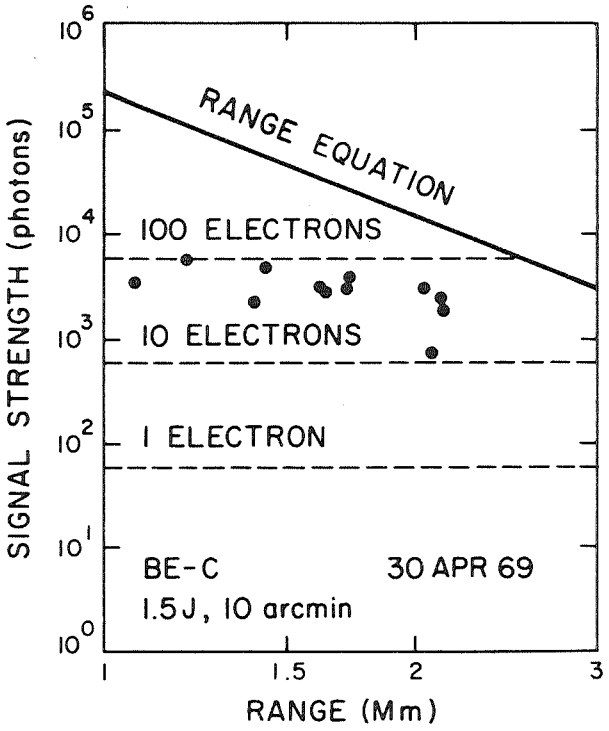

Figure 1a. Laser returns.

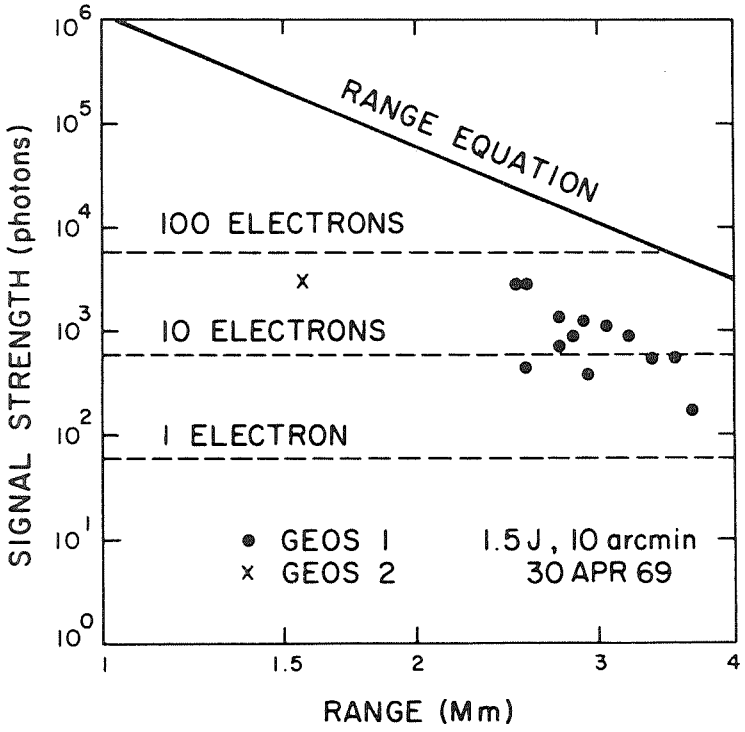

Figure 1b. Laser returns.

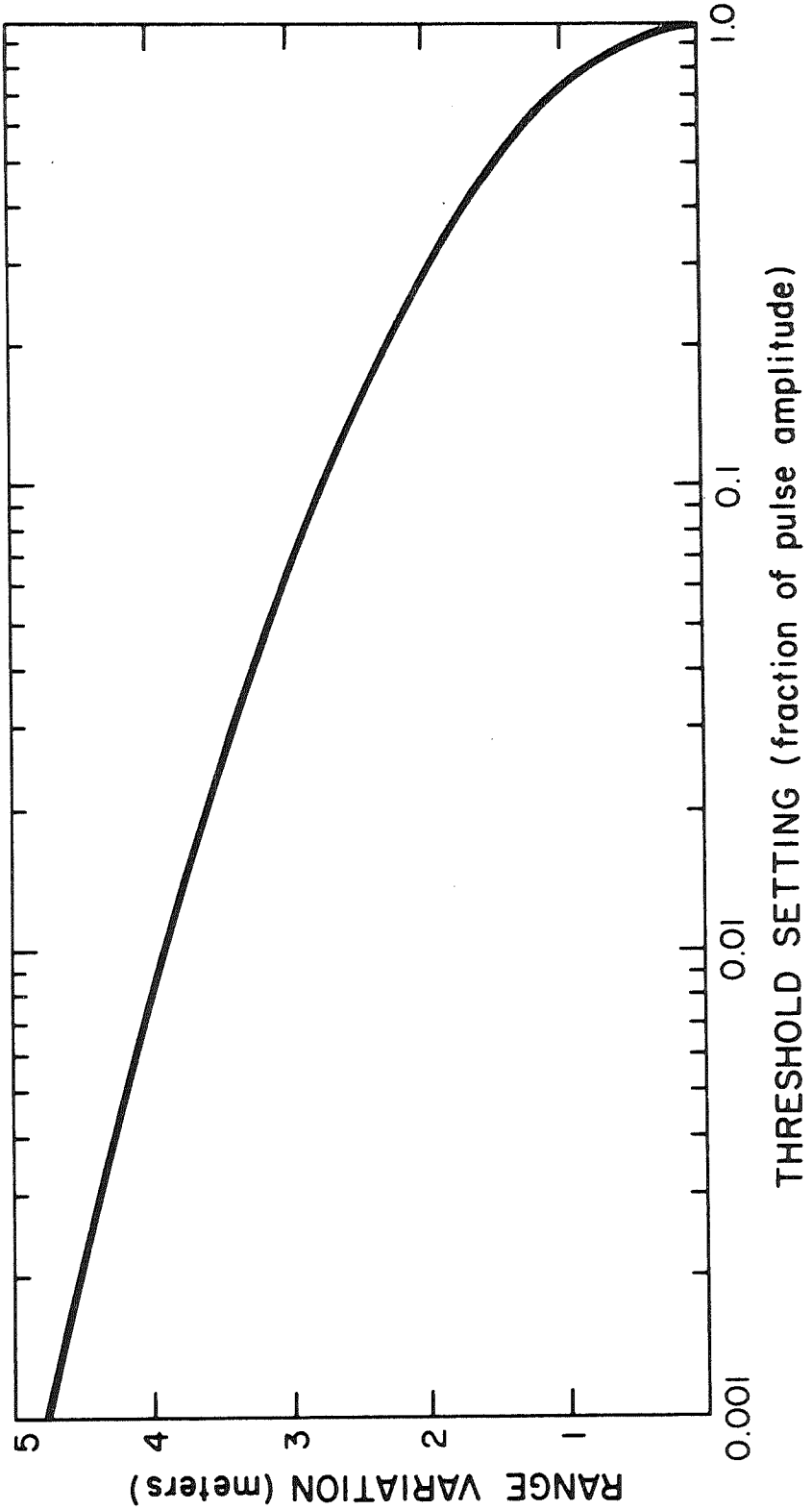

Figure 2. Range variation vs. threshold setting.

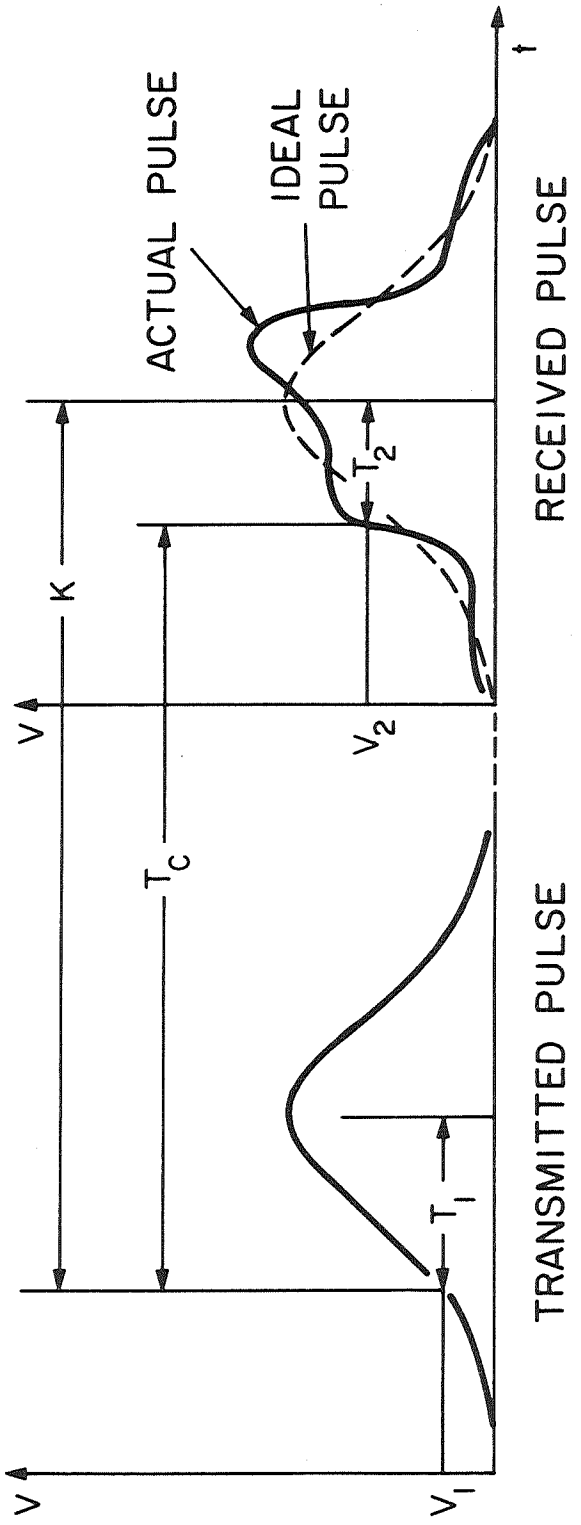

Figure 3. Transmitted and received pulses.

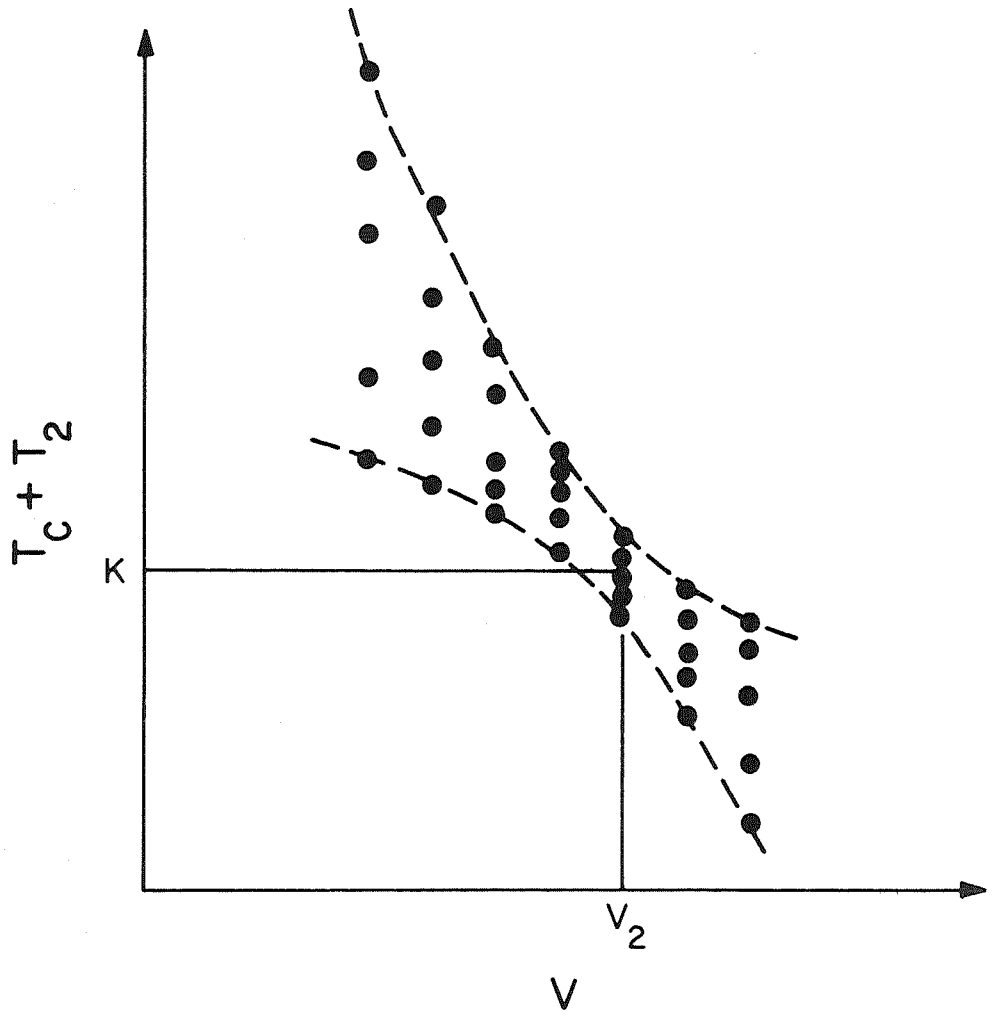

Figure 4. Transit time vs. assumed threshold voltage.

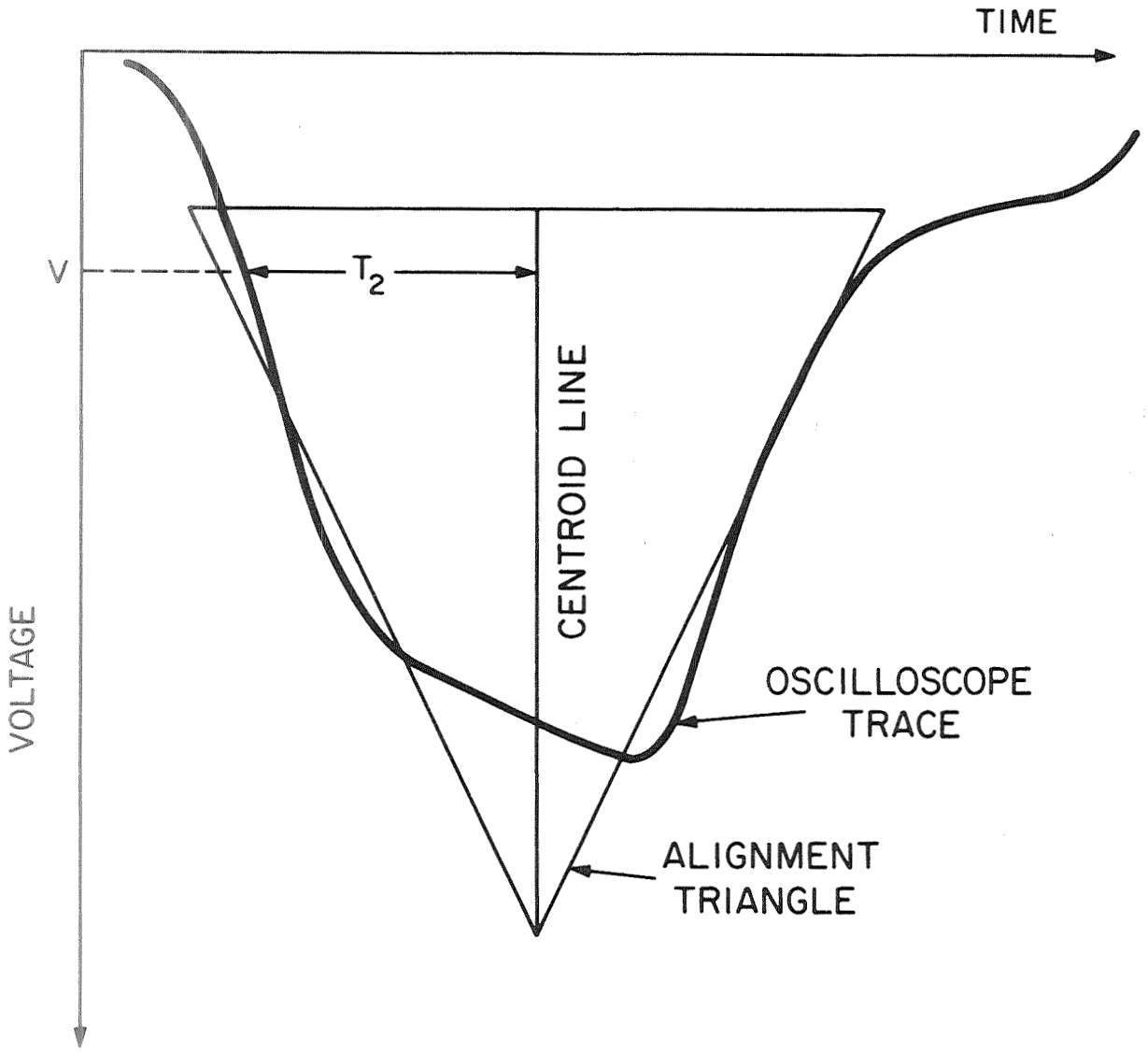

Figure 5. The determination of the centroid and the measurement of T_2.

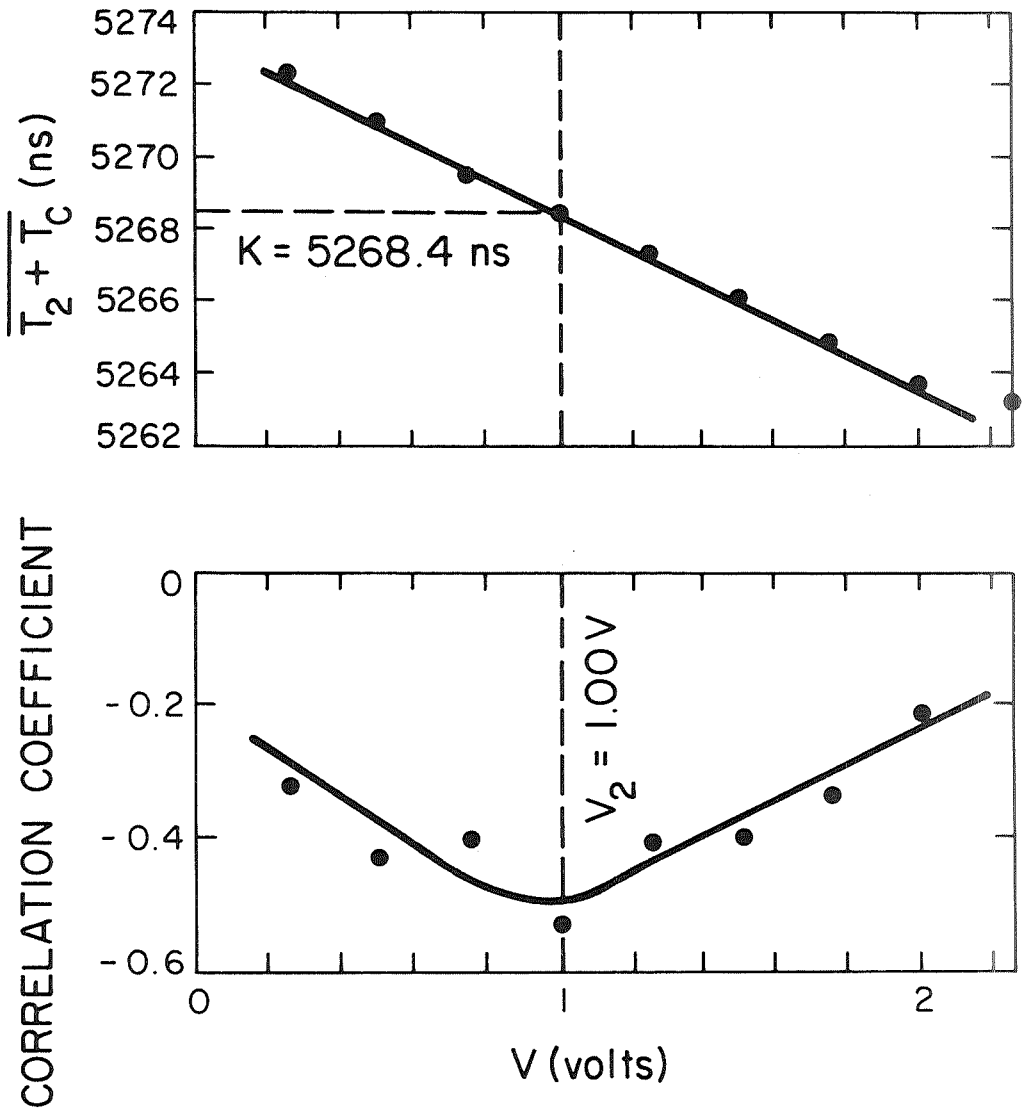

Figure 6. Threshold setting 1.5 v.

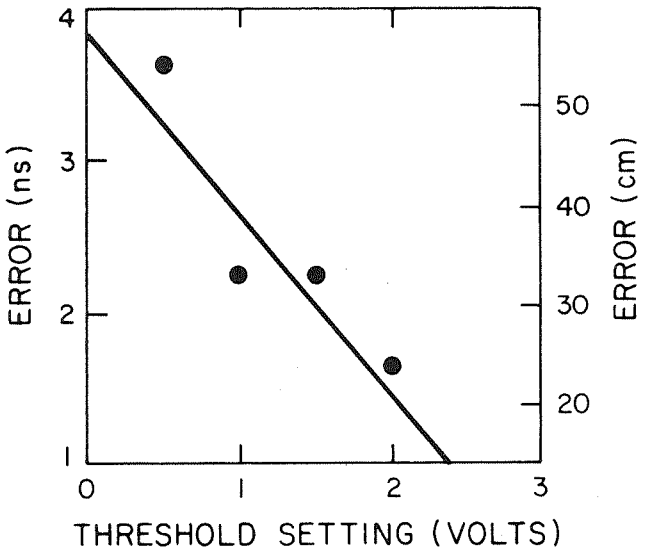

Figure 7. Range error vs. threshold setting.

SOME COMMENTS ON THE PRESENT AND FUTURE VALUE OF GEOMETRIC SATELLITE GEODESY

K. Lambeck

To be presented at the Geos 2 Review Meeting

Goddard Space Flight Center, Greenbelt, Maryland

June 1970

Smithsonian Institution
Astrophysical Observatory
Cambridge, Massachusetts 02138

006-63

SOME COMMENTS ON THE PRESENT AND FUTURE VALUE OF GEOMETRIC SATELLITE GEODESY

K. Lambeck

1. PRESENT STATUS OF GEOMETRIC SATELLITE GEODESY

Geometric satellite geodesy using simultaneous optical direction observations is a very powerful method for obtaining accurate information on relative station positions in the form of directions between stations. This method has the advantage over dynamic techniques in that it is independent of any orbital theory; consequently, a minimum of assumptions have to be made when relating physical observations to the mathematical model. On the other hand, simultaneous directions do not give information on the scale or the translation of the system, and unless the station positions are geometrically well distributed, the propagation of the uncertainties in the station coordinates increases rapidly if they are not constrained by some form of scale control. This is seen in Figure 1, which graphically represents the results obtained from the geometric satellite solution that is part of the 1969 Smithsonian Standard Earth (Gaposchkin and Lambeck, 1970). The origin has been fixed at station 9010 (Florida), and the scale has been fixed by the distance 9001 (New Mexico) to 9010. Despite the large uncertainties in some coordinates, such as stations 9005 (Japan) and 9002 (South Africa), the accuracy of directions between stations is still very high. This is illustrated in Table 1 for some selected lines where directions have not been directly observed but have been computed from the overall geometric solution. Table 2 shows some directional accuracies for directly observed lines.

This work was supported in part by grant NGR 09-015-002 from the National Aeronautics and Space Administration.

These accuracies approach 1 μrad for lines for which many data are available. For a 2000-km line this represents about 2 m. For numerous lines SAO has large numbers of unreduced data that could provide, when reduced, directional accuracies of this order. Comparisons with these attained accuracies and with the theoretically expected values have indicated that the influence of systematic or model errors in the data has been reduced very considerably. One important feature of the SAO geometric solution that helped reduce some of the temporal systematic errors — for example, star catalog errors and refraction — is that the observing campaign was carried out over a time interval of at least 2 years, and in many cases 5 or 6 years. Thus, SAO has built up a data set that will provide a very valuable basis for future observing programs.

The importance of the geometric solution in establishing a geocentric reference system is illustrated by the results of the 1969 Smithsonian Standard Earth. In this new solution a comparison was made between the station positions determined by the geometric and the dynamic methods before a final combination was made. These comparisons enabled us to verify the accuracy estimates made for the individual solutions and to adopt an optimum weighting procedure in the final combination. Based on the results of these comparisons, we feel justified in saying that the position accuracy of the fundamental Baker-Nunn network is better than 10 m. The importance of the geometric solution is further emphasized when we compare the results of the new Standard Earth with those of the 1966 Standard Earth (Lundquist and Veis, 1966). Table 3 gives the coordinate differences. For the stations where it was possible to make comparisons and combinations in both solutions, the difference between the two Standard Earth solutions lies within the accuracy claims made for the respective solutions.

For stations where the 1966 geometric solution was poor (the Z components of stations 9007 and 9011) or nonexistent (all coordinate components of stations 9002 and 9003), the difference between the two Standard Earth results is larger. For stations 9007, 9011, and to a lesser degree, 9002, considerably more data were used in the new solution, and comparisons between the geometric and the dynamic solutions support the accuracy claims for the new solution.

Some comparisons are given in Figure 2, which shows projections of the station–station vector – as determined from the geometric and the dynamic solutions – onto a plane normal to this vector. Both vectors have been constrained to pass through the same point at one of the stations so that the difference in the diagrams between the geometric and the dynamic solutions reflects the uncertainties in the coordinates of both stations.

In addition to contributing to the coordinates of the global system, the geometric solution assists in separating two important and correlated factors in the dynamic solution: namely, the difference between the computed and the observed satellite positions is a function of uncertainties in the station coordinates and certain terms in the earth's gravity field. These differences are analyzed in order to compute corrections to the coordinates and to the gravity field. From combination of the geometric coordinate information with the dynamic results, an improved separation of these two factors is possible, leading to a gravity field that gives better comparisons against surface gravity than does the gravity field determined solely from the dynamic solution.

2. FUTURE REQUIREMENTS FOR GEOMETRIC SATELLITE GEODESY

The orbital theories developed at SAO include all perturbations with magnitudes greater than 0.5 m. Thus, laser data of 1-m accuracy will enable station coordinates to be determined with an accuracy also of about 1 m.

At this level of accuracy and sophistication of orbital theory, the application of geometric satellite geodesy of comparable accuracy is essential for both comparison and combination purposes in order to detect and eliminate any uncertainties in the results and to separate the orbital perturbations caused by uncertainties in the station positions and in the earth's gravity field.

The geometric solution to date has been almost entirely based on direction observations, but some initial work on the combination of laser range data with optical direction data has been carried out in France and at SAO. The results have already indicated the importance of this method for obtaining station positional information that is of an accuracy comparable to the expected results from dynamic satellite geodesy.

The simplest approach is to observe the satellite simultaneously with a combination of lasers and cameras from two stations: lasers and cameras at both stations, cameras at both stations but a laser at only one, or lasers at both stations and a camera at only one. An optimization of the many variables that enter into solutions of this kind has already been discussed. The feasibility of such a program has been shown in terms of available satellites, instrumentation, and observing time span (Lambeck, 1968). But one of the problems of combining laser results with optical data is their difference in accuracies. Laser ranging now gives accuracies of about 1 to 2 m, or better than 1 in 10^6, whereas directions can be obtained with an accuracy of about 1" to 2", or 1 in 10^5. Another problem is to obtain exactly simultaneous observations. The partial answer to the first problem is related to the second – namely, the use of curve-fitting methods, interpolating for a fictitious instant. This reduces random errors in the data and ensures strict simultaneity. For the Baker-Nunn camera, however, the accuracy of such a fictitious observation is currently about 1".5 and can be improved to about 1".0 with minor modifications in the reduction process (Lambeck, 1969). This still represents an accuracy of only about 5 in 10^6, as compared to 1 in 10^6 for laser range data.

But there is still another possibility for making optimum use of the laser data. First, we must employ directional data between the stations; these data, determined by simultaneous direction observations collected over the years, can reach accuracies approaching 1 in 10^6. This information can be introduced into the adjustment of simultaneous laser optical data as quasi-observed quantities. Second, we must observe the satellites in favorable positions such that the variances in the direction observations have

a minimum influence on the accuracy of the desired distance of the station–station vector.

For example, if the satellite P_s is observed by cameras from stations P_a and P_b and by a laser from station P_a, the distance L of the station–station vector is related to the observed quantities by

$$L = r_a \frac{\sin(\theta_a + \theta_b)}{\sin \theta_b} ,$$

where θ_i is the angle subtended at point P_i by the other two points in the triangle $P_a P_b P_s$, and r_a is the observed station–satellite range from P_a.

Applying the law of combination of variances gives

$$\left(\frac{\sigma_L}{L}\right)^2 = \left(\frac{\sigma_r}{r_a}\right)^2 + \cot(\theta_a + \theta_b)\, \sigma^2_{\theta_a} + \frac{\sin^2 \theta_a}{\sin^2 \theta_b \sin^2(\theta_a + \theta_b)}\, \sigma^2_{\theta_b} ,$$

and the problem becomes one of finding, for given variances of the observed range and the observed angles θ_a, θ_b, the geometrical configuration required for (σ^2_L) to be minimum. Several possible examples are discussed in the next section.

Geometric satellite geodesy using laser range observations may also take the form of trilateration – simultaneous range observations from at least four stations. The advantage of this method is that no directional data are required, so the full accuracy potential of the laser is used; with laser data accurate to about 20 cm, relative station positions can be determined with an accuracy of perhaps 10 cm.

As an example, given four stations situated on the corners of a 1000-km square and a satellite of height H, with n observations uniformly distributed through the common visibility area of the four stations, the relative accuracy of the station positions can be expressed by

$$\sigma^2_{L_x} = 260\left(\frac{L}{H} - 0.55\right)\frac{\sigma_r^2}{n}\ m^2 \quad , \qquad \begin{cases} L = 1000\ \text{km} \\ 500 < H < 1500 \\ z_{max} = 60° \end{cases}$$

for a maximum zenith distance of observation of 60°. For $z_{max} = 75°$,

$$\sigma^2_{L_x} = 50\left(\frac{L}{H}\right)\frac{\sigma_r^2}{n}\ m^2 \quad , \qquad \begin{cases} L = 1000\ \text{km} \\ 500 < H < 1500\ \text{km} \\ z_{max} = 75° \end{cases} .$$

For $\sigma_x = \sigma_r = 20$ cm, about 120 observations are required in the former case, and about 25 in the latter.

For global geodesy, however, the method does require a dense distribution of stations, particularly with the satellites currently in orbit, and its application appears to be limited to areas where continental drift or large-scale crustal motions are suspected. Laser-reflector-carrying satellites with altitudes of about 3500 to 4000 km are very desirable for this purpose.

More important, trilateration does not give any absolute directional information, so it cannot contribute to kinematic studies of polar motion or earth rotation.

Several combinations of laser and direction observations are possible, each of which has some advantage, depending on the situation in which they are employed. In the following section three instances are treated.

A. Range observations from both stations, directions from one station, and the direction between the two stations are known with a high degree of accuracy.

B. Range and directions from both stations are known, but there is no a priori knowledge of the direction of the station–station vector.

C. Range and directions from both stations, as well as the direction of the station–station vector, are known.

3. AN OPTIMIZATION OF PARAMETERS FOR SIMULTANEOUS RANGE AND DIRECTION OBSERVATIONS

Case A

The observed quantities are the distances r_a and r_b and the direction $\overrightarrow{P_a P_s}[\delta_{as}, (\alpha - \theta)_{as}]$. The direction $\overrightarrow{P_a P_b}$ has been determined a priori from, for example, simultaneous direction observations. The angle θ_a is given by

$$\cos \theta_a = \ell_{ab}\ell_{as} + m_{ab}m_{as} + n_{ab}n_{as} \quad , \tag{1a}$$

with

$$\begin{pmatrix} \ell \\ m \\ n \end{pmatrix} = \begin{bmatrix} \cos \delta \cos (\alpha - \theta) \\ \cos \delta \sin (\alpha - \theta) \\ \sin \delta \end{bmatrix} \quad . \tag{1b}$$

The distance L can be expressed as

$$L = r_a \cos \theta_a + r_b \cos \theta_b \quad , \tag{2a}$$

with

$$\theta_b = \sin^{-1} \left(\frac{r_a}{r_b} \sin \theta_a \right) \quad . \tag{2b}$$

Applying the law of propagation of variances to equations (2) yields the accuracy S with which L can be determined as a function of the accuracy of the observed quantities. If we assume that the two ranges are measured with equal accuracy, i. e., $\sigma^2_{r_a} = \sigma^2_{r_b} = \sigma^2_r$, then

$$S^2 = \left[\frac{\cos^2(\theta_a + \theta_b) + 1}{\cos^2 \theta_b}\right] \sigma^2_r + r_b^2 \frac{\sin^2(\theta_a + \theta_b)}{\cos^2 \theta_b} \sigma^2_{\theta_a} \quad .$$

Differentiating equation (1a) yields

$$-\sin \theta_a \, d\theta_a = (\ell mn)_{as} \begin{pmatrix} d\ell \\ dm \\ dn \end{pmatrix}_{ab} + (\ell mn)_{ab} \begin{pmatrix} d\ell \\ dm \\ dn \end{pmatrix}_{as} \quad , \qquad (3)$$

and if we assume that the accuracy of the direction $\overrightarrow{P_a P_s}$ can be written as

$$\sigma^2_{as} \begin{pmatrix} 1 & 0 \\ 0 & 1 \end{pmatrix}$$

and the accuracy with which the direction $\overrightarrow{P_a P_b}$ is known as

$$\sigma^2_{ab} \begin{pmatrix} 1 & 0 \\ 0 & 1 \end{pmatrix} \quad ,$$

then propagating variances through equation (3) gives

$$\sigma^2_{\theta_a} = \frac{1}{\sin^2 \theta_a} (\sigma^2_{as} + \sigma^2_{ab}) \quad .$$

Hence,

$$S^2 = \left[\frac{\cos^2(\theta_a + \theta_b) + 1}{\cos^2 \theta_b}\right] \sigma^2_r + \frac{r_b^2 \sin^2(\theta_a + \theta_b)}{\cos^2 \theta_b \sin^2 \theta_a} (\sigma^2_{as} + \sigma^2_{ab}) \quad , \qquad (4a)$$

or, alternatively,

$$S^2 = \left[\frac{\cos^2(\theta_a + \theta_b) + 1}{\cos^2 \theta_b}\right] \sigma_r^2 + \frac{L^2 \sin^2(\theta_a + \theta_b)(\sigma_{as}^2 + \sigma_{ab}^2)}{\cos^2 \theta_b} \quad . \quad (4b)$$

If n sets of observations have been made, the accuracy with which the distance L can be determined is

$$\sigma_L^2 = \frac{1}{n} \sum S_i^2 \quad , \quad i = 1 \ldots n \quad ;$$

S^2 will be a minimum when $\theta_b = 0°$ or $180°$ and will be infinity when $\theta_b = 90°$.

The curvature of the earth, the satellite height, and the maximum zenith distance at which observations can be made impose limits on the possible values for θ_a and θ_b. To express θ_a and θ_b as functions of zenith distance z, satellite height H, subsatellite distance η, and azimuth β_a of the subsatellite point relative to $\overrightarrow{P_a P_b}$, we use the following relations (see Figure 3), where R is the radius of the earth:

$$\sin \eta_a = \sin z_a \cdot \frac{r_a}{R + H} \quad ; \quad \sin \eta_b = \sin z_b \cdot \frac{r_b}{R + H} \quad ,$$

$$\sin \frac{\psi}{2} = \frac{L}{2R} \quad ,$$

$$\cos \beta_a = \frac{\cos \eta_b - \cos \psi \cos \eta_a}{\sin \psi \sin \eta_a} \quad ; \quad \cos \beta_b = \frac{\cos \eta_a - \cos \psi \cos \eta_b}{\sin \psi \sin \eta_b} \quad ,$$

$$\cos \theta_a = \cos \beta_a \sin z_a \cos \frac{\psi}{2} - \cos z_a \sin \frac{\psi}{2} \quad ,$$

$$\cos \theta_b = \cos \beta_b \sin z_b \cos \frac{\psi}{2} - \cos z_b \sin \frac{\psi}{2} \quad .$$

The function S^2 is evaluated as a function of η and β in Figure 4 for some typical values of L and H for $\sigma_r^2 = 2$ m, $\sigma_s = (\sigma_{as}^2 + \sigma_{ab}^2)^{1/2} = 1''.0$, and $z_{max} = 75°$ and $z_{max} = 60°$.

For a given maximum zenith distance at which observations can be made and for $\alpha_b = 0$, $\cos \theta_b$ is largely independent of the distance L (or angular distance ψ). This is verified when the minimum value of S^2 is computed for satellites with different heights and for various values of L. Figure 5 gives these minimum values of S^2 as well as the number of observations required to determine the distance L with an accuracy equal to σ_r if the observations are made when the satellite is near the optimum positions. The results are given for 1) $z_{max} = 75°$, $\sigma_r = 2.0$ m, $\sigma_s^2 = 1''.0$; 2) $z_{max} = 60°$, $\sigma_r = 2.0$ m, $\sigma_s^2 = 1''.0$; 3) $z_{max} = 75°$, $\sigma_r = 2.0$ m, $\sigma_s^2 = 2''.0$; and 4) $z_{max} = 75°$, $\sigma_r = 1.0$ m, $\sigma_s^2 = 1''.0$. Clearly, it becomes desirable to observe as close to the horizon as possible at all times and to measure the angle θ_a with as great an accuracy as possible. An improvement in the accuracy of the range observations does not significantly reduce the number of observations required.

With Baker-Nunn cameras the accuracy of an interpolated direction observation is currently about $1''.5$ but can be improved to about $1''.0$. Then, if the direction $\overrightarrow{P_a P_b}$ is known a priori with high accuracy, $\sigma_s^2 \approx 1.0$ arcsec^2.

If the direction has not been determined from simultaneous observations but can be computed from the coordinates derived from a dynamic determination, then σ_{as} is of the order of about $1''$ and $\sigma_s^2 \approx 2.0$ arcsec^2. The dynamic and geometric solutions for the length L would, however, no longer be independent.

If there are cameras at both stations, the satellite can be observed simultaneously with both lasers and cameras; but the optimum configuration will be different, since θ_b is now an observed quantity. This is discussed further below. Alternatively, we can observe the satellite with one camera and the two lasers when the optimum configuration occurs for this combination, or we can observe the satellite with the two lasers and the other camera

when the appropriate configuration occurs. The advantage of this alternative approach is that the satellite need be visible only from the camera site if the laser at the other site is powerful enough to obtain daylight returns.

The requirement that the satellite be observed in a very limited part of the sky is rather stringent and could result in a long observing program. But this should not be a real problem, since only a small number of observations is required, the laser at P_b can be operated in daylight if it is powerful enough, and several retroreflector-carrying satellites are available. This point is illustrated further by examples in Section 4.

Case B

Let us consider now the case where the satellite is observed simultaneously with both cameras and lasers from the two sites and where no precise information is available on the relative stations positions. Then,

$$L = (r_a^2 + r_b^2 - 2r_a r_b \cos\theta_s)^{1/2} \quad , \tag{5}$$

where

$$\cos\theta_s = \ell_{as}\ell_{bs} + m_{as}m_{bs} + n_{as}n_{bs} \quad .$$

With

$$\sigma^2_{\theta_s} = \frac{1}{\sin^2\theta_s}(\sigma^2_{as} + \sigma^2_{bs}) = \frac{2\sigma^2_s}{\sin^2\theta_s} \quad ,$$

if

$$\sigma^2_{as} = \sigma^2_{bs} (= \sigma^2_s) \quad ,$$

propagating variances through equation (5) gives

$$S^2 = \left\{(r_a^2 + r_b^2)[1 + \cos^2(\theta_a + \theta_b)] + 4r_a r_b \cos(\theta_a + \theta_b)\right\} \frac{\sigma_r^2}{L^2}$$

$$+ \left(\frac{r_a r_b}{L}\right)^2 \sigma_s^2 \quad . \tag{6}$$

For given L and H, S^2 is a minimum for a satellite position midway between P_a and P_b (see Figure 6), and the larger the distance L, the smaller will be S^2. The relation between L, H, and S^2_{min} is given in Figure 7 for σ_r = 2.0 m and σ_s^2 = 1".0. We see that for this case, S^2_{min} is very dependent on both L and H. On the other hand, the results in Figure 7 are independent of z_{max}, at least in the range of 60° to 75°, since when the satellite is midway between the two stations, it is generally at a zenith distance of less than 60°.

For the Case B combination of observations, the satellite must always be visible from both stations and daylight observations are not possible.

Case C

If, in addition to both directions and ranges, the direction of the station–station vector is known, we obtain two estimates for the length L:

$$L_1 = \frac{r_a \sin(\theta_a + \theta_b)}{\sin \theta_b} \quad ,$$

$$L_2 = \frac{r_b \sin(\theta_a + \theta_b)}{\sin \theta_a} \quad ,$$

and an adjustment must be made to obtain a unique and most probable value for L. The accuracy estimate for this adjusted length is given by

$$S^2 = \left\{ \left(\frac{L}{r_a r_b} \right) \sigma_r^4 + [1 + \cos^2 (\theta_a + \theta_b)] \left(\frac{\sin^4 \theta_a + \sin^4 \theta_b}{\sin^4 \theta_a \cdot \sin^4 \theta_b} \right) \sigma_r^2 \cdot \sigma_s^2 \right.$$

$$\left. + \frac{L^2 \sigma_s^4}{\sin^2 \theta_a \sin^2 \theta_b} \right\} \Bigg/ \left(\left(\frac{r_a^2 + r_b^2}{r_a^2 r_b^2} \right) \sigma_r^2 \right.$$

$$+ \left\{ \frac{[\cos (\theta_a + \theta_b) \sin \theta_a + \sin \theta_b]^2}{\sin^4 \theta_a} \right.$$

$$\left. \left. + \frac{[\cos (\theta_a + \theta_b) \sin \theta_b + \sin \theta_a]^2}{\sin^4 \theta_b} \right\} \frac{\sigma_s^2}{\sin^2 (\theta_a + \theta_b)} \right) ,$$

with

$$\sigma_r^2 = \sigma_{r_a}^2 = \sigma_{\theta_b}^2 ,$$

$$\sigma_s^2 = \sigma_a^2 + \sigma_{ab}^2 = \sigma_b^2 + \sigma_{ab}^2 .$$

In Figure 8, S^2 is evaluated for L = 1500 km, H = 1000 km, by use of σ_r = 2.0 m and σ_s = 1".0.

The function S^2 is a minimum for a given L and H when either θ_a or θ_b is as large as possible, which occurs when $(\theta_a + \theta_b)$ is a maximum — i.e., when the angle subtended at the satellite by the two stations is a minimum.

The minimum values of S^2 as a function of L and H are given in Figure 9 for z_{max} = 75°. For z_{max} = 60°, the relationship becomes less dependent on H. The average values of S^2 as a function of L are indicated by the broken line in Figure 9.

4. SOME EXAMPLES

As part of the ISAGEX observing program scheduled for 1970-71, it is intended to obtain simultaneous range and direction observations between several stations:

8015	Haute Provence (laser)
9004	San Fernando (laser and Baker-Nunn)
9029	Natal (laser and Baker-Nunn – daylight laser observations will be possible)
9091	Athens (laser and Baker-Nunn)
9041	Dakar (laser and Baker-Nunn) .

Determination of the following distances will be attempted:

8015–9004	1306 km
8015–9091	1656 km
9004–9091	2648 km
9004–9041	2600 km
9029–9041	3000 km .

From the 1969 Smithsonian Standard Earth results and from the Centre National d'Études Spatiales RCP-133 results, the directions of the triangle 8015–9004–9091 have been accurately determined by the geometric method. For lines 8015–9004 and 8015–9091, Case A is therefore appropriate, while for the line 9004–9091, Case C is the most suitable. For the lines 9004–Dakar and 9029–9041, Case B has to be used, since no directional information on these vectors is currently available. Figure 10 gives the number of observations necessary to determine the station–station vector with an accuracy of 2 m, assuming the optimum conditions are satisfied. Curves for three satellites are given. These and others can be constructed from the general cases given in Figures 5, 7, and 9. If σ_s = 1!'0, σ_r = 2.0 m, and z_{max} = 75°, only 14 observations are required to determine the distance 8015–9004 with an accuracy of about 2.0 m, and 18 observations are required for the distance 8015–9091. For these lines any satellite at any height can be observed with equal effectiveness. For the line 9004–9091 the

number of observations required varies between about 10 and 16, depending on the satellite height. For the remaining two lines the situation is less favorable. In both instances the satellites must be observed when they are near perigee, as height now plays a very critical role. For example, using Geos 1 for the line 9004–9041, about 94 observations are required if the satellite is observed near apogee, whereas only 16 observations are required when the satellite is near perigee. A similar number is required for Geos 2 observations at perigee.

The long line Natal–Dakar will present some problems, since observations near perigee will not always be possible because of the earth's curvature. For a height of about 1200 km, at least 20 observations are required.

For both these lines the situation will be considerably improved if the station–station direction is also known (Case C).

5. CONCLUSIONS

For a successful program of simultaneous direction and range observations, the following points must be considered:

1. The satellite–station configuration is extremely critical in Cases A and B if the number of observations are to be kept to a minimum. The conditions are such that a particular satellite satisfies them only very occasionally, but with the six retroreflector-carrying satellites now available, sufficient data can be collected in an observational period of about 6 months.

2. It is important that the direction of the station–station vector be independently observed by simultaneous direction observations with an accuracy of about 0!!5 or better. This can be done by use of more favorable satellites and the optimizations discussed by Lambeck (1969).

3. The direction observations should be accurate to about 1".0 or better. With care, this can be achieved for synthetic Baker-Nunn observations, particularly as the lines discussed here are mostly in the Northern Hemisphere and stars of far south declinations are not required in the film-reduction process.

4. Laser range accuracies of about 1 or 2 m are adequate for this observational program. Improved range accuracies do not significantly reduce the number of observations required.

5. If the interstation distances are to be determined with accuracies better than about a meter, range observations only in the form of spatial trilateration should be used. High-altitude retroreflector-carrying satellites will be required for this.

6. For the 1-m range accuracy and for low laser-firing repetition rates, interpolation methods for obtaining synthetic simultaneous observations are adequate if the direction observations are taken on either side of the range measurement and if the interpolation is carried out at the instant at which the latter observation is made.

7. For spatial trilateration either very rapid repetition rates are required or the lasers must be synchronized so that exactly simultaneous observations are possible. For 20-cm accuracies, this means that the absolute time at each station must be known to within about 20 μsec and that the laser can be fired on command. Lasers employing Pockel cells for triggering the firing are appropriate for this.

6. REFERENCES

GAPOSCHKIN, E. M., and LAMBECK, K.

1970. 1969 Smithsonian Standard Earth (II). Smithsonian Astrophys. Obs. Spec. Rep. No. 315, 93 pp.

LAMBECK, K.

1968. Scaling a satellite triangulation net with laser range measurements. Studia Geophys. et Geod., vol. 12, pp. 339-349.

LAMBECK, K.

1969. On the reduction and accuracy of Baker-Nunn observations. In Reduction of Satellite Photographic Plates, ed. by J. Kovalevsky and G. Veis, COSPAR Transactions No. 7.

LUNDQUIST, C. A., and VEIS, G., Eds.

1966. Geodetic parameters for a 1966 Smithsonian Institution Standard Earth. Smithsonian Astrophys. Obs. Spec. Rep. No. 200, 3 vols., 686 pp.

Table 1. Direction cosines and accuracies of selected long lines.

Line		L	M	N	Distance	σ^2_δ arcsec^2	$\sigma_{\delta,\alpha-\theta}$ arcsec^2	$\sigma^2_{\alpha-\theta}$ arcsec^2
9004	9005	-0.9175731	0.3975023	-0.0071827	9.8655413	0.22	0.05	2.57
9004	9012	-0.9752180	-0.1705706	-0.1409100	10.8403546	0.16	0.07	0.59
9007	9008	0.1254920	0.8932594	0.4316705	11.4279447	0.26	-0.15	0.25
9011	9114	-0.3787809	0.1546661	0.9124711	9.3601113	0.06	0.04	0.07
9001	9006	0.2333572	0.9720264	-0.0266289	10.9443275	0.16	-0.02	0.74
9009	9028	0.2614842	-0.9645428	0.0358218	10.1417612	0.39	-0.16	0.24
9029	9117	-0.9531798	0.2164585	0.2111728	11.7438257	0.28	0.19	0.37
9005	9028	0.9534319	0.0645153	-0.2946276	9.2827560	0.56	0.50	0.78

Table 2. Direction cosines of station–station vectors.

Station	L	M	N	σ_δ^2	σ_α^2	$\sigma_{\alpha-\theta}^2$
90019007	.5533024	-.1013374	-.8267933	.08	.04	-.02
90019009	.8673538	-.1488313	-.4749175	.04	.05	-.02
90019010	.9654354	-.1669486	-.2001564	.05	.06	-.03
90019012	-.7952943	.5590340	-.2344950	.22	.26	.16
90019113	-.8398600	.4984305	.2149468	.55	.44	.18
90019114	.1092630	.6856665	.7196687	.48	.16	-.02
90019117	-.7167568	.6500002	-.2525064	.22	.29	.15
90029008	-.2634801	.2647682	.9276185	.26	.86	-.41
90029028	-.0386285	.3164744	.9478142	.65	.47	.17
90049006	-.5590305	.8242178	-.0902773	.14	.17	-.10
90049008	-.3267921	.9374792	-.1197483	.20	.13	-.11
90049009	-.4414247	-.8138821	-.3778096	.31	.37	.25
90049010	-.6274848	-.7668084	-.1351580	.29	.40	.22
90049028	-.0379168	.8490277	-.5269860	.38	.38	-.06
90049029	.0149787	-.5736286	-.8189785	1.09	.38	.30
90049091	-.1927372	.9797634	.0540006	.31	.31	-.15
90049115	-.6890483	.3985934	.6052568	.72	.51	-.21
90059006	.9152361	.3880019	-.1086161	.52	.42	.38
90059012	-.2473509	-.9394576	-.2371432	1.06	.27	1.19
90059117	-.3907736	-.8491932	-.3551997	2.04	.42	1.62
90069008	.9110432	-.4121827	.0102782	.62	.28	.23
90069028	.8289764	-.3212882	-.4577905	.68	.44	.16
90069115	.3606918	-.8366851	.4121402	.23	.37	.15
90079009	.0984437	-.0040855	.9951342	.05	.10	.03
90079010	-.2021848	.0424032	.9784290	.05	.06	.02
90079011	.1850049	.4871412	-.8535026	.22	.15	.08
90079029	.7997417	.5301435	.2817112	.34	.74	-.03
90079031	-.0766857	.5210859	-.8500522	.65	.58	.17
90089028	.5673330	-.1630395	-.8071873	1.47	.09	.28
90089115	-.0568149	-.8471896	.5282441	.46	.20	.14
90099010	-.6310609	.1066281	.7683701	.10	.17	.04
90099011	.0060328	.1892182	-.9819165	.08	.03	.02
90099029	.7072600	.5213013	-.4775230	.75	.75	.01
90109114	-.5807344	.5531073	.5973440	.16	.14	.06
90119029	.6980520	.3028520	.6488482	.50	.81	-.10
90129114	.8019840	-.2028475	.5618492	.46	.40	-.00
90129117	-.3703243	.8841374	-.2848877	1.70	.43	.96
90289091	-.0872703	-.5447064	.8340736	1.22	.90	-.03
90299031	-.6643695	-.0872138	-.7422984	.43	.73	-.04
91139114	.5223308	.5101516	.6833124	.55	.45	-.12
91149115	.7328034	.6782404	.0546731	1.22	.74	.20
80159004	.4036878	-.7757363	-.4850458	.51	.32	.18
80159066	-.6962356	.3087623	.6480138	8.83	.68	1.29
80159074	-.7231334	.4996525	.4768914	1.31	.42	-.53
80159080	-.6121440	-.5512713	.5669035	1.42	.65	.35
90049066	-.4796719	.6955520	.5349041	.34	.18	-.08
90049074	-.6073169	.6246964	.4908366	.44	.14	-.17
90049080	-.6703400	.2377845	.7029245	.45	.19	-.01
90669074	-.7225951	.5377779	.4343400	2.01	.66	-.75
90669080	-.4578721	-.7820683	.4227555	1.68	.48	.49
90749091	.6757205	.2958945	-.6751653	1.91	.55	.21
90021043	-.4604214	.8202075	.3395169	1.16	0.89	1.09

Table 3. Differences in the coordinates as determined in the 1966 and 1969 Standard Earth solutions. The large discrepancies occurred at stations where no comparisons or combinations of independent solutions were possible in the 1966 solution.

Station	X (m)	Y (m)	Z (m)
9001	+ 1.7	- 0.6	+ 1.0
9002	- 0.7	+26.0	+32.1
9003	-26.0	-13.8	+26.5
9004	- 4.7	+ 3.7	- 7.1
9005	+ 4.3	+13.4	-11.3
9006	- 2.2	+ 3.3	+ 8.6
9007	+ 5.6	- 3.4	+27.8
9008	+11.2	- 9.0	- 4.2
9009	+ 8.6	- 3.6	- 4.1
9010	+ 9.2	- 9.2	- 2.5
9011	+14.2	- 4.0	+30.9
9012	+ 1.8	- 6.8	+ 0.7
9114	+ 1.4	+ 8.4	- 8.0
9115	+ 4.9	+14.6	+ 5.6
9117	+ 3.1	+13.9	+ 4.5

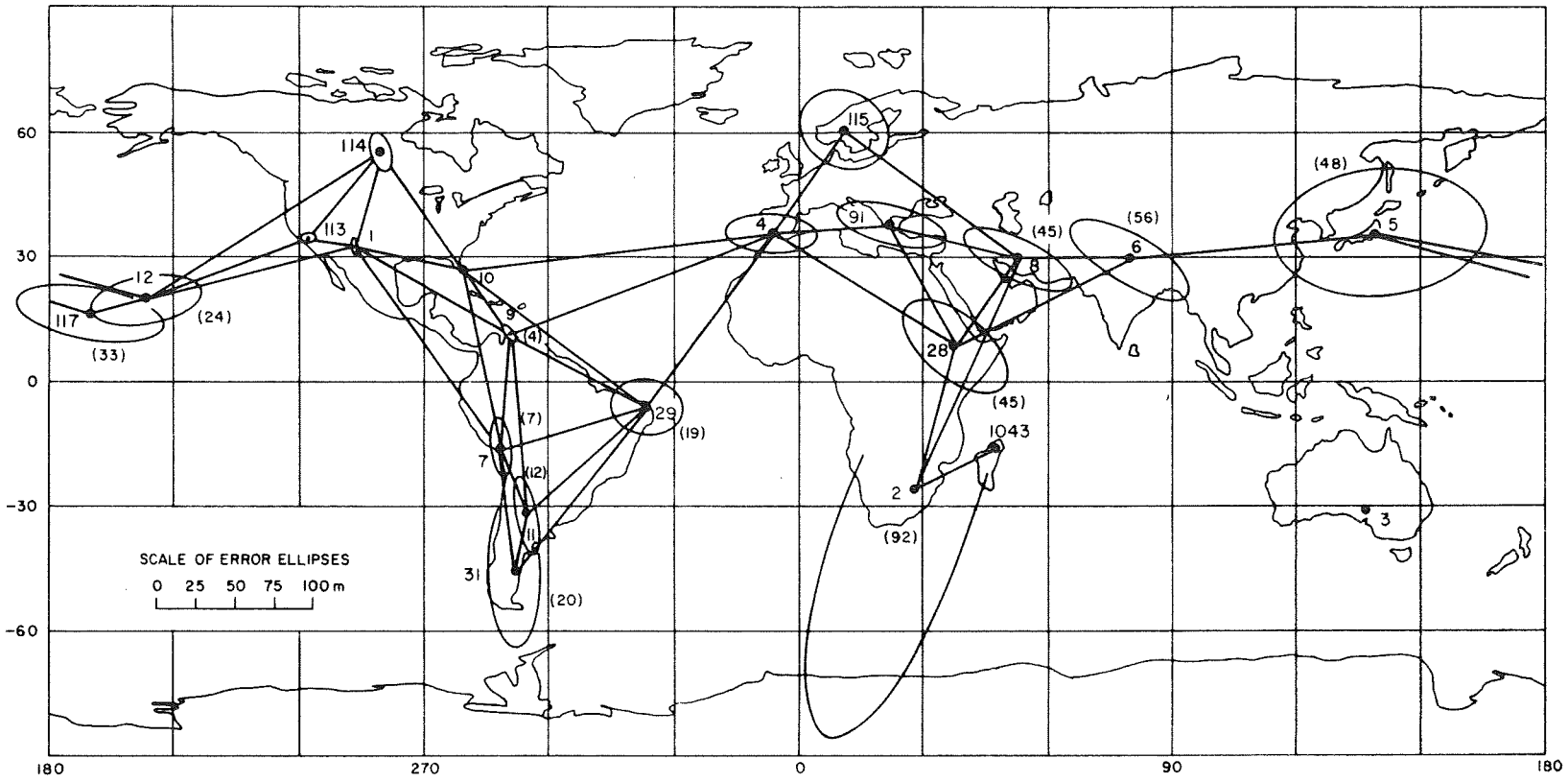

Figure 1. Error ellipses for the Baker-Nunn camera coordinates derived from the geometric solution. The origin is station 9010, and the scale is the distance 9001–9010. The number in parentheses at each station refers to the standard deviation of the height determination.

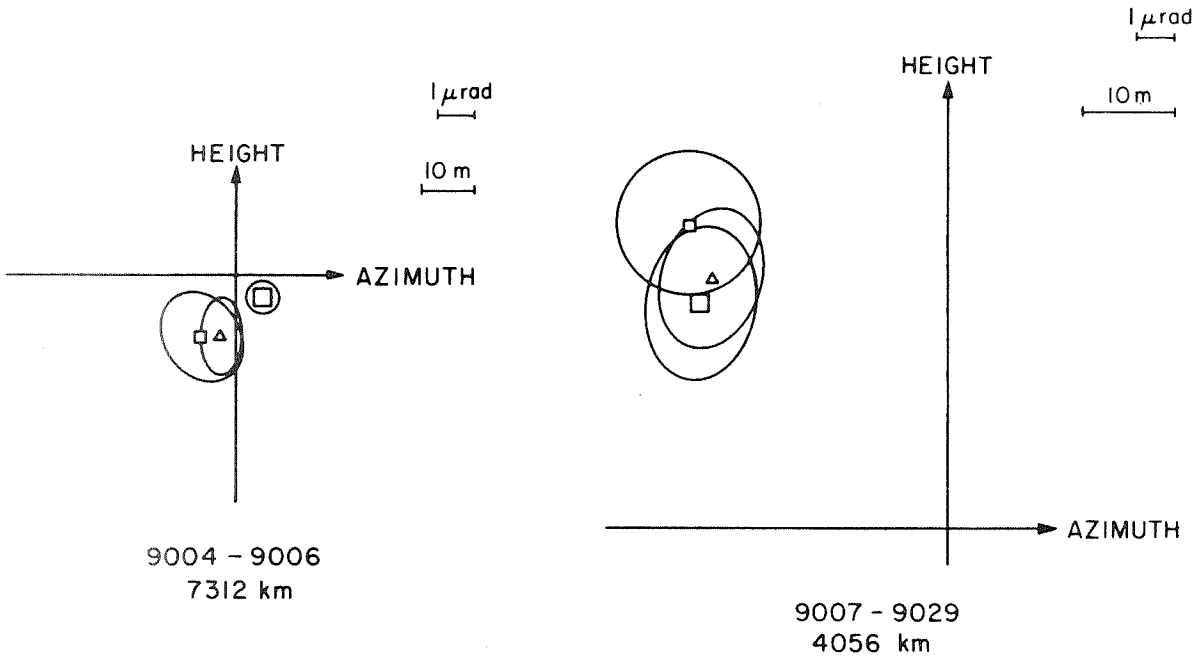

Figure 2. Representation of some comparisons for directions between stations derived from the geometric solution △, the dynamic solution □, and the combination solution ▢.

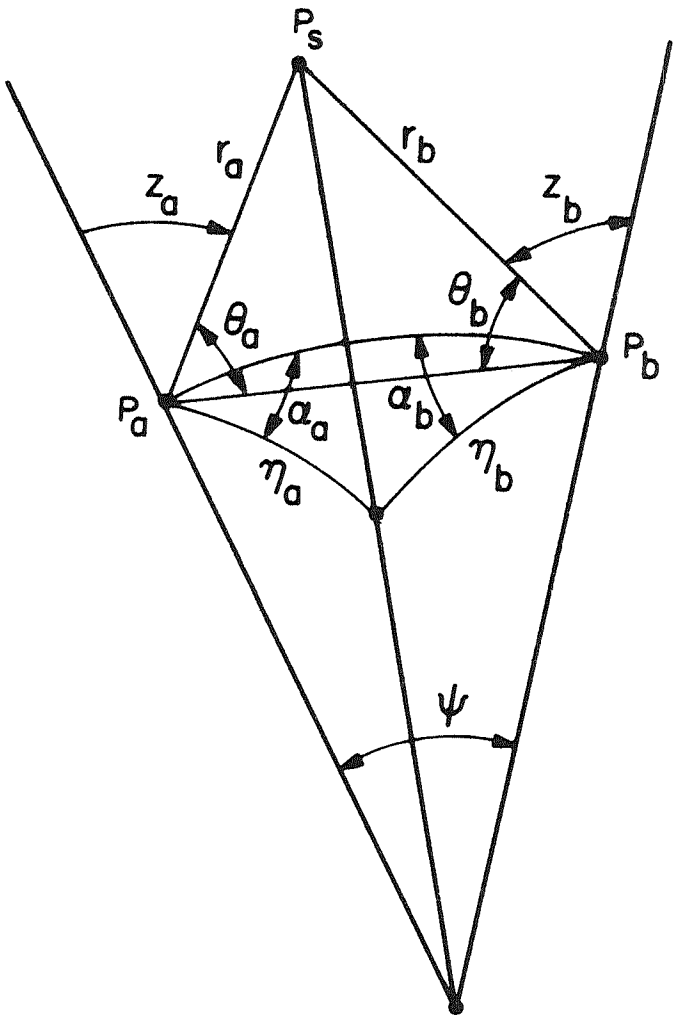

Figure 3. Station–satellite configuration geometry.

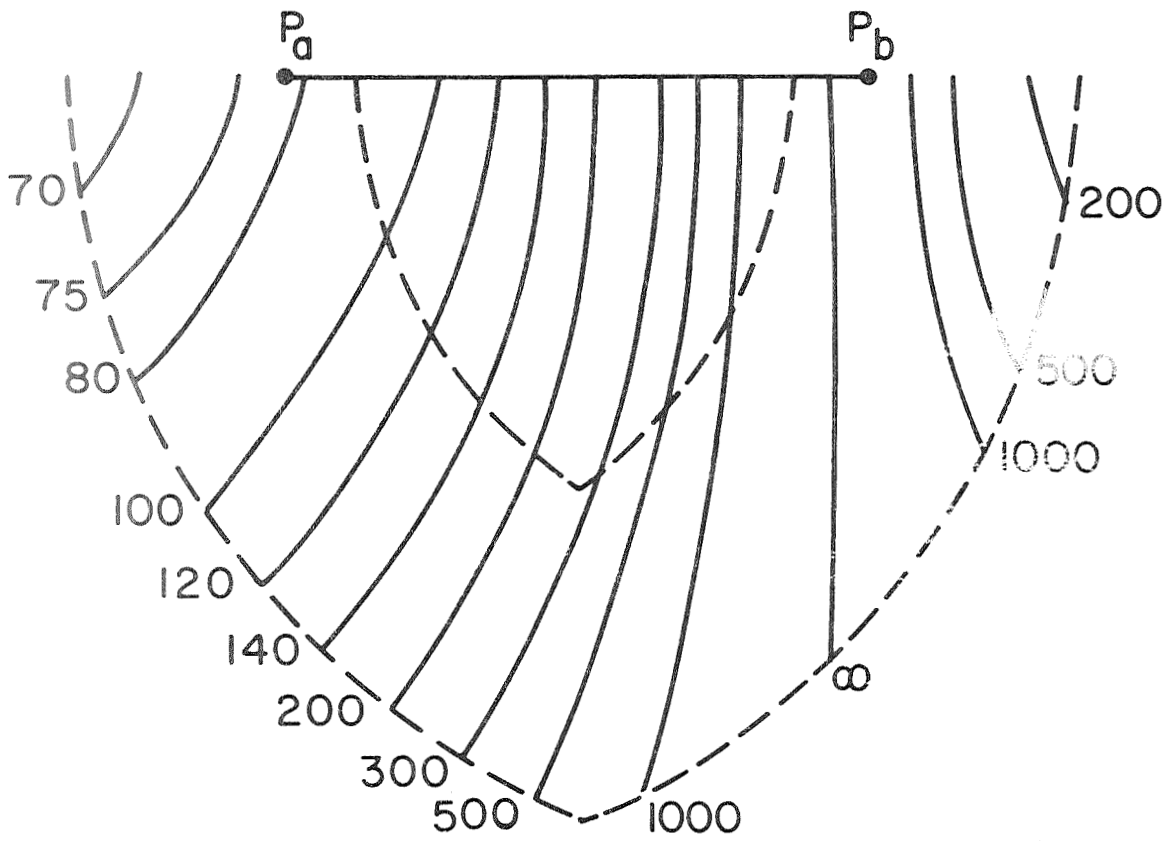

Figure 4. Evaluation of S^2 for L = 1500 km, H = 1000 km for the case of range observations from P_a and P_b. The direction observations from P_a and the direction of $\overrightarrow{P_aP_b}$ are known (Case A). The limits of the common coverage area are shown for $z_{max} = 60°$ and $z_{max} = 75°$.

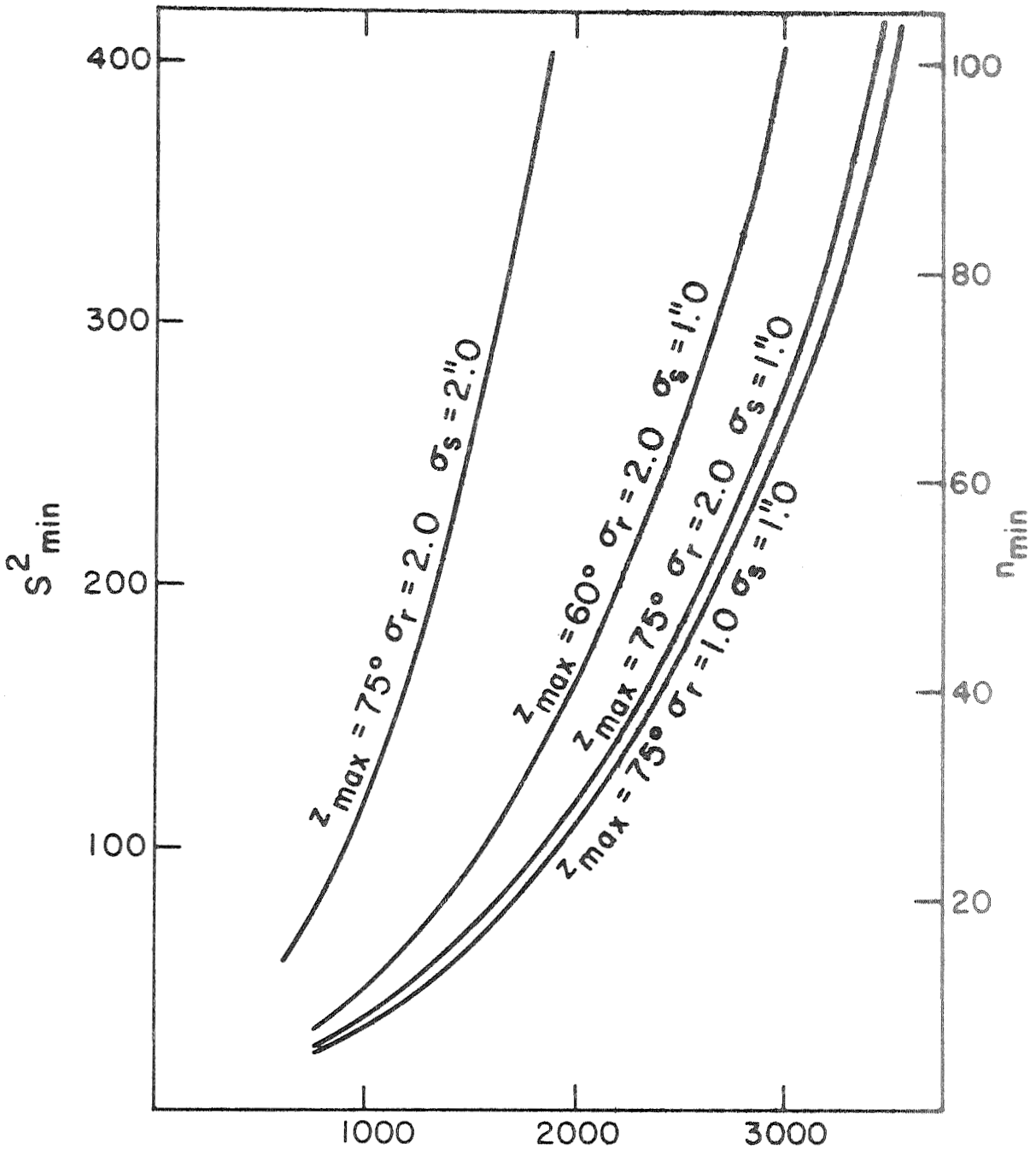

Figure 5. Evaluation of S^2_{min} for Case A and the minimum number of observations required (N) to determine the distance between the stations with an accuracy of 2 m.

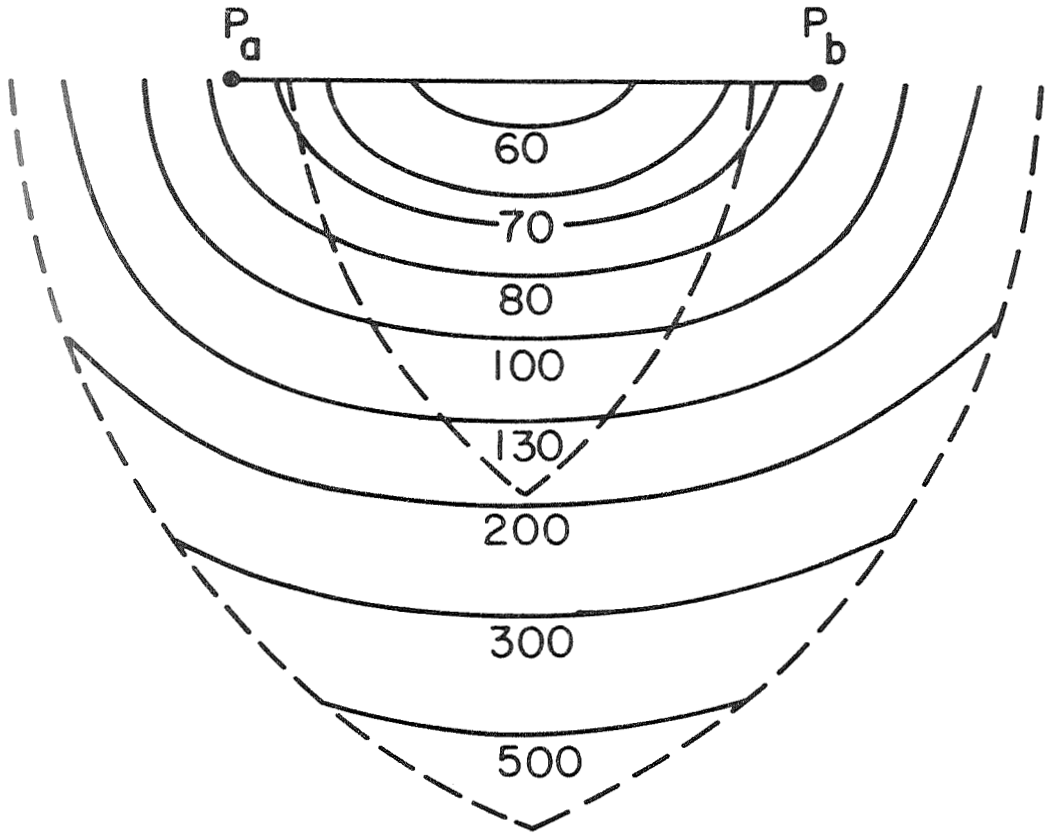

Figure 6. Evaluation of S^2_{min} for L = 1500 km, H = 1000 km for the case of range and directions observed from both P_a and P_b, but with no information on the direction $\overrightarrow{P_aP_b}$ (Case B). The limits of the common coverage area are shown for $z_{max} = 60°$ and $z_{max} = 75°$.

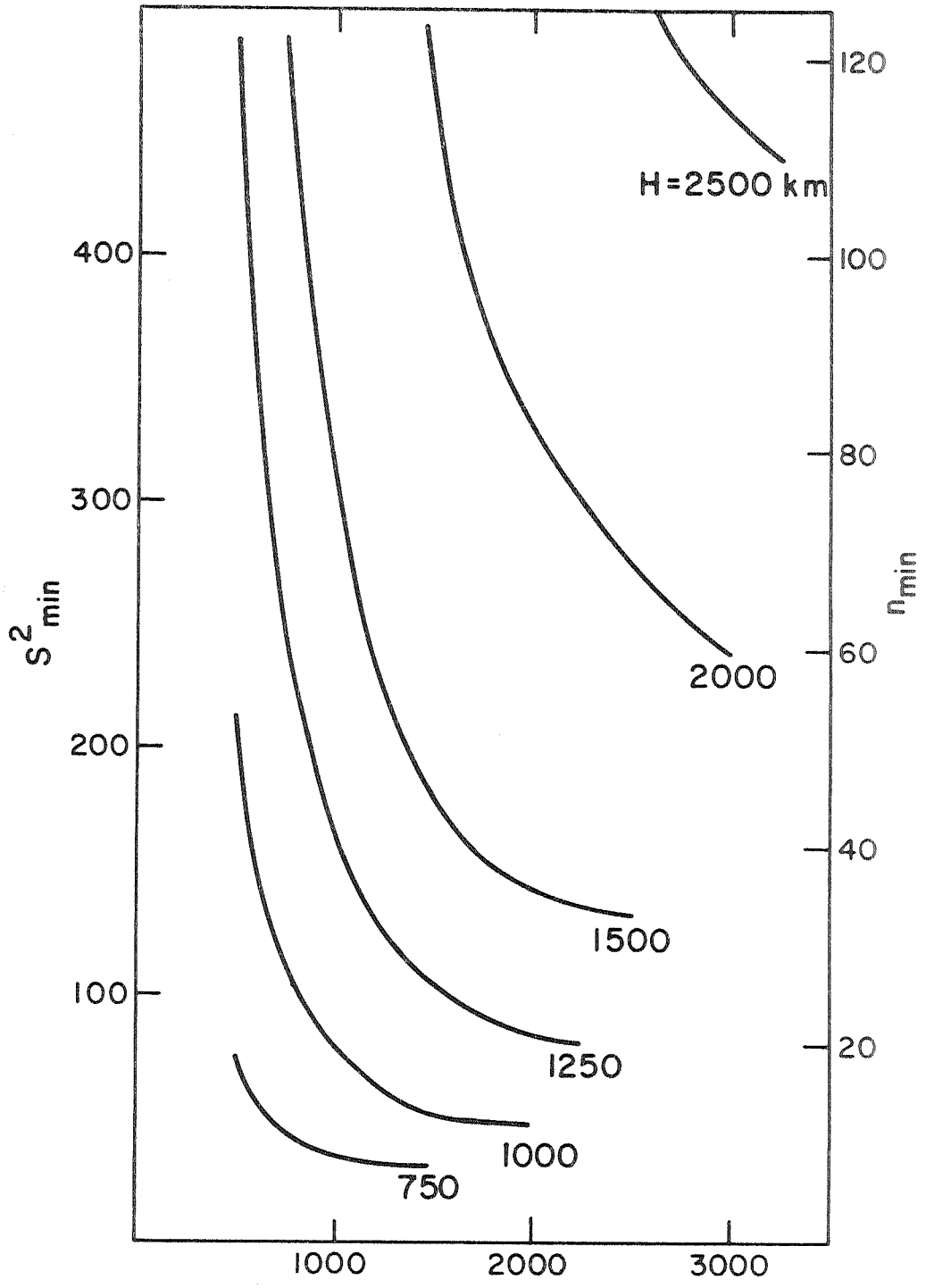

Figure 7. Evaluation of S^2_{min} and n_{min} for Case B as a function of satellite height H and interstation distance L. σ_r = 2.0 m, σ_s = 1".0, z_{max} = 75°.

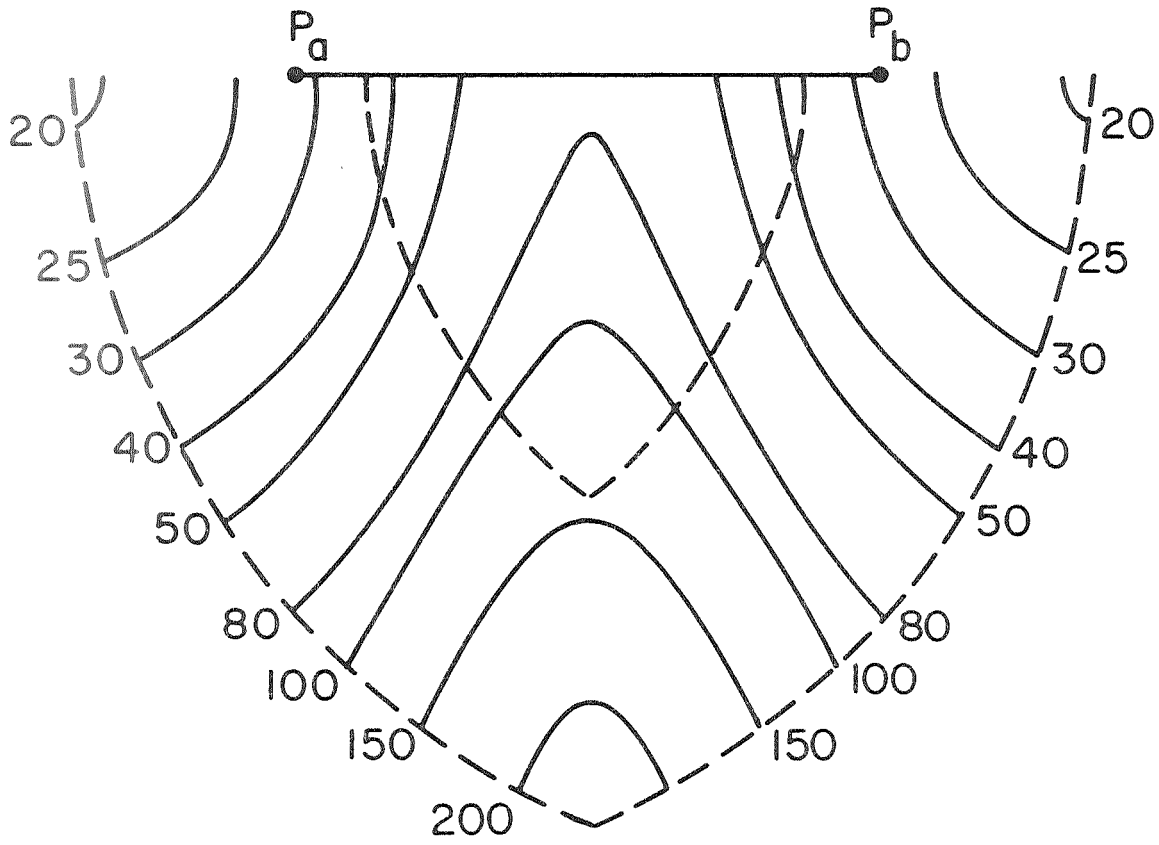

Figure 8. Evaluation of S^2 for L = 1500 km, H = 1000 km for the case of range and direction observations from P_a and P_b and with precise direction information for the vector $\overrightarrow{P_a P_b}$ (Case C). The limits of the common coverage area are shown for $z_{max} = 60°$ and $z_{max} = 75°$.

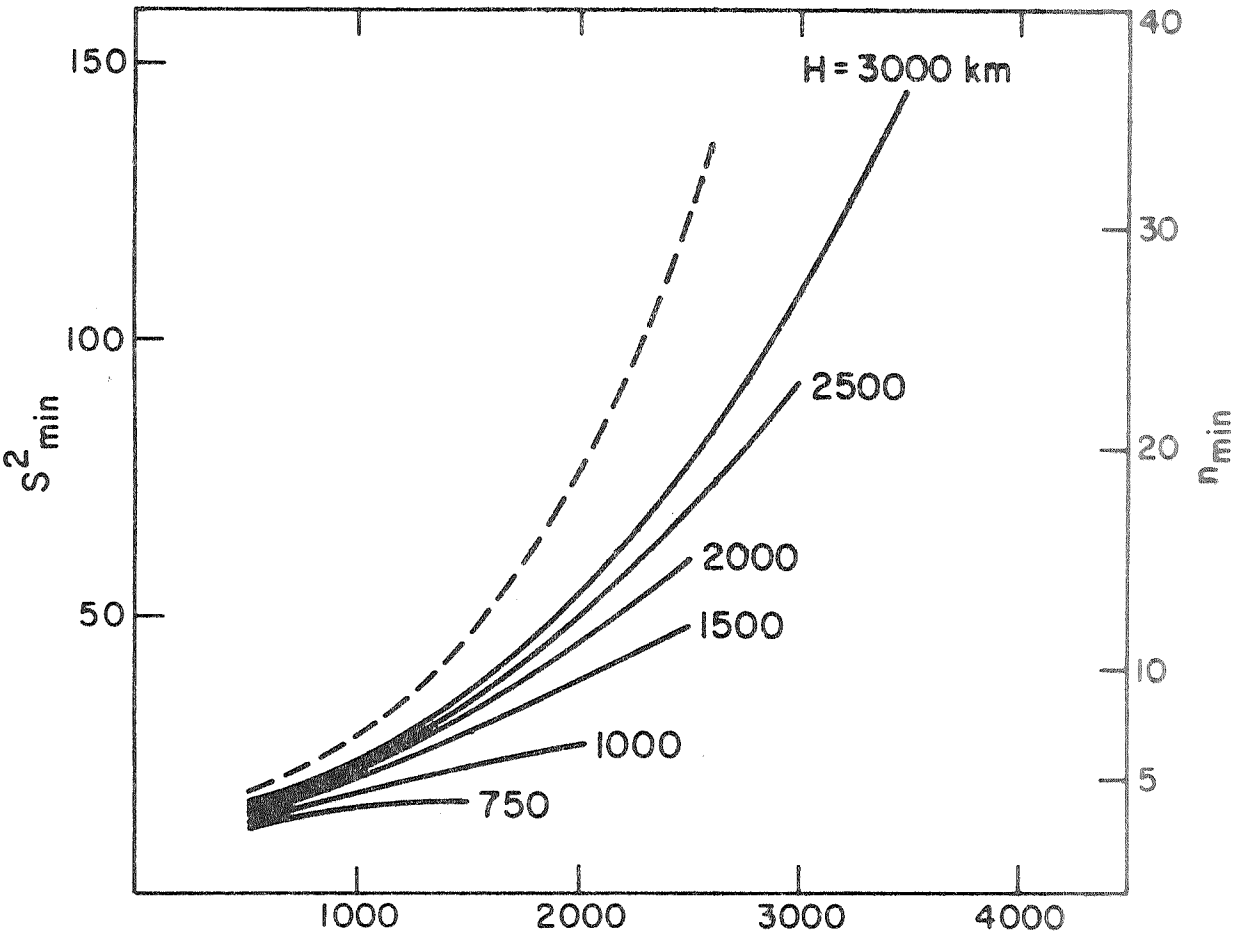

Figure 9. Evaluation of S^2_{min} and n for Case C as a function of satellite height and interstation distance. σ_r = 2.0 m, σ_s = 1.0, z_{max} = 75°.

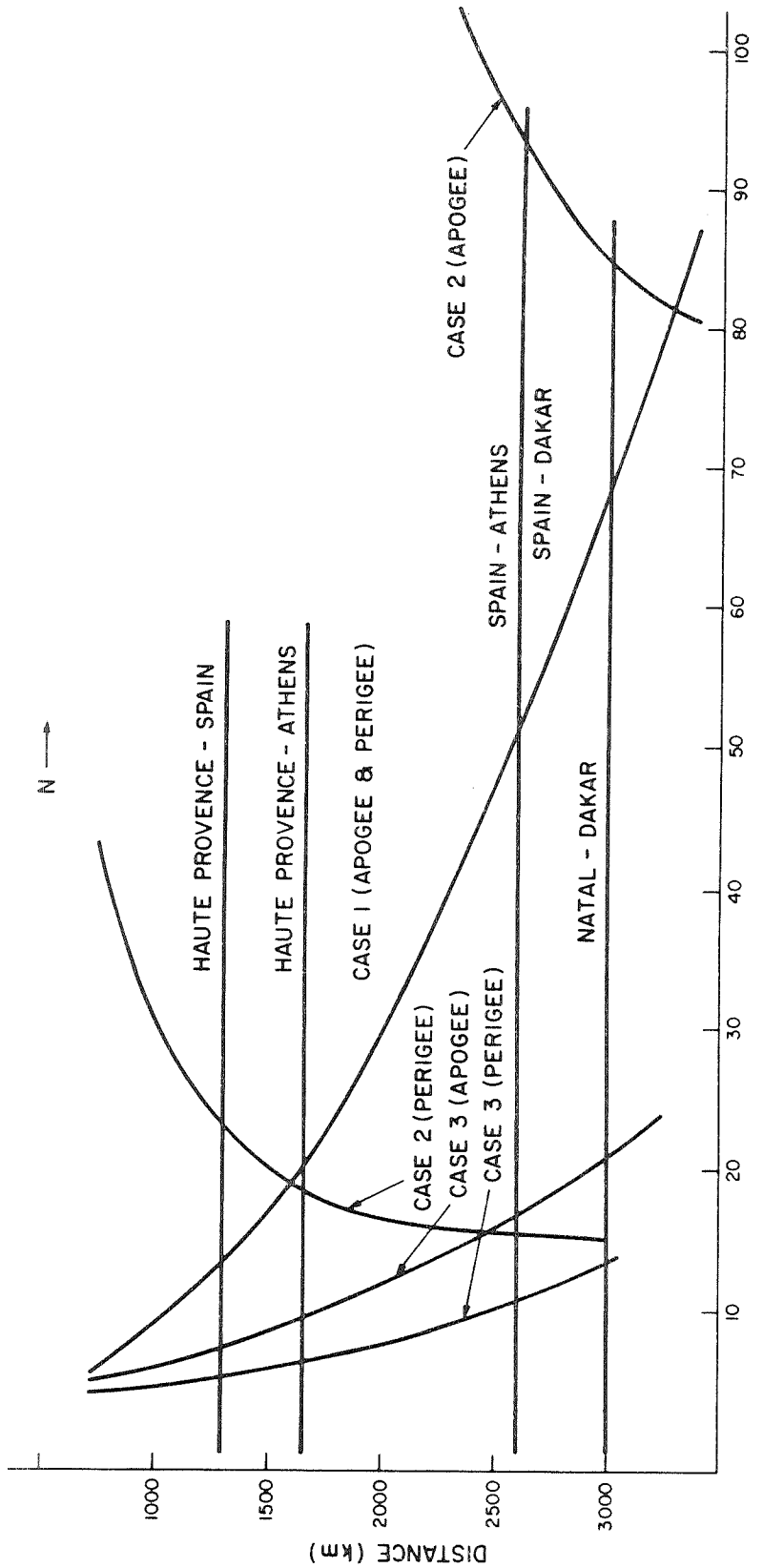

Figure 10a. Number of observations N required to determine the interstation distance with an accuracy of 2 m as a function of satellite height for Geos 1. σ_r = 2.0 m, σ_s = 1".0, z_{max} = 75°. Curves for the three cases discussed in text are given.

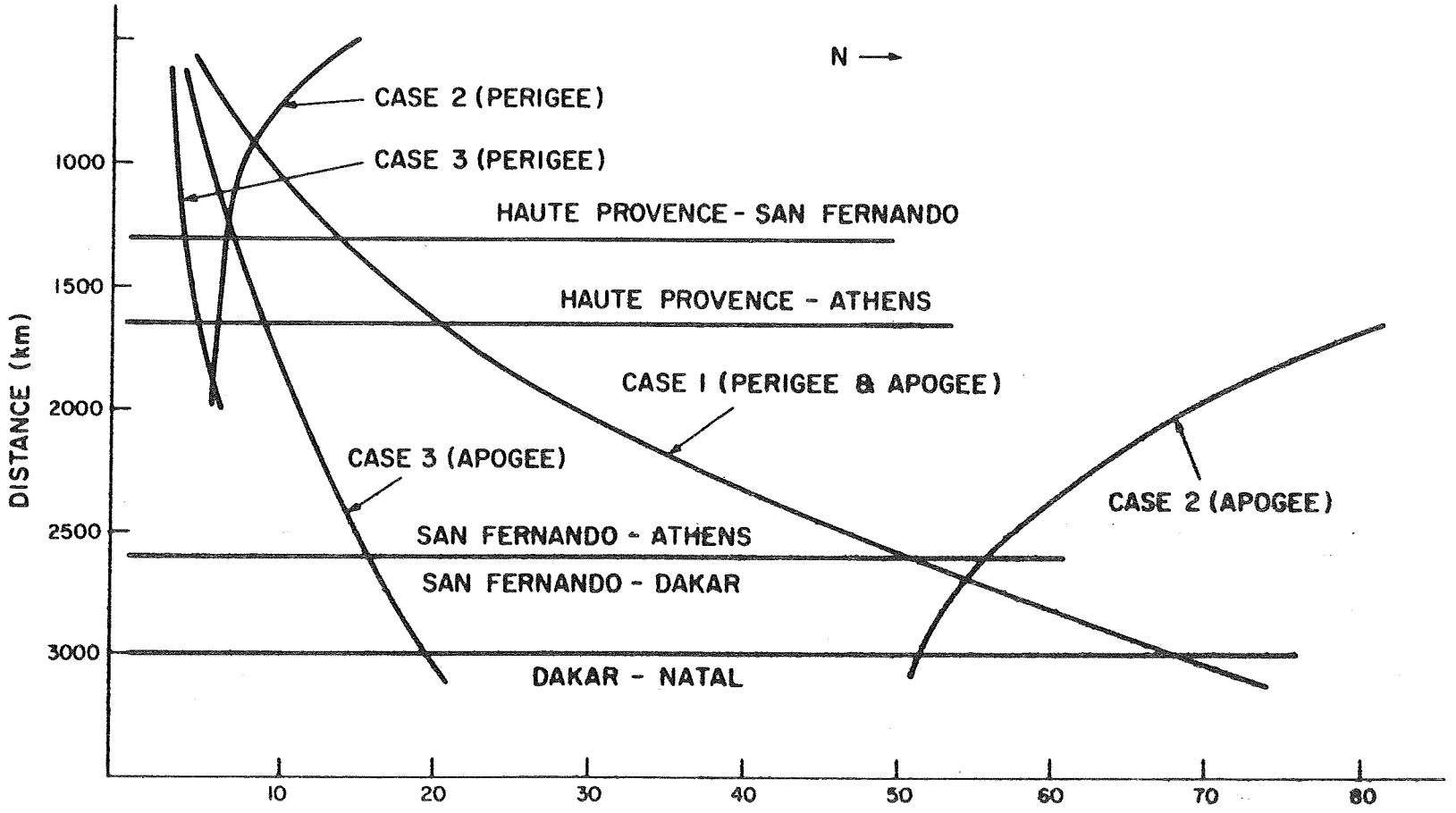

Figure 10b. Number of observations N required for satellite DID. σ_r = 2.0 m, σ_s = 1.''0, z_{max} = 75°.

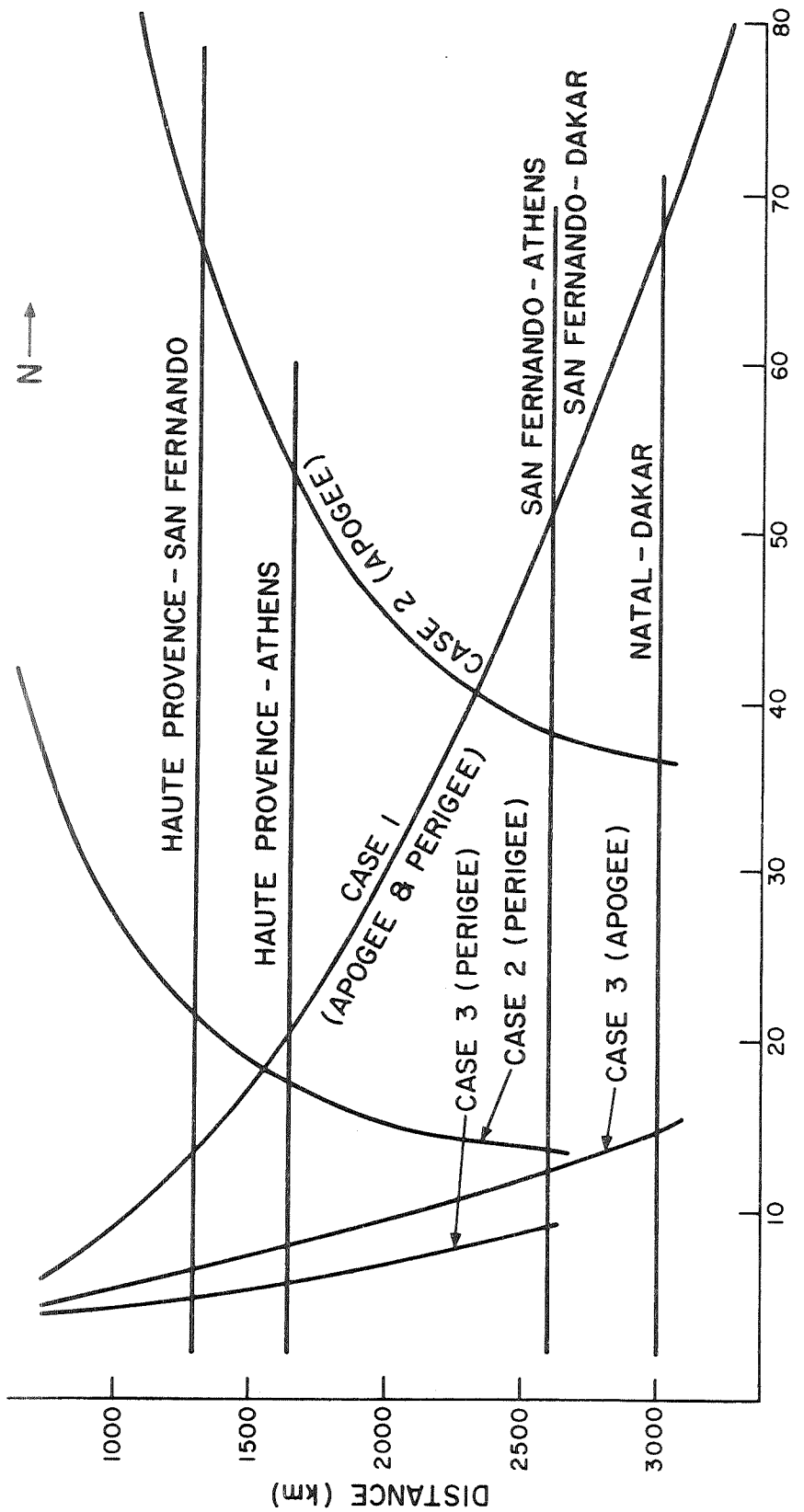

Figure 10c. Number of observations N required for satellite 6800801. $\sigma_r = 2.0$ m, $\sigma_s = 1.0$, $z_{max} = 75°$.

GODDARD MOBILE LASER (MOBLAS) SYSTEM DESCRIPTION

DON A. PREMO
GODDARD SPACE FLIGHT CENTER
GREENBELT, MARYLAND

Presented at the GEOS-2 Review Conference at
Goddard Space Flight Center 22-24 June 1970

GODDARD MOBILE LASER (MOBLAS) SYSTEM DESCRIPTION

by Don A. Premo

Introduction

The Goddard Mobile Laser Tracking System (MOBLAS) is a pulsed ruby laser radar designed primarily to track satellites equipped with optical corner reflectors. The system began operations in late 1968 at Goddard along side the Goddard Experimental Laser Tracker with which it was intercompared. It was during this initial series of tests that the MOBLAS first demonstrated the ability to track satellites in daylight. Since then, the tracker has been moved to Carnarvon, Australia; Mt. Hopkins, Arizona; and back to Goddard for collocation tests and participation in various world-wide concentrated tracking efforts. Presently, the MOBLAS is in New York state for three months in support of the Preliminary Polar Motion Experiment (PPME).

Figure 1 shows the MOBLAS installation at Carnarvon. The Tracking Pedestal is visible at the far right and the Control Van can be seen just to the left of a small building near the Tracking Pedestal. Not shown is a Power Van containing diesel generators for use when adequate power is not available.

The Tracking Pedestal can be seen in greater detail in Figure 2. The laser is located within the air conditioned enclosure just visible in the lower left corner of the picture. The laser is stationary and the light is directed to the telescope on the left through a coelostat, a portion of which is visible on the azimuth axis just above the platform level. The central telescope collects the reflected pulse and the telescope on the right is for operator use.

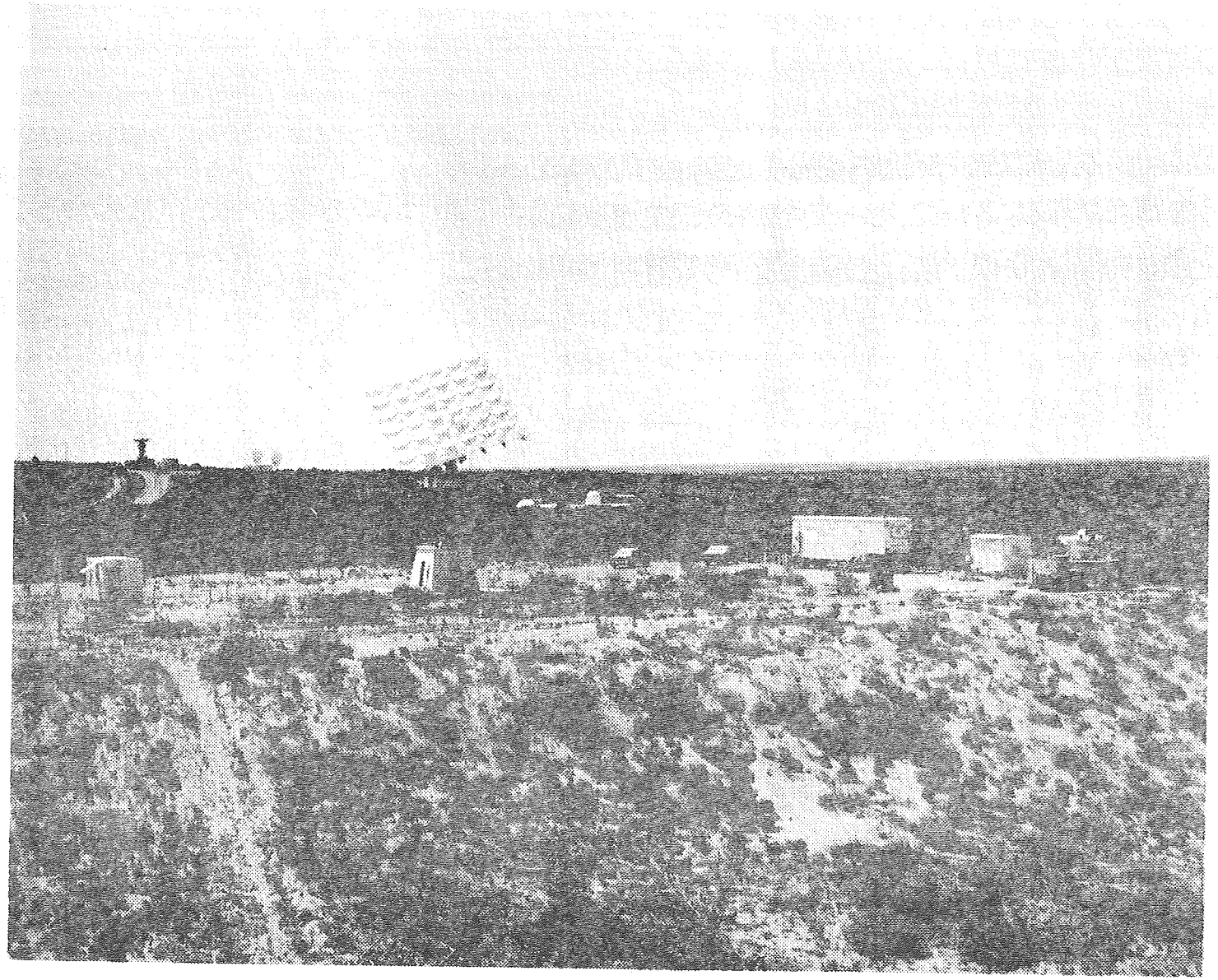

Figure 1

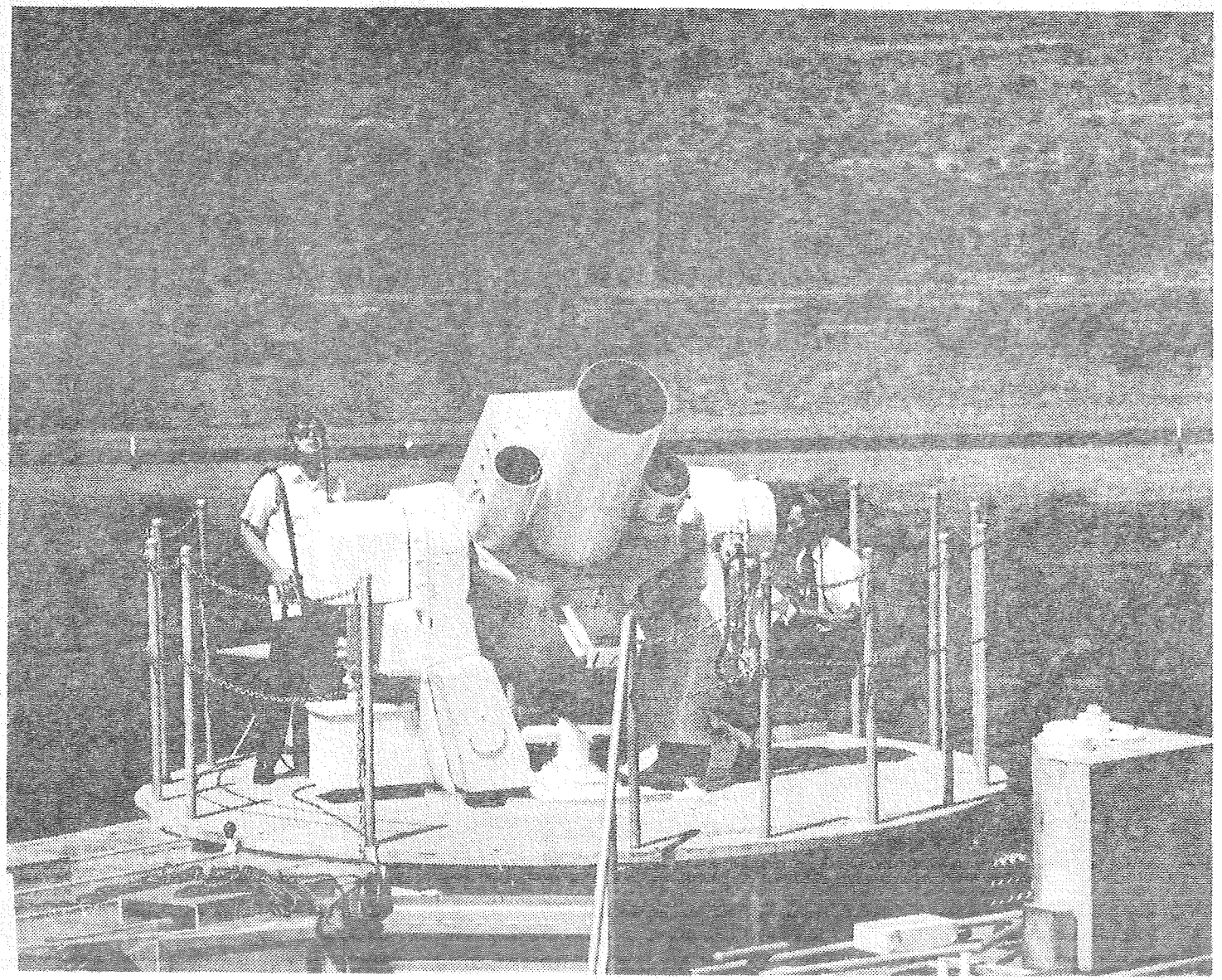

Figure 2

System Characteristics

The characteristics to be described do not include improvements soon to be incorporated for the PPME, but are valid for all prior measurements. The characteristics are shown in Figure 3.

The 0.5 joule output is obtained from a Goddard-built q-switched laser oscillator whose active element is a ruby rod 3/8 inch in diameter and nominally 6 inches long. The q-switch, a rotating prism with bleachable dye cell, is adjusted so that a single 18 nanosecond, 0.5 joule pulse is emitted each time the laser is triggered. These parameters are measured at least once each shift by use of a suitable thermopile and oscilloscope and monitored at all other times by an oscilloscope. The laser is water cooled and has been operated up to 10 minutes at a time at a one pulse per second rate with output characteristics remaining constant within 30%. The beam divergence figure is based on a nominal 5 milliradian total angle at the laser which is reduced to the 1/3 milliradian value by the 15 power transmitting optics. These optics are of sufficient diameter to prevent vignetting.

The receiver aperture shown is the nominal value. The effective value is more nearly 15 inches. The receiving telescope is a cassegrain type and has a focal length of 227 inches and a field of view of 5 milliradians. However, to reduce background noise, especially during daylight operations, the field of view is reduced by a field stop to match the transmitted beam width. Additional noise reduction is achieved by placing a 10Å filter centered at 6943Å in the optical path. This configuration has been found satisfactory for ranges out to at least 2000 km when operating in daylight with GEOS-B.

MOBLAS SYSTEM CHARACTERISTICS

LASER ENERGY/PULSE	0.5 JOULE
PULSE WIDTH	15-25 NANOSECONDS
REPETITION RATE	1 PPS
BEAM DIVERGENCE	1/3 MILLIRADIAN
RECEIVER APERTURE	16 INCHES
RECEIVER FIELD OF VIEW	1/3 MILLIRADIAN
SPECTRAL FILTER	10 Å AT 6943 Å
RANGE RESOLUTION	10 NANOSECONDS (1.5 METERS)
TIMING ACCURACY	+ 50 MICROSECONDS TO USNO

FIGURE 3

The range resolution is limited to 10 nanoseconds by the Range Time Interval Counter presently being used. The accuracy of this counter as quoted is ± 10 nanoseconds ± time base accuracy. To date, the time base accuracy has been held to within 2 parts in 10^{11} referred to the standard offset frequency broadcast by WWVL.

The timing accuracy stated is conservative, insofar as the MOBLAS time standard is concerned. By the use of VLF measurements and flying clocks, it is estimated that time was known to within ± 15 microseconds at Carnarvon and to ± 5 microseconds elsewhere. The reason for the ± 50 microseconds is that the laser firing time is not measured to a greater accuracy.

Block Diagram

To understand the MOBLAS from a functional viewpoint, one might start with Figure 4, the Block Diagram. Most of the Figure is self-explanatory, the system being relatively a simple one. However, one should note that the Range Time Counter is activated by the leading edge of the start and stop pulses. The effect is that large amplitude variations in the received energy can and do cause the range measurements to appear biased. However, the magnitude of the bias is limited roughly to the width of the laser pulse; i.e., to less than 3 meters. In future versions of the system, the detection circuitry will be modified to overcome this source of error.

Pointing and data handling are performed by the computer. Experience has shown that tracking operations, especially in daylight, are much improved if real time adjustments can be made to satellite predictions.

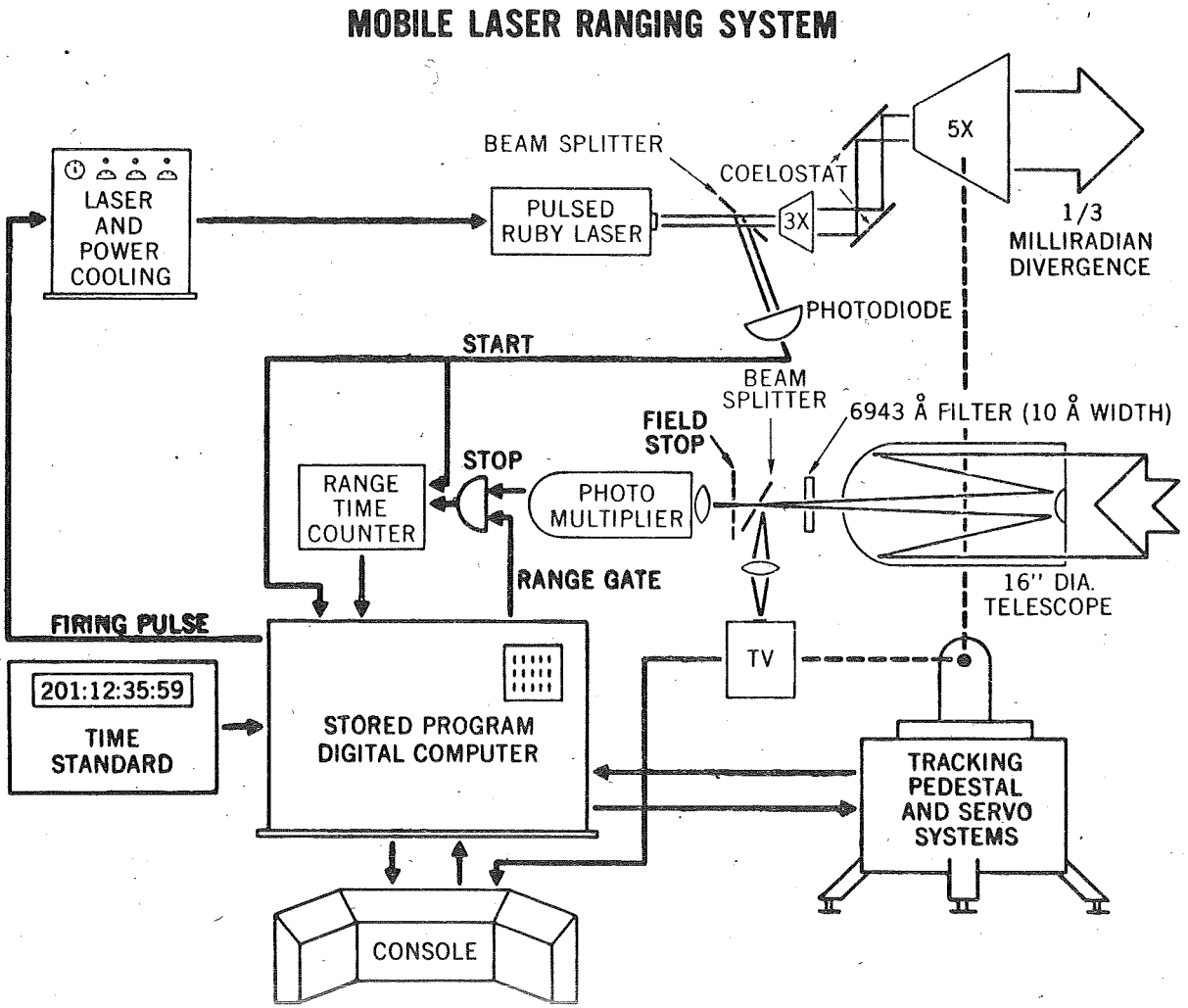
MOBILE LASER RANGING SYSTEM
LASER AND POWER COOLING
PULSED RUBY LASER
BEAM SPLITTER
COELOSTAT
3X
5X
1/3 MILLIRADIAN DIVERGENCE
PHOTODIODE
START
BEAM SPLITTER
6943 Å FILTER (10 Å WIDTH)
FIELD STOP
STOP
RANGE TIME COUNTER
PHOTO MULTIPLIER
RANGE GATE
16" DIA. TELESCOPE
FIRING PULSE
TV
201:12:35:59
TIME STANDARD
STORED PROGRAM DIGITAL COMPUTER
TRACKING PEDESTAL AND SERVO SYSTEMS
CONSOLE

Figure 4

The major source of prediction error encountered so far has been the uncertainty in the instantaneous value of mean anomaly. The correction to this problem in an operational sense has been to evaluate the predictions immediately after each pass to obtain eventually a history of adjustment values that can be extrapolated.

To improve pointing accuracy, a periodic astronomical calibration is performed on the instrument. The procedure is to track 40 or 50 stars spread throughout the visible hemisphere and to use the measurements to adjust the coefficients of a pointing error model to reduce in a least square sense the difference between observed and calculated positions. The rms of the residuals after the adjustment is typically from 6 to 8 arc seconds. The coefficients are used during a pass to adjust pointing angles to the correct values and afterwards to correct recorded angular data.

The computer has turned out to be a powerful tool, both for the determination of the adjustment values and for their use.

Data Handling

The MOBLAS is geared to the handling of a fair amount of tracking data per pass. As an example, Figure 5 shows a plot of the residuals for two passes of GEOS-B taken at Carnarvon. The upper one contains 457 observations, the lower, 402. One advantage is that it is easy to decide which points are acceptable. A second is that operational functions such as satellite acquisition and continuity of track are immeasurably easier to implement, thus, assuring an adequate accumulation of data. A third is that usually a good range of measurement geometry is obtained for collocation type experiments. To illustrate the accumulation of data,

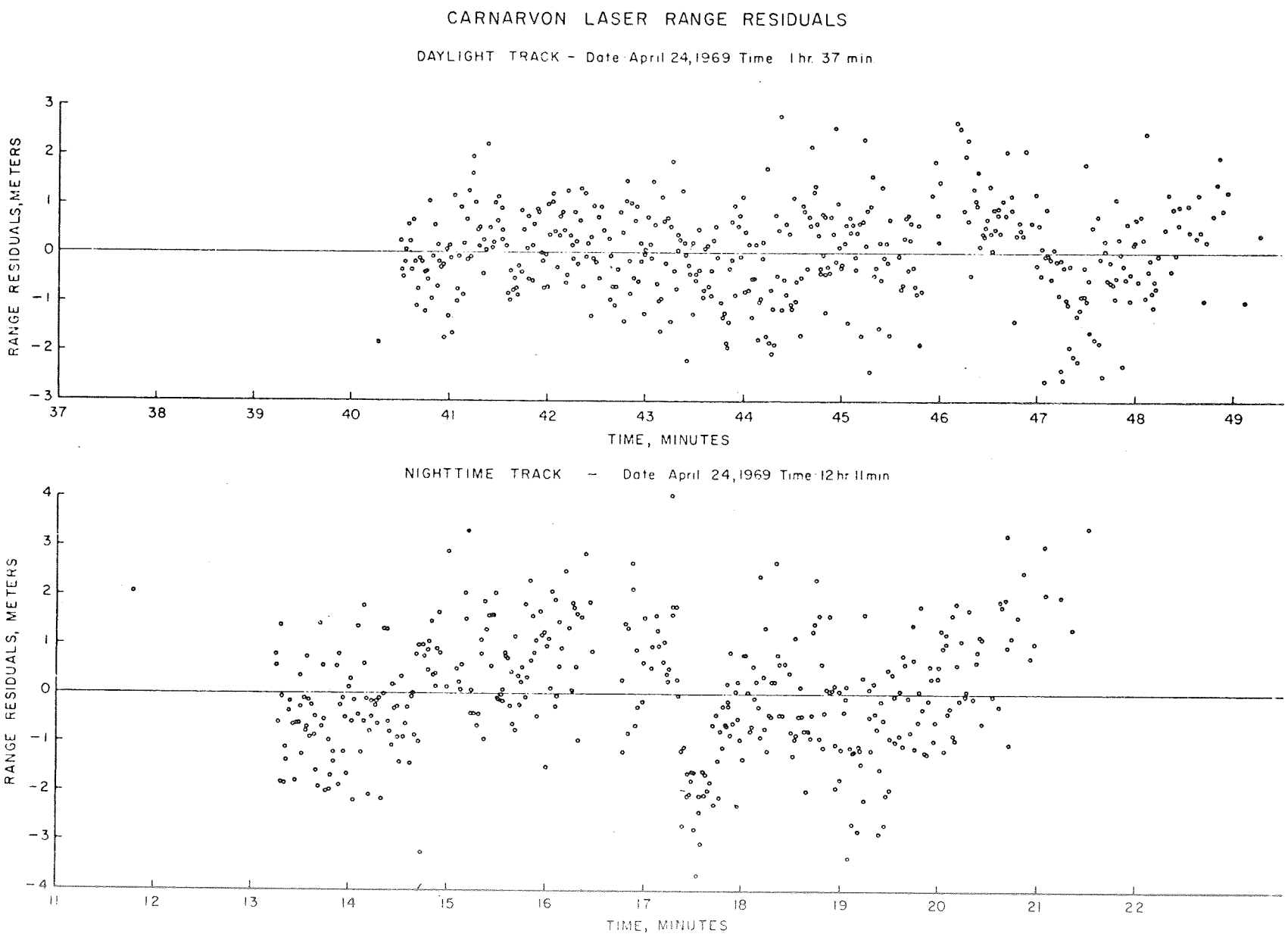
CARNARVON LASER RANGE RESIDUALS
DAYLIGHT TRACK - Date April 24, 1969 Time 1 hr. 37 min.
RANGE RESIDUALS, METERS
TIME, MINUTES
NIGHTTIME TRACK - Date April 24, 1969 Time 12 hr 11 min
RANGE RESIDUALS, METERS
TIME, MINUTES

Figure 5

SUMMARY OF CARNARVON LASER RANGE DATA

FIGURE 6

Date	Time	Day(D) or Night(N)	No.of Obs.	Rms (Meters)
Feb. 6	2320	D	55	1.06
6	956	D	349	1.29**
7	2340	D	292	1.20**
8	1019	D	122	1.34**
15	1040	D	115	1.76**
16	1100	D	146	1.22
16	2252	D	164	1.31*
17	1121	D	25	0.87
17	2311	D	239	1.58
18	2329	D	335	1.44**
19	1007	D	252	1.24**
19	2350	D	371	1.41**
20	1026	D	294	1.52**
21	0009	D	224	1.05**
21	1044	D	159	1.61**
23	2316	D	310	1.74**
25	1011	D	245	1.08
25	2354	D	358	1.38**
26	1030	D	386	1.35**
27	0014	D	409	1.09*
27	1050	D	398	1.41*
28	0034	D	272	1.29
28	1108	D	370	1.10
Mar. 2	2348	D	91	0.98
3	1017	D	207	1.23
5	1054	D	57	1.62
6	0037	D	227	1.16
6	1115	D	397	1.26**
9	1022	D	242	0.96
10	1041	D	303	1.23
11	0023	D	437	0.95**
11	1100	D	396	1.53
12	1119	D	308	1.25**
13	1138	N	336	1.21**
13	2332	D	361	1.04
14	1157	N	100	1.14
17	0029	D	498	1.29**
17	1104	D	427	1.59**
18	0044	D	427	1.12**
18	1123	D	363	1.55**
19	0107	D	103	1.09
19	1142	N	315	1.26**
19	2337	D	174	1.22
20	2355	D	281	1.22
22	0013	D	158	1.70**
24	1130	N	402	1.48**
25	0112	D	208	1.40
25	1151	N	141	1.23
31	1153	N	330	1.39**
Apr. 1	1211	N	276	1.88**
5	0104	D	205	1.37**
Apr. 5	1140	N	243	1.55**
6	0122	D	198	1.24**
6	1157	N	397	1.49
8	1236	N	76	1.51
9	1106	N	217	1.31
10	0049	D	470	1.07**
10	1124	N	468	1.34
11	0109	D	540	1.07*
11	1152	N	449	1.45**
12	138	D	501	1.00
14	17	D	189	1.09
14	206	D	14	2.29**
14	1240	N	309	1.80
15	35	D	302	1.22
16	1130	N	268	1.40
17	1132	N	88	1.80
21	0040	D	336	1.17**
21	1116	N	223	1.08
21	1305	N	144	0.97
22	1134	N	366	1.41
23	1154	N	415	1.08**
24	0137	D	457	0.95**
24	1211	N	402	1.27**
25	1231	N	502	1.39**
28	0110	D	132	1.16*
29	1200	N	223	1.06
30	0143	D	452	1.05*
30	1219	N	65	1.01
May 1	0202	D	175	1.01
1	1237	N	98	1.24
2	1256	N	549	1.31**
4	1145	N	414	1.07**
5	0130	D	515	1.24**
5	1205	N	400	1.02
6	0148	D	326	1.22**
6	1222	N	492	1.01**
10	0116	D	222	1.18**
11	1208	N	480	1.38**
12	0154	D	459	1.25**
12	1227	N	112	1.27
14	0234	D	27	1.15
15	1329	N	257	1.56*
16	0121	D	309	1.16*
OVERALL		D	17384	1.26
OVERALL		N	9557	1.34

* - Indicates Residuals are Significantly Non-Random - 5 Percent Level.

** - Indicates Residuals are Significantly Non-Random - 1 Percent Level.

Figure 6

Figure 6 shows a summary of the data taken at Carnarvon.

Availability of the data is certainly another factor that must be considered. The MOBLAS can process its own data and transmit all or part by teletype to the experimenter within hours after it is taken. This was started at Carnarvon and has been continued during every experiment since then. Although in earlier tests not fully corrected for refraction effects, the data now is fully corrected for all known parameters and is as accurate as that submitted to the Data Center; i.e., average rms of fit to short arc of 1.2 meters.

Future Plans

In the near future, modifications will be incorporated to increase range time measurement resolution by an order of magnitude and to eliminate sources of bias and error such as that inherent in the present range measurement technique and in certain time measurements. The methods are known, only the implementation remains.

GEODETIC LOCATION OF A SHIP AT SEA WITH C-BAND RADAR RANGE DATA

by

MILTON HILLHOUSE

AIR FORCE EASTERN TEST RANGE

MAY 1970

Presented at the GEOS-II Review Conference at Goddard Space Center

22-24 June 1970

INTRODUCTION

This study was directed towards the problem of obtaining a geodetic position of a transponder array in the broad ocean. The transponder array is used for scoring the accuracy of impact of missiles, hence the location of the array must be known quite accurately. The approach used in the investigation was to have a ship locate itself by tracking a satellite whose orbit is accurately determined by land based sensors. Then the ship may interrogate the transponders in the target array and thus locate the geodetic position of the array. The problem as a whole becomes somewhat complex, involving the determination of the relative positions of the transponders and the orientation as well as the latitude and longitude of the array. This presentation will be confined to a discussion of the methods and accuracy achieved in ship location only.

All data were obtained from beacon track of the GEOS-B satellite. The orbit of GEOS-B was determined in every case from tracking data obtained by AFETR pulse radars. Clearly a single observation in range, azimuth and elevation from the ship would serve to locate the ship. Such a simple non-redundant piece of data would, however, give very poor accuracy. In practice it is desirable to have ship radar track from satellite rise to satellite set. During this interval, of course, the ship may travel two miles in not necessarily uniform motion, and this motion is a very important consideration in the solution. Three methods of determining ship motion were investigated: (1) Direct

solution for average ship velocity vector in least squares solution, (2) Use of ship navigation data (SINS) for relative ship position, and (3) Use of ocean bottom transponder interrogation data for relative ship position.

The results of the ship location tests conducted at the AFETR were evaluated to an accuracy of about five feet by a network of land based theodolites which tracked the moving ship as the ship tracked the satellite. The theodolite measurements were also used to simulate an "ideal" transponder array to provide relative ship positions. The complete test design included simulation tests as well as tests with real data. Simulations were used to study the following variables:

a. Recovery of radar range bias

b. Maximum elevation of satellite

c. Use of radar range-only versus azimuth and elevation with range data.

d. Various portions of satellite pass.

This abbreviated discussion will be limited to a review of some of the representative results.

DATA COLLECTION

The data for these tests were collected at separate periods. The first test was conducted July 22-23, 1969. Due to priority problems, no additional passes were scheduled until September 1969. The second test was scheduled and seven passes were collected in December 1969. The latter test has no absolute reference. Table 1 shows the revolution number and the dates of radar track. It was intended to collect more land based radar data for the reference orbit but priority prevented using more than two land based radars in some cases.

TABLE 1

GEOS-B SATELLITE TRACK BY TWIN FALLS

Date	Revolution Number*	Number Passes
July 22, 1969	7156, 7157	2
July 23, 1969	7169, 7170	2
Sept 2-5, 1969	7708, 7709, 7715, 7721, 7722 7728, 7734, and 7735	8
Dec 7-15, 1969	8939, 8940, 8979, 8953, 8954, 9004 and 9030	7

*NOTE: Land based radars also were scheduled to track GEOS-B. In most cases a minimum of two radars provided tracking data for the reference trajectory.

DATA REDUCTION

Two separate data reduction routines were evaluated for this study. The first method treats the data exactly like a fixed land based radar site. Ship's radar data are transformed to a fixed site. Each data point requires a relative position for the ship. The ship's radar data were processed for input to the NITE computer program as follows:

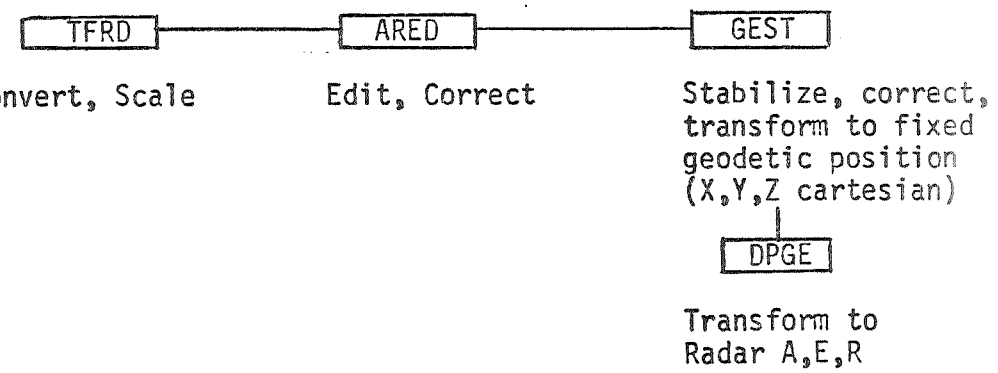

The second data reduction method utilized the radar range data after processing through GEST. The range only ship data are input along with earth fixed E, F, G satellite data into the HESP computer program. Input information required consists of (1) satellite trajectory points in an earth centered, earth fixed coordinate system (2) ship radar range data at times coincident with the satellite trajectory coordinates, and (3) either relative ship position points or a priori estimates of ship position and velocity at epoch.

As indicated above, if the ship does not have uniform position changes or velocity, relative ship position coordinates may be input directly and the equations of motion for the ship are by-passed and the adjustment process is entirely unaffected by erratic ship motion.

TEST RESULTS

a. NITE Computer Program. The land based radar range data and the ship's radar range data are used to simultaneously estimate the orbit and to locate the position of the ship. The NITE computer program is capable of adjusting for a range bias. Results for this limited series of tests indicated no significant improvement when radar range bias is also adjusted. The results also indicate that a one revolution or two revolution fit are about equal. Since the ship moves during the test, it was not considered feasible to constrain the survey adjustment in the same manner as a fixed radar site.

Results of the control tests conducted near the Florida mainland appear in Table 2. The second test was far out in the ocean and no absolute accurate reference was available. The dispersion was computed about the arithmetic mean. All data were referenced to a fixed transponder. The results of the second test are summarized in Table 3. The forward motion of the ship was determined by ASPS interrogation for the second test (Dec 69). Previous survey results had determined the relative position or base line length between three transponders. The ASPS ranging data were recorded at one minute intervals and relative ship position data were smoothed for this computer run.

TABLE 2

TWIN FALLS GEODETIC SURVEY ERROR FROM NITE COMPUTER

Rev No.	Single Rev Orbit Fit		Two Rev Orbit Fit	
	Delta Lat (feet)	Delta Long (feet)	Delta Lat (feet)	Delta Long (feet)
7156	-28.0	101.0	-39.7	53.8
7157	-40.0	109.0	-63.0	-162.0
7169	-35.0	16.5	-2.4	69.0
7170	*	*	156.3	-125.4
7708	1.2	-19.6	-26.8	-64.2
7709	** 566	**1322.6	**533.1	**1302.5
7715	3.1	-107.0	NA	NA
7721	-1.7	-32.4	64.0	54.9
7722	-2.4	100.0	9.6	128.0
7728	4.3	-150.9	NA	NA
7734	96.8	125.3	3.4	56.8
7735	-79.0	-190.1	-5.9	32.2
Mean**	-13.5	-4.8	-24.1	40.8
SD **	51	115	61	88

* Rev 7170 was not processed as a single pass since only one land-based radar tracked during this pass.

** Rev 7709 results were excluded - high PCA elevation may have caused a poor reference orbit.

TABLE 3

NITE COMPUTER SOLUTION FOR C12 ARRAY
RADAR RANGE ONLY DATA FOR GEOS-B

Rev No	PCA Elev	Delt Lat (ft)	Delta Long (ft)	Radar Random Noise (ft)
8939	50	-125	- 7	9
8940	24	+ 37	+31	6
8979	50	+280	+386	20
8953	69	-198	-316	12
8954	17	- 81	-112	6
9004	36	+ 33	-94	6
9030	59	+ 45	+117	10
Std Dev		155	218	
Mean Off Set*		180	113	

Circular Std Dev = (155 + 218)/2 = 186 feet

Standard Error = $186/\sqrt{7}$ = 72 feet

*NOTE: Mean off set from a reference transponder with the geodetic location established by a different system.

TABLE 4

ESTIMATE OF SHIP POSITION AND VELOCITY
WITH RADAR RANGE ONLY DATA

GEOS-B Revolution No.	7708	7715	7721	7722	7728	7734	7735
MIPIR Radars in Fit*	7, 0, 19	7, 19	7, 19, BER	7, 19	7, 19	7, 19	7, 19
MIPIR Data Density	10 sec	10 sec	10 sec	10 sec	10 sec	10 sec	10 sec
Ship Heading (deg)	179	259	229	69	299	228	50
Rise, Max, Set Elev for Ship (deg)	9, 17, 1	7, 27, 15	5, 23, 4	10, 72, 2	22, 36, 7	2, 30, 2	8, 55, 5
Ship Data Density	10 sec	10 sec	10 sec	10 sec	10 sec	10 sec	10 sec
Ship Path Parameters Forced	None	None	None	None	None	None	None
Ship Path Parameters Adjusted	Pos&Vel	Pos&Vel	Pos&Vel	Pos&Vel	Pos&Vel	Pos&Vel	Pos&Vel
Error in Ship Speed (knots)	+0.37	+1.31	+0.58	+1.14	-0.04	+3.04	+1.66
Error in Ship Heading (deg)	+2.0	+6.0	+0.0	+0.6	+0.0	+5.0	-10.0
Error in Adjusted Ship Position	153 ft	696 ft	146 ft	147 ft	15	1553 ft	523 ft
Direction of Ship Error (deg)	295	179	347	346	180	322	184

*GEOS-B orbit was determined from land-based MIPIR radar data using TRACE-66 computer program.
**Rev 7734 is not included in evaluation due to poor ship velocity estimate.

TABLE 5
ESTIMATE OF SHIP POSITION
WITH RADAR RANGE ONLY DATA

GEOS-B Revolution Nr	7156	7157	7169	7170	7708	7715	7721	7722	7728	7734	7735
MIPIR Radars in Fit*	91,7,19	91,7,19	91,7	91,7	7,0,19	7,19	7,19,BER	7,19	7,19	7,19	7,19
MIPIR Data Density	10 sec	10 sec	10 sec	10 sec	10 sec	10sec	10 sec	10 sec	10 sec	10 sec	10 sec
Ship Heading (deg)	230	89	239	86	179	259	229	69	299	228	50
Rise, Max, Set Elev for Ship (deg)	18,18,14	62,69,36	19,24,14	24,50,13	9,17,1	7,27,15	5,23,4	10,72,2	22,36,7	2,30,2	8,55,5
Ship Data Density	1 sec	1 sec	1 sec	1 sec	10 sec	10 sec	10 sec	10 sec	10 sec	10 sec	10 sec
Ship Path Parameter Forced*	Rel Position	Rel Pos	Rel Pos	Rel Pos	Rel Pos	Rel Pos	Rel Pos	Rel Pos	Rel Pos	Rel Pos	Rel Pos
Ship Path Parameter Adjusted	None	None	None	None	None	None	None	None	None	None	None
Error in Adjusted Ship Position	97 ft	92 ft	76 ft	101 ft	35 ft	59 ft	71 ft	129 ft	15 ft	30 ft	34 ft
Direction of Ship Error (deg)	264	29	256	260	201	330	72	243	120	192	71

*GEOS-B orbit was determined from land-based MIPIR radar data using TRACE-66 computer program.
Relative position of ship determined from theodolite.

b. HESP Computer Program. The HESP computer program requires a reference orbit. Input data are ships radar range and the adjusted parameters may be varied. We adjusted position and velocity in one study (see Table 4). It may be noted that the estimated velocity of the ship was in error but the ship's position errors are small. The ship location accuracy was much improved when only position was estimated (see Table 5). The ship's relative position was input as a known parameter. Relative position was based on theodolite data. If the ship has uniform velocity during the tracking period, it is not necessary to know the point-by-point position during the tracking period. Only a good estimate of the velocity is required. Slight deviations from uniform velocity will have only a minor effect.

Data were to be processed in the HESP program for the C-12 array using SINS velocity. A delay in data reduction has caused the results to be delayed. Preliminary data review indicated that ship's radar acquired track of GEOS-B satellite late approximately fifty per cent of the time. A further review of data acquisition is needed to resolve the problem. Previous studies have indicated that horizon-to-horizon track by the radar is highly desirable. The real ship's radar data for Air Force Eastern Test Range were less than the anticipated track time. This possibly could degrade the results below the optimum solution.

SIMULATED DATA

Figure 1-A depicts the location of three AFETR land based radar trackers and four ships. The ship location was generally chosen to study the effect of geometry on geodetic survey error. Also depicted is the ground trace to describe the three different satellites (Pegasus, Transit and GEOS-B).

Table 1-A indicates the orbital elements for the simulated satellites. The error free data used for this simulation were generated for each ship location shown. Bias and random errors were added to the data as shown in Table II-A for each tracker and to each ship. The only tracker error that was adjusted was Range Rate (R dot).

Satellite trajectory errors resulted from geopotential errors and tracker errors and appear in Table III-A. The errors are shown in the conventional H, C, L coordinate system.

Note that the errors in the satellite position are about the same for Range only data as for Range rate (R dot). However, the orbital errors are much larger for Pegasus than for Transit or GEOS-B. It will be seen later that the orbital errors in Pegasus are the dominant source of error in the survey adjustment.

Table IV-A shows the latitude and longitude for each ship for the simulated data obtained for each of the three satellites. The maximum elevation (PCA) is shown for each ship also. When the satellite pass was almost overhead with high maximum elevation (PCA) poor survey results were obtained for each case.

Table V-A shows the speed and course (heading) for each ship. When the survey adjustment was made for position only, an error of 0.5 knots and (-0.5) degree heading was always present in the a priori offset for the ship.

Table VIa-A - A geodetic survey adjustment was attempted for each ship simulation as shown in Table VIa-A. In one case no solution could be obtained. Results are very poor for ship No. 2 which has a high PCA and poor geometry. All of the other results in Table VIa-A are essentially the same and ship heading has little influence. The errors can be largely explained by large orbital errors in the trajectory of Pegasus.

Table VIb-A shows the results for Transit. Ship No. 1 gave poor results because of high max elevation (PCA). It appears that range rate (R-dot) gives less accurate results than does range-only data. Also, the velocity of the ship can be adjusted when range data is used. If the ship velocity error is large (0.5 knots) it appears to improve the survey adjustment when ship velocity is also adjusted. The residual error is shown for the ship but the residual does not appear to represent the magnitude of the survey error. Also, the R-dot data are sensitive to the heading of the ship during a pass. A large effort should be made to ascertain a better description of survey error associated with range rate (R-dot) and ship heading. The survey errors obtained here for R-dot indicate a survey bias could very easily occur. The errors are not considered random for the R-dot data.

Table VIc-A shows the simulated survey adjustment for GEOS-B. Results for ship No. 1 are poor because of high elevation (PCA). The R-dot data are inferior to the range only data. Better results are also obtained for range-only data when ship's speed is adjusted.

Table VIIa-A shows the results for range only data to compare results with and without orbital errors. (Refer back to Table VIa-A). As already indicated, Pegasus results are not very good here and require further study. Results for ships 1, 3 and 4 are good for the case of no orbital errors. However, it may prove difficult to obtain a perfect orbit in actual practice.

Table VIIb-A shows Range-only solutions for Transit. Very little difference is indicated between passes with and without orbital errors. It should be recalled that the orbital errors were small. In every case except high elevation passes (ship No. 1), the results are very good. Survey errors are typically 200 feet when ship velocity errors of 0.5 knots are present. There is also some indication that heading does influence the results but further study is needed to ascertain how much.

Table VIIc-A indicates the simulated results for GEOS-B with and without orbital errors. The orbital errors in this case do not strongly influence the survey error when ship's velocity is not adjusted. It appears feasible to adjust for ship's velocity but in actual practice it should be recalled that horizon-to-horizon tracking data are required. More effort is required to determine the best procedure to use. However, the author would prefer to rely on independent means to determine the ship's motion. The ship's ASPS ranging data may prove to be the best source for ship's motion. This has not been completely resolved at AFETR.

FIGURE 1 - A

SATELLITE GROUND TRACES, LAND BASED TRACKING SITES, AND SHIP POSITIONS

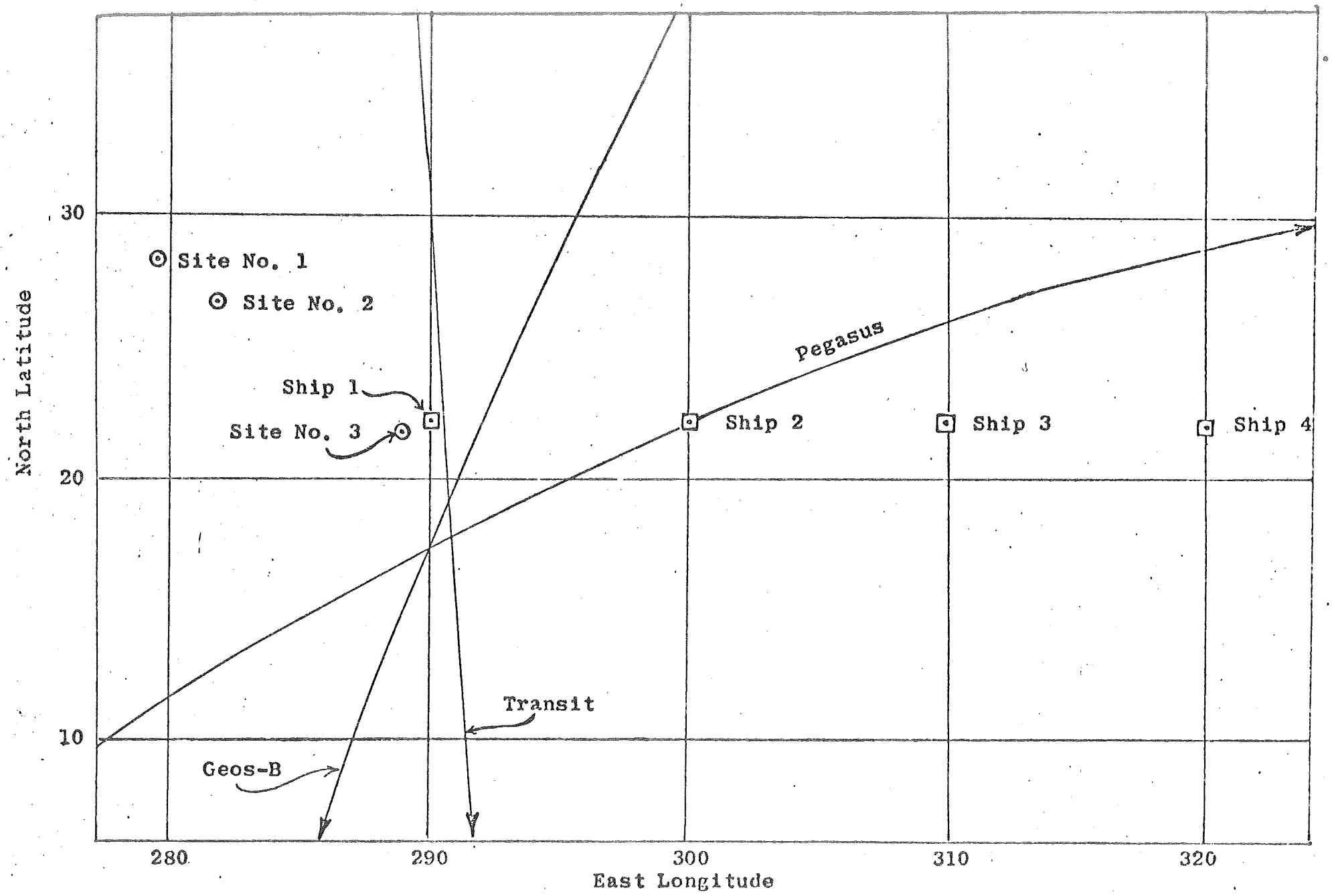

TABLE I - A

ORBITAL ELEMENTS FOR SIMULATED SATELLITES

	PEGASUS	TRANSIT	GEOS-B
Perigee (n.m.)	256	602	602
Apogee (n.m.)	352	605	861
Inclination (deg.)	31.7	90.0	105.8

TABLE II - A

TRACKER ERRORS

	SITE #1	SITE #2	SITE #3	SHIPS
R - Bias (ft.)	30	30	30	30
$\dot{R}$ - Bias (ft./sec.)*	100	100	100	100
R - Random (ft.)	25	25	25	10
$\dot{R}$ - Random (ft./sec.)	.15	.15	.15	.10

* This represents the error remaining prior to adjustment. The error remaining in $\dot{R}$ after adjustment was of the order of .1 ft/sec. No adjustment was made for R-bias.

TABLE III - A

SATELLITE TRAJECTORY ERRORS IN VICINITY OF SHIPS

	SATELLITE	H (ft)	C (ft)	L (ft)	Total (ft)
Range Data	Pegasus	78	102	822	832
	Transit	35	9	6	37
	GEOS-B	27	66	88	113
Range Rate Data	Pegasus	117	85	720	734
	Transit	35	41	45	70
	GEOS-B	12	48	127	136

TABLE IV - A

MAXIMUM ELEVATION OF EACH SATELLITE FROM EACH SHIP POSITION

SATELLITE	SHIP NUMBER	SHIP POSITION N. LAT. (DEG.)	SHIP POSITION E. LONG. (DEG.)	MAX. ELEVATION (DEGREES)
Pegasus	1	22	290	43
	2	22	300	89
	3	22	310	49
	4	22	320	32
Transit	1	22	290	86
	2	22	300	42
	3	22	310	18
	4	22	320	5
GEOS-B	1	22	290	81
	2	22	300	56
	3	22	310	30
	4	22	320	15

TABLE V - A

TRUE SHIP SPEED AND HEADING*

Satellite	Ship	Speed (knots)	Heading from** North (deg.)	Heading from** Satellite Ground Trace (deg.)
Pegasus	No. 1	5.5	+90	+28
			+45	-17
			0	-62
	No. 2	5.5	+90	+24
			+45	-21
			0	-66
	No. 3	5.5	+90	+19
			+45	-26
			0	-71
	No. 4	5.5	+90	+13
			+45	-32
			0	-77
Transit	No. 1	5.5	+90	-86
			+45	-131
			0	-176
	No. 2	5.5	+90	-86
			+45	-131
			0	-176
	No. 3	5.5	+90	-86
			+45	-131
			0	-176
	No. 4	5.5	+90	-86
			+45	-131
			0	-176
GEOS-B	No. 1	5.5	+90	-116
			+45	-161
			0	+154
	No. 2	5.5	+90	-116
			+45	-161
			0	+154
	No. 3	5.5	+90	-116
			+45	-161
			0	+154
	No. 4	5.5	+90	-116
			+45	-161
			0	+154

* A priori off-sets from these values were (-.5) knots in speed and (-.5) degree in heading for all simulation runs.

** Heading is the angle from the reference direction to the direction of the ship velocity vector measured positively clockwise as seen by an observer looking downward on the ocean surface.

TABLE VIa - A

SHIP POSITION ERROR AT PCA IN SITUATIONS INVOLVING ORBITAL ERRORS

			Ship	No. 1			No. 2			No. 3			No. 4		
			Heading from North	90°	45°	0°	90°	45°	0°	90°	45°	0°	90°	45°	0°
PEGASUS	Using Range Data	Adj. for Position Only	Error at PCA (ft.)	880	860	780	20180	23560	12660	750	790	810	740	810	850
			RMS Residuals (ft.)	80	100	50	49	48	14	130	130	60	120	120	40
		Adjustment for Position and Velocity	Error at PCA (ft.)				6050	4400	4150	800	820	770	730	700	670
			RMS Residuals (ft.)				11	10	10	9	8	9	10	10	11
			Error in Recovered Speed (knots)				-.77	+.16	-.32	+.39	-.22	-.06	-.08	+.20	+.56
			Error in Recovered Heading (deg.)				-21.	-5.7	+1.1	+9.4	+5.8	+.40	-1.8	-3.2	-1.1
	Using Range Rate Data	Adjustment for Position and R-Dot Bias	Error at PCA (ft.)	730	690	660	16170	20020	11230	760	800	760	680	760	780
			RMS Residuals (ft./sec.)	.3	.3	.2	.2	.1	.1	.3	.3	.2	.2	.2	.1
			Error in Recovered R-Dot Bias (ft./sec.)	-.12	-.18	-.03	+.14	+.16	+.12	+.01	+.06	+.04	-.01	+.02	+.10

TABLE VIb - A

SHIP POSITION ERROR AT PCA IN SITUATIONS INVOLVING ORBITAL ERRORS

			Ship	No. 1			No. 2			No. 3			No. 4		
			Heading from North	90°	45°	0°	90°	45°	0°	90°	45°	0°	90°	45°	0°
TRANSIT	Using Range Data	Adj. for Position Only	Error at PCA (ft.)	670	2060	3500	120	170	260	230	190	130	350	230	40
			RMS Residuals (ft.)	31	110	190	20	120	200	10	94	135	12	37	48
		Adjustment for Position and Velocity	Error at PCA (ft.)				79	30	37	78	130	70	28	27	190
			RMS Residuals (ft.)				9	9	10	9	10	10	12	9	8
			Error in Recovered Speed (knots)				-.35	-.07	+.01	-.18	-.17	+.01	-.02	-.01	-.02
			Error in Recovered Heading (deg.)				.0	-.7	+1.2	-.2	-2.3	+1.4	-.2	-.5	+2.5
	Using Range Rate Data	Adjustment for Position and R-Dot Bias	Error at PCA (ft.)	1600	5100	8360	170	480	790	280	520	750	490	620	840
			RMS Residuals (ft./sec.)	.1	.3	.5	.1	.2	.3	.1	.1	.2	.1	.1	.1
			Error in Recovered R-Dot Bias (ft./sec.)	+.07	0.04	-.09	-.02	+.03	+.07	-.05	-.02	+.09	-.28	+.07	+.28

TABLE VIc- A

SHIP POSITION ERROR AT PCA IN SITUATIONS INVOLVING ORBIT ERRORS

			SHIP	No. 1			No. 2			No. 3			No. 4		
			Heading from North	90°	45°	0°	90°	45°	0°	90°	45°	0°	90°	45°	0°
GEOS-B	Using Range Data	Adj. for Position Only	Error at PCA (ft.)	800	1750	1890	250	490	520	220	260	270	290	180	200
			RMS Residuals (ft.)	10	260	280	90	220	230	80	170	170	60	110	100
		Adjustment for Position and Velocity	Error at PCA (ft.)	280	280	270	140	100	310	80	250	140	370	80	70
			RMS Residuals (ft.)	10	9	10	9	10	10	8	9	10	10	11	9
			Error in Recovered Speed (knots)	+.08	-.07	+.07	-.70	-.04	-.31	-.05	+.14	-.07	+4.3	-.02	+.01
			Error in Recovered Heading (deg.)	-.1	-2.8	-.7	+2.6	-.9	+12.3	-.2	-.7	+1.3	+2.6	.0	-.3
	Using Range Rate Data	Adjustment for Position and R-Dot Bias	Error at PCA (ft.)	870	3210	3600	290	1060	1120	290	790	810	410	820	820
			RMS Residuals (ft./sec.)	.1	.2	.3	.1	.2	.3	.1	.2	.2	.1	.1	.1
			Error in Recovered R-Dot Bias (ft./sec.)	+.04	+.04	+.01	-.04	-.02	-.05	-.07	-.05	-.02	-.09	-.11	-.02

TABLE VIIa-A

SHIP POSITION ERROR AT PCA IN SITUATIONS WITH AND WITHOUT ORBITAL ERRORS

(Only Radar Range Data Used in Solutions)

			Ship	No. 1			No. 2			No. 3			No. 4		
			Heading from North	90°	45°	0°	90°	45°	0°	90°	45°	0°	90°	45°	0°
PEGASUS	With Orbital Errors	Adj. for Position Only	Error at PCA (ft.)	880	860	780	20180	23560	12660	750	790	810	740	810	850
			RMS Residuals (ft.)	80	100	50	49	48	14	130	130	60	120	120	40
		Adjustment for Position and Velocity	Error at PCA (ft.)				6050	4400	4150	800	820	770	730	700	670
			RMS Residuals (ft.)				11	10	10	9	8	9	10	10	11
			Error in Recovered Speed (knots)				-.77	+.16	-.32	+.39	-.22	-.06	-.08	+.20	+.56
			Error in Recovered Heading (deg.)				-21.	-5.7	+1.1	+9.4	+5.8	+.4	-1.8	-3.2	-1.1
	Without Orbital Errors	Adj. for Position Only	Error at PCA (ft.)	110	110	20	21020	24860	7540	130	140	60	100	100	80
			RMS Residuals (ft.)	80	100	50	17	16	37	120	130	50	110	110	40
		Adjustment for Position and Velocity	Error at PCA (ft.)				4470	4190	3370	93	65	47	42	65	96
			RMS Residuals (ft.)				9	10	10	9	8	9	10	10	10
			Error in Recovered Speed (knots)				+1.14	-.25	-1.64	+.32	-.21	+.03	-.08	+.14	+.48
			Error in Recovered Heading (deg.)				+16.	+13.	+13.	+8.7	+4.7	-.2	-.9	-2.7	-1.1

TABLE VIIb - A

SHIP POSITION ERROR AT PCA IN SITUATIONS WITH AND WITHOUT ORBITAL ERRORS

(Only Radar Range Data Used in Solutions)

			Ship	No. 1			No. 2			No. 3			No. 4		
			Heading from North	90°	45°	0°	90°	45°	0°	90°	45°	0°	90°	45°	0°
TRANSIT	With Orbital Errors	Adj. for Position Only	Error at PCA (ft.)	670	2060	3500	120	170	260	230	190	130	350	230	40
			RMS Residuals (ft.)	31	110	190	20	120	200	10	94	135	12	37	48
		Adjustment for Position and Velocity	Error at PCA (ft.)				79	30	37	78	130	70	28	27	190
			RMS Residuals (ft.)				9	9	10	9	10	10	12	9	8
			Error in Recovered Speed (knots)				-.35	-.07	+.01	-.18	-.17	+.01	-.02	-.01	-.02
			Error in Recovered Heading (deg.)				.0	-.7	+1.2	-.2	-2.3	+1.4	-.2	-.5	+2.5
	Without Orbital Errors	Adj. for Position Only	Error at PCA (ft.)	1240	1480	2930	140	150	220	240	190	120	370	250	30
			RMS Residuals (ft.)	41	110	180	31	110	190	14	86	130	12	34	45
		Adjustment for Position and Velocity	Error at PCA (ft.)				65	44	72	49	92	110	56	47	240
			RMS Residuals (ft.)				9	9	10	9	10	10	12	9	8
			Error in Recovered Speed (knots)				-.21	+.01	-.01	-.08	-.13	-.03	+.07	+.02	-.06
			Error in Recovered Heading (deg.)				+.3	+.6	+2.6	+.2	-1.3	+2.4	+.2	+.5	+3.4

TABLE VIIc - A

SHIP POSITION ERROR AT PCA IN SITUATIONS WITH AND WITHOUT ORBITAL ERRORS

(Only Radar Range Data Used in Solutions)

			Ship	No. 1			No. 2			No. 3			No. 4		
			Heading from North	90°	45°	0°	90°	45°	0°	90°	45°	0°	90°	45°	0°
GEOS - B	With Orbital Errors	Adj. for Position Only	Error at PCA (ft.)	800	1750	1890	250	490	520	220	260	270	290	180	200
			RMS Residuals (ft.)	10	260	280	90	220	230	80	170	170	60	110	100
		Adjustment for Position and Velocity	Error at PCA (ft.)	280	280	270	140	100	310	80	250	140	370	80	70
			RMS Residuals (ft.)	10	9	10	9	10	10	8	9	10	10	11	9
			Error in Recovered Speed (knots)	+.08	-.07	-.07	-.70	-.04	-.31	-.05	+.14	-.07	+.43	-.02	+.01
			Error in Recovered Heading (deg.)	-.1	-2.8	-.7	+2.6	-.9	+12.3	-.2	-.7	+1.3	+2.6	.0	-.3
	Without Orbital Errors	Adj. for Position Only	Error at PCA (ft.)	690	1630	1780	240	480	650	250	260	250	320	190	200
			RMS Residuals (ft.)	8	250	270	81	220	230	73	170	170	60	110	110
		Adjustment for Position and Velocity	Error at PCA (ft.)	210	200	180	200	160	60	60	40	5	32	130	40
			RMS Residuals (ft.)	9	9	10	9	10	10	10	11	9	10	10	10
			Error in Recovered Speed (knots)	+.25	-.02	-.01	-.83	+.34	+.07	+.10	+.03	+.03	+.02	+.06	+.03
			Error in Recovered Heading (deg.)	+.6	-1.0	+1.0	-4.7	+6.7	-1.0	+.3	+.4	-.3	-.1	+1.9	-.1

TABLE VIII - A

MAXIMUM ELEVATION OF EACH SATELLITE
FROM EACH LAND BASED SITE

SATELLITE	SITE NUMBER	SITE POSITION N. LAT. (DEG.)	E. LONG. (DEG.)	MAX. ELEVATION (DEGREES)
Pegasus	1	28.226	279.401	8.8
	2	26.636	281.732	13.2
	3	21.473	288.868	42.4
Transit	1	28.226	279.401	39.5
	2	26.636	281.732	46.5
	3	21.473	288.868	78.8
GEOS-B	1	28.226	279.401	35.9
	2	26.636	281.732	43.1
	3	21.473	288.868	76.3

CONCLUSION

The geodetic location of a ship at sea can be accurately determined from pulse radar range-only data. This study has not included the relative location of one transponder to another as this was considered to be a different problem which involves the ASPS measurements obtained by the ship. Also, the ASPS measurements can degrade the attained accuracy of the transponder survey, if not properly used.

The actual survey accuracy achieved and the number of separate satellite passes required depends to a large extent upon (1) the accuracy of the reference orbit, (2) the accuracy of the ship's tracking data and ship's motion determination and (3) the geometry of the different passes used. Where unknown and unmodeled errors exist, it will be essential to obtain sufficient passes to examine the errors present for each test. It is always desirable to obtain satellite passes on each side of the ship for which the geodetic survey is desired.

ACKNOWLEDGEMENTS

The author gratefully acknowledges the contributions of RCA Technical Evaluation. In particular, I wish to thank John J.O'Connor for his technical advice.

REFERENCES

1. Bush, N.; Pfingsten, D.R.; Greene, J.A.; et al, "MISTRAM MRS Survey Improvement Study" AFETR TR-69-6, Pan American World Airways, RCA International Service Corp, Patrick AFB, Florida, dated October 1969.

2. Boroughs, S.P., "Surveying a Marine Benchmark Using Ship Radar Track of an Orbiting Satellite" RCA International Service Corporation Report No. 61-SR-69-6, dated 31 December 1969.

3. O'Connor, J.J., "Estimation of Ship Position and Velocity Using Ship Radar Range Data from Satellite Track" RCA Technical Evaluation Special Report No. 83-SR-69-13, dated 22 July 1969.

4. O'Connor, J.J., and Rowe, R.R. "Use of SINS Input in Estimation of Ship Position from Satellite Track" RCA Technical Evaluation Special Report No. 83-SR-69-23, dated 17 November 1969.

5. Christ, O.J.W., IBM 360 Program HESP-6 (Estimated Ship Position) RCA Technical Evaluation Computer Program, dated 19 November 1969.

6. O'Connor, J.J., and Rowe, R.R., "Ship Location from Satellite Track Using Real Data" RCA Technical Evaluation Report No. 83-SR-69-24, dated 19 December 1969.

ABSTRACT

"Geodetic Survey Improvement with C-Band Radar"

AUTHOR

D. R. Pfingsten - RCA International Service Corporation, MTP

Survey adjustments and improved accuracies were obtained for four AFETR downrange Mistram/MRS sites. This presentation describes the role played by C-Band tracking radars in obtaining these results. Comparisons between the C-Band radar results and other systems are also discussed.

GEODETIC SURVEY IMPROVEMENT WITH C-BAND RADAR

By: D. R. Pfingsten

SLIDE 1

This presentation describes the role played by C-band tracking radars in reducing survey uncertainties for the Mistram/MRS System.

This special effort was undertaken because survey uncertainties at the Mistram/MRS sites at Grand Turk, Antigua, Bermuda, and Trinidad affected the Minuteman III (MM III) velocity accuracies after burnout. The flight interval of interest was between 300-900 seconds. This accuracy requirement caused the AFETR to deploy the Mistram/MRS vans at new locations. It had been shown that if a survey improvement could be effected for the above four X-band sites relative to the Florida mainland, this would be a significant contribution towards improving the MM III velocity accuracies.

Briefly, as shown in the figure, the Mistram/MRS system is a CW X-band system which consists of transmitter and receiver systems at Valkaria and Eleuthera, the rate stations at Miami Beach, Pier Road, Bermuda, Grand Turk, Antigua, and Trinidad. The Valkaria and Eleuthera systems provide unambiguous target position both for real time and postflight purposes.

These rate stations provide a measurement of range sum from the transmitter to the missile to the receiver, but the measurements are ambiguous up to the initialization constant, and are used in postflight reductions.

The Mistram/MRS data are processed postflight in the NITE (N Interval Trajectory Estimation Program) which is a minimum variance trajectory and error model coefficient estimation program designed to process tracking data from free fall and powered flight trajectories. All the solutions discussed, processed at AFETR, were processed through the NITE Program.

SLIDE 2

In addition to the desirability of the reduction in survey uncertainties, data from the first MM III Test 1721 which occurred on 16 August 1968 indicated some type of problem in the data. One aspect of the problem is shown by the residuals from two of the rate stations -- Antigua and Trinidad. This figure will be shown again. At this time, note that the magnitude of the residuals, especially late in flight, were relatively large. Past experience yielded residual standard errors typically on the order of 0.04 ft/sec.

SLIDE 3

Theoretical studies performed early in the calibration satellite effort had indicated that, even with a moderate amount of data, a significant improvement over existing uncertainties could be obtained. The limitation on studies of this type is that the physical situation assumed in the study may not completely describe the actual situation under which the data are collected relative to data availability, noise in the data, and the significant parameters in the solution. The last two limitations apply to the error propagation obtained from the actual reduction.

This slide shows the satellite revolutions for one of the two solutions from the GEOS-B data. This particular solution involved 9 revolutions. This solution included those revolutions for which ballistic camera data were obtained. When processed with radar only data, this solution is identified as NITE 1R. When processed with both radar and camera data, it is identified as NITE 6.

The pulse radars principally used were 0.18, 19.18, 7.18, 91.18 and 67.18. The first two are located in the Cape Kennedy area at Patrick Air Force Base and Merritt Island. The last three are located at Grand Turk, Antigua and Bermuda. A particular revolution typically included data from three to four radars. The ballistic cameras included 1000 mm cameras at the above sites as well as Homestead Florida, Atlantic Field North Carolina, and Trinidad. Data from 600 mm cameras at Vero Beach Florida and Grand Bahama Island were also used as well as some additional data supplied by NASA.

SLIDE 4

This slide shows the satellite revolutions for the second solution from the GEOS-B data. This particular solution involved only radar data. In addition to the GEOS-B data shown on the last two slides, passive ballistic camera data from the Echo II and Pageos Satellites were collected during the same time period the GEOS-B ballistic camera data were collected. These data with other available data from past programs were used to generate another solution. Finally, Mistram/MRS data from three Minuteman III tests were used. The failure to significantly change geometry between tests and the attendant flame, aspect angle, and staging problems associated with powered flight are limitations for these data. However, these tests provided data with vehicle motion in an east-west direction contrasted to the north-south satellite data as well as data from another type of instrumentation.

SLIDE 5

When the decision was made in September 1968 to concentrate on the Mistram/MRS Survey Improvement Study, it was also decided to confine the radar data used in the solutions to range measurements. This decision was based upon studies which indicated that exclusion of the radar angle data had little effect on the results. It also greatly reduced the quantity of data used in the reduction.

The corrections made to the data prior to input to NITE were:

1. Zero-set (including pulse width)
2. Editing
3. Transit time
4. Refraction
5. Signal strength
6. Filtering and reduced sample rate

The zero-set correction was based upon the pre- and post-calibrations and included a nominal correction for the difference between the calibrate and beacon pulse widths.

SLIDE 5 (Continued)

The refraction correction was computed from a ground index value of refractivity, determined from measurements, and an assumed exponential variation with height. A ray trace computation was performed. Data below 10° elevation were not used to minimize residual refraction errors. The signal strength correction was a small correction which attempted to account for the variation of beacon delay about its nominal value. The filtering took the data at 10 samples per second through a 101 point filter constrained to pass a 3rd degree polynomial. Output data were used at 1 sample every 10 seconds. A moderate amount of noise reduction was achieved.

SLIDE 6

The GEOS-B NITE solutions were structured as follows:

Survey adjustments were made for Grand Turk, Bermuda, and Antigua whenever pulse radar data were available. Survey adjustments were also made for Trinidad in NITE 6 using the available ballistic camera data. Short arc orbital constraints were used in all solutions and the orbital parameters were estimated for each revolution as well as a distinct range zero-set for each radar. For all range measurements, a scale factor equal to 5×10^{-7} was propagated as an unmodeled error and was also combined with the a priori noise estimates to weight the measurements. A 10° elevation angle cutoff was used on all radar measurements to minimize the residual refraction effect. In all revolutions involving the Bermuda radar, a timing offset, distinct for each revolution, was estimated. The original basis for using this rather extensive error model was to reduce the risk of obtaining biased survey adjustments at the expense of less precise estimates. For example the inclusion of the Bermuda timing offset was not on positive evidence that such an offset existed but rather on the possibility that it might exist, since it alone of all the radars did not receive ETR timing.

SLIDE 7

This slide shows the RMS radar range residual values from the two solutions. As can be seen the residuals were small. When considered across a single revolution the RMS residual values varied from 2 to 6 feet. The residuals were also unbiased and the mean value was consistently under 1 foot. This of course was not entirely unexpected to the extent that range zero-sets were modeled. However, the residuals at least gave no positive indication of unaccounted systematic error.

SLIDE 8

This slide shows the adjustments obtained. The results are presented in terms of a local coordinate system at the ballistic camera site with X-east, Y-north, and Z-up. These coordinates are used as a means of presentation. Within the NITE Program geodetic coordinates are employed. For the islands the radar positions were input relative to the ballistic camera sites and this relative position was held fixed. Recall that solutions NITE 4 and NITE 1R are radar only solutions, and that NITE 6 is NITE 1R supplemented with ballistic camera data. The pooled results are based upon NITE 4, NITE 6 and also upon additional camera and Mistram/MRS data. There was no C-band pulse radar at Trinidad. The Trinidad adjustment under NITE 1R is a combination of the Antigua adjustment with an adjustment of Trinidad relative to Antigua.

As can be seen, the radar solutions agreed very well at all sites in the X and Z coordinate adjustments. In these coordinates both radar solutions also show good agreement with the pooled results. The disagreement in the Y coordinates is attributed at least in part to a confounding of these coordinate adjustments with the Bermuda timing adjustments. This effect was also evident in terms of little variance reduction in the Bermuda X and Y adjustments.

SLIDE 9

This slide shows the a priori estimates of site uncertainties and the uncertainties based upon the pooled results. The pooled results are also repeated. As can be seen relative to

SLIDE 9 (Continued)

the a priori uncertainties, the major shifts occurred at Trinidad, Antigua X, and Grand Turk Y. The relatively large Trinidad shift was explained by an accidental error that had occurred in obtaining the previously held values.

The pooled results were obtained by computing a weighted mean across the various solutions. In this computation which involved pooling results from various types of instrumentation and geometry, the tacit assumption was made that the relative weights within a solution, based on the computer outputs, were correct but scaled improperly.

SLIDES 10 & 11

These slides show a comparison between the MRS residuals shown earlier and the residuals from the same test with the new survey values. It can be seen that the residuals are reduced particularly late in flight. These residuals are of course only one aspect of the problem. For this particular test the survey shifts produced a significant shift in the trajectory estimated by the system. The shifted trajectory proved to be more consistent internally and also agreed better with trajectory solutions from other systems. The large shift at Trinidad accounts for a major part of these changes. While this large shift was indicated from other sources including the Mistram/MRS data, the similar results from the GEOS-B data were important. This was due to the fact that the test shown was the first test supported at the Trinidad site by the MRS van and it would have been difficult to establish by other means that the shift determined was in fact a survey error and was not some other unknown error functionally similar to survey.

SLIDE 12

Subsequent to the adoption of the values previously shown, four additional Minuteman III tests provided Mistram/MRS data suitable for adjustments. In these solutions an accurate trajectory was the primary objective and the survey adjustments were performed as a means to properly weight the

SLIDE 12 (Continued)

observations for trajectory determinations. This slide shows the mean values from these four tests and the uncertainties as of August 1969. These mean values correspond to an additional shift relative to the shifts previously shown on Slide 9. The fact that they are in general small and within the uncertainties quoted supports the consistency of the changes adopted. The one exception to this is the Bermuda X shift. The problem here does not, however, appear to be due to the GEOS-B data used.

SLIDE 13

This study was the first attempt at AFETR to use C-band pulse radar data from satellites in short arc solutions for survey improvement. The conclusions reached were as follows:

1. The method can properly determine any major inconsistencies.

2. Weaknesses in the adjustment will be identifiable from internal comparisons.

3. When the results were internally consistent, comparison with adjustments obtained by other means were for the most part consistent within the uncertainties quoted.

4. The results were obtained relatively fast compared to results using ballistic cameras.

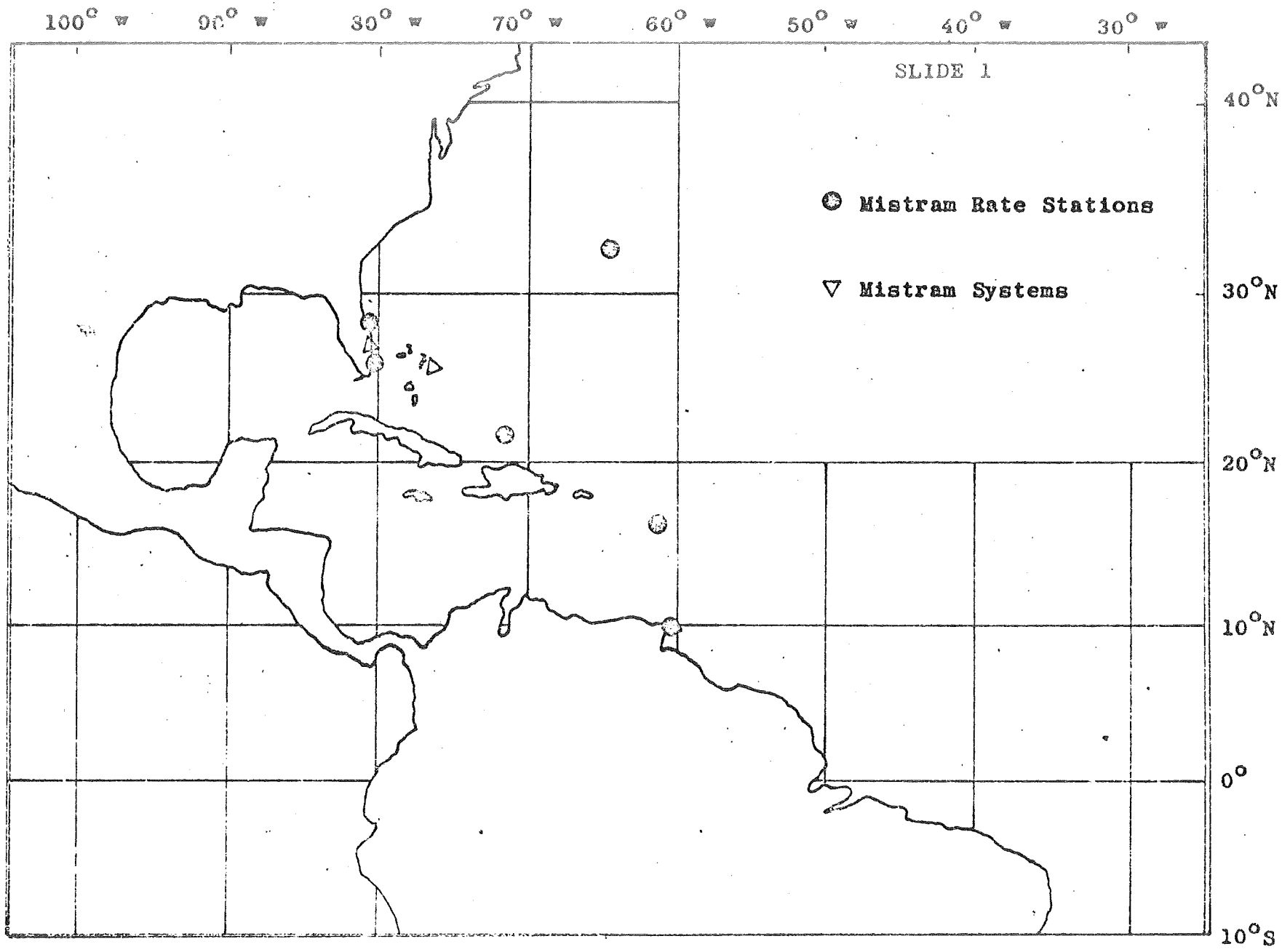
100° W
90° W
80° W
70° W
60° W
50° W
40° W
30° W
SLIDE 1
40°N
30°N
20°N
10°N
0°
10°S
Mistram Rate Stations
Mistram Systems

SLIDE 2

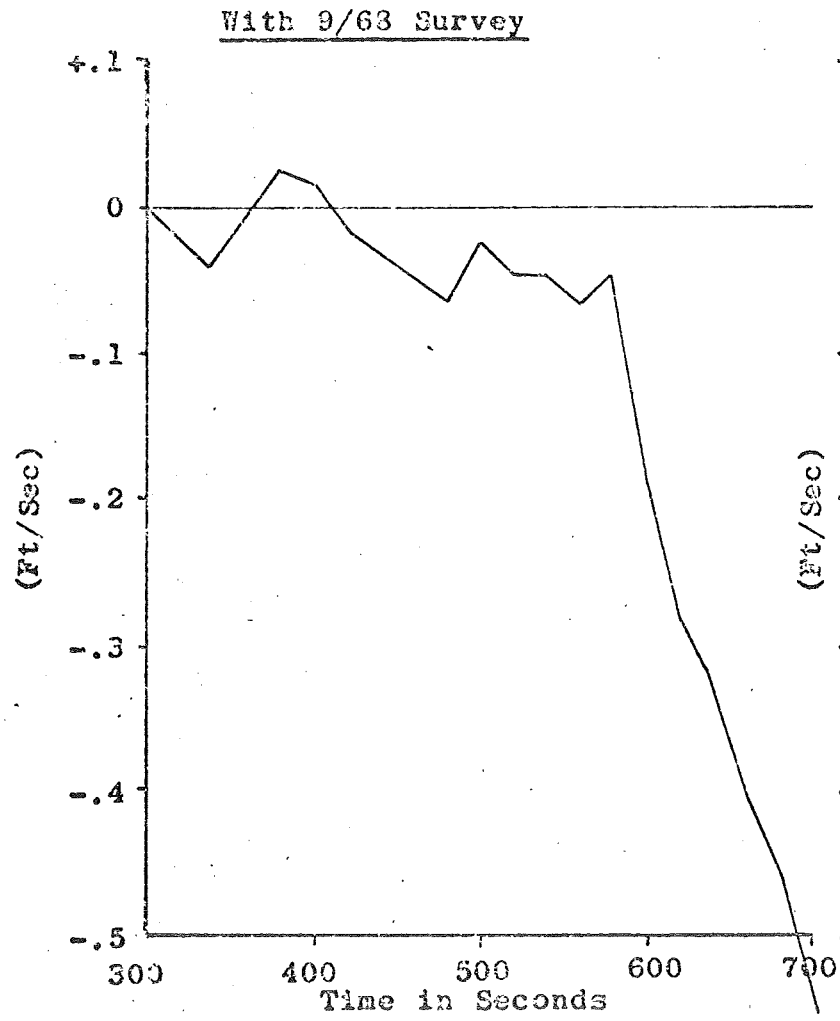

TRINIDAD RS VELOCITY RESIDUALS
(MM T-1721, 300-700 Sec)

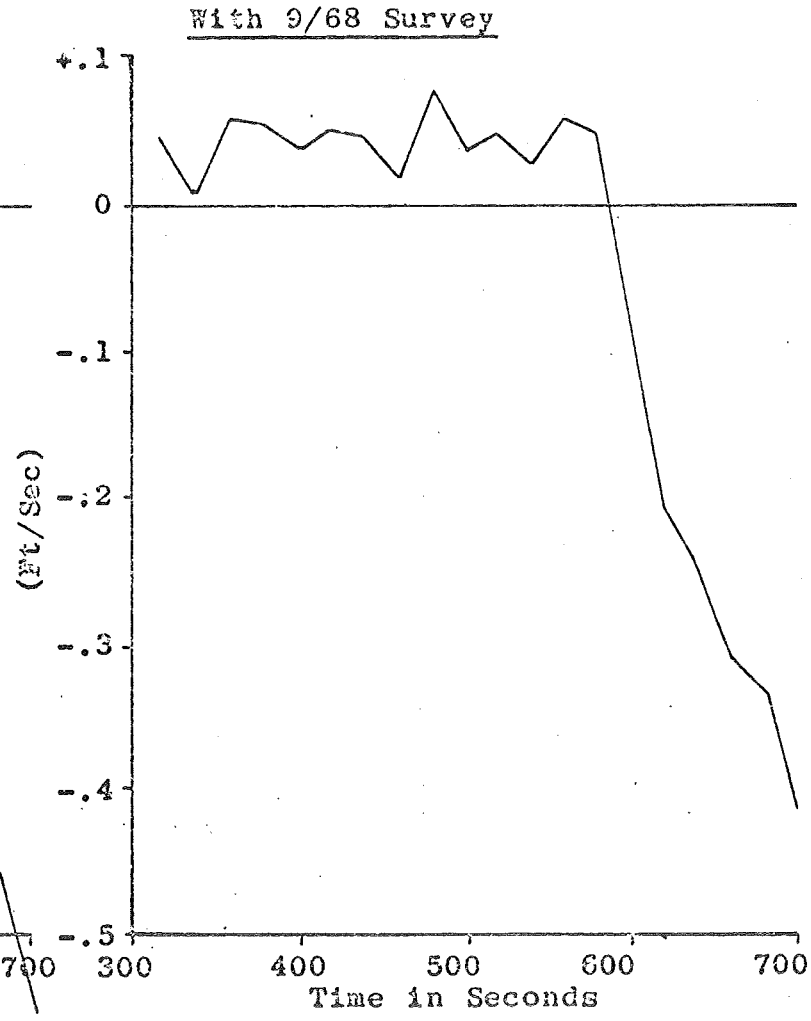

ANTIGUA RS VELOCITY RESIDUALS
(MM T-1721, 300-700 Sec)

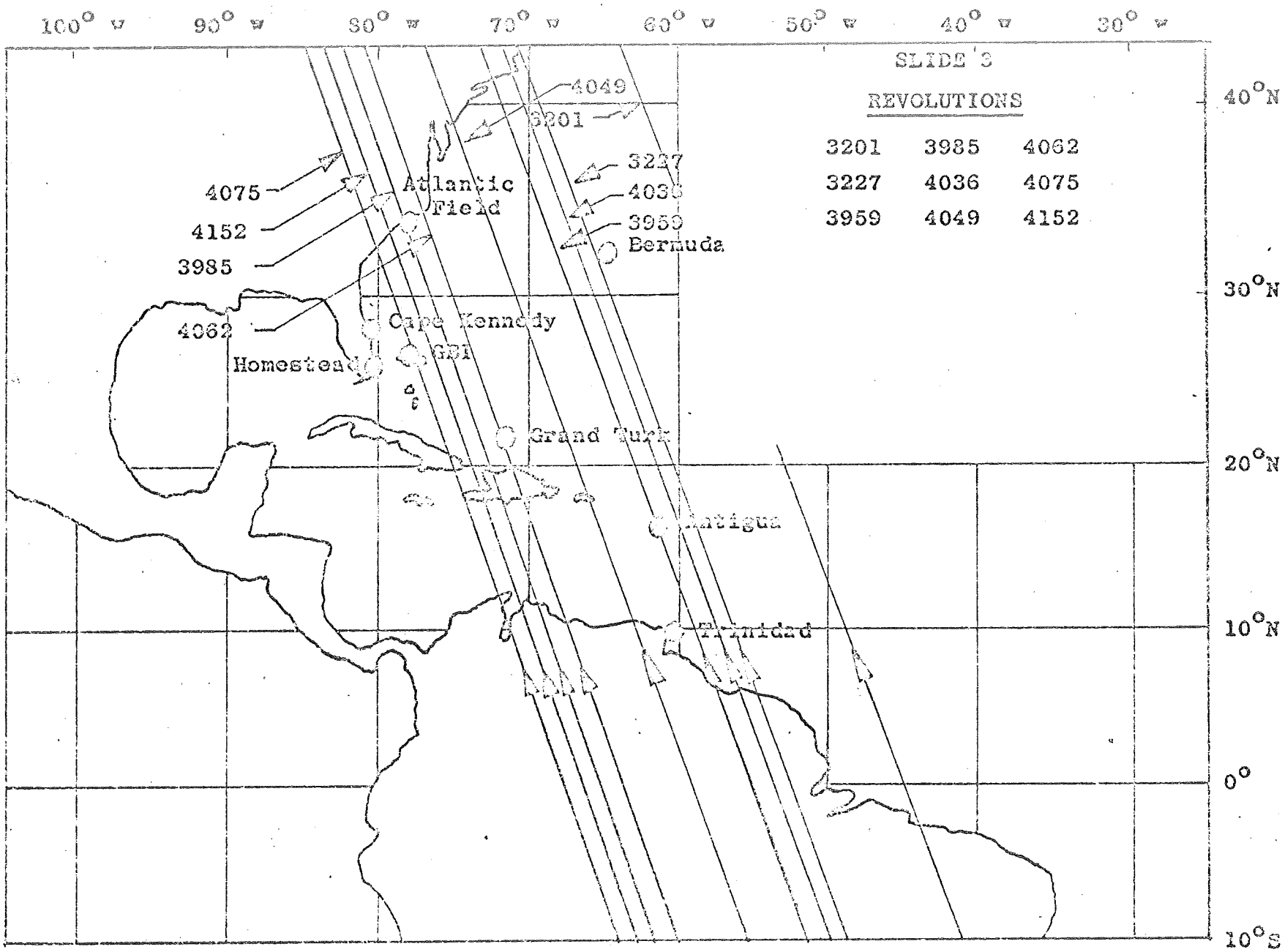
100° W
90° W
80° W
70° W
60° W
50° W
40° W
30° W
40°N
30°N
20°N
10°N
0°
10°S
SLIDE 3
REVOLUTIONS
3201 3985 4062
3227 4036 4075
3959 4049 4152
4049
3201
3227
4036
3959
Bermuda
4075
4152
3985
4062
Atlantic Field
Cape Kennedy
GBI
Homestead
Grand Turk
Antigua
Trinidad

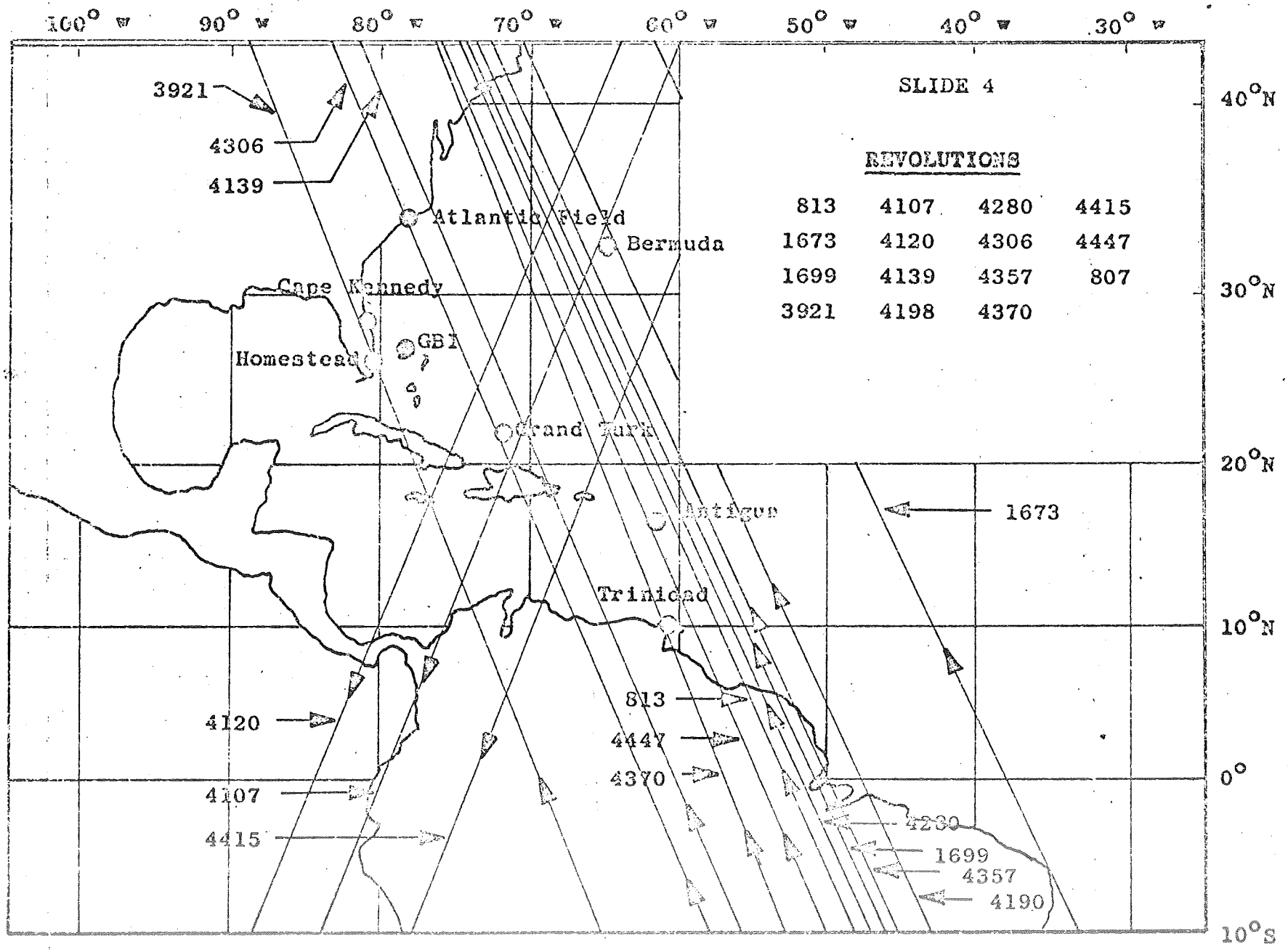
100° W
90° W
80° W
70° W
60° W
50° W
40° W
30° W
40°N
30°N
20°N
10°N
0°
10°S
SLIDE 4
REVOLUTIONS
813 4107 4280 4415
1673 4120 4306 4447
1699 4139 4357 807
3921 4198 4370
3921
4306
4139
Atlantic Field
Bermuda
Cape Kennedy
Homestead
GBI
Grand Turk
Antigua
1673
Trinidad
813
4447
4370
4120
4107
4415
4280
1699
4357
4190

SLIDE 5

RADAR RANGE DATA PROCESSING

1. Zero-set
2. Edit
3. Transit Time
4. Refraction
5. Smooth and Reduce Sample Rate

SLIDE 6

STRUCTURE OF NITE SOLUTIONS

Parameters - Orbital Elements

Range Zero-sets

Time Bias

Survey

Weighting - Random and Scale Factor

WGS 66 Spheroid

NWL 8D Geopotential Model

SLIDE 7

RADAR RESIDUAL ANALYSIS
(RMS Values in Feet)

Station	NITE 6	NITE 4
Grand Turk	4	4
Merritt Island	2	3
Antigua	3	4
Patrick AFB	3	4
Bermuda	2	3

SLIDE 8

SURVEY RESULTS

POSITION CHANGE FEET

		NITE 4	NITE 1R	NITE 6	Pooled
Grand Turk	X	-3	1	1	3
	Y	12	-5	-33	-21
	Z	-0	-3	-3	-5
Antigua	X	49	53	48	65
	Y	24	-11	-75	-25
	Z	-29	-38	-8	-26
Bermuda	X	-16	-11	25	-10
	Y	-6	-1	1	-4
	Z	7	9	1	6
Trinidad	X		121	134	126
	Y		-164	-202	-177
	Z		-20	-42	-39

SLIDE 9

POSITION CHANGES AND
UNCERTAINTIES
(Feet)

		Pooled	Uncertainty As of 9/68	Uncertainty As of 8/69
Grand Turk	X	3	11	7
	Y	-21	11	5
	Z	-5	14	7
Antigua	X	65	33	12
	Y	-25	28	9
	Z	-26	24	11
Bermuda	X	-10	20	11
	Y	-44	11	10
	Z	6	26	11
Trinidad	X	126	34	20
	Y	-177	37	22
	Z	-39	16	15

SLIDE 10

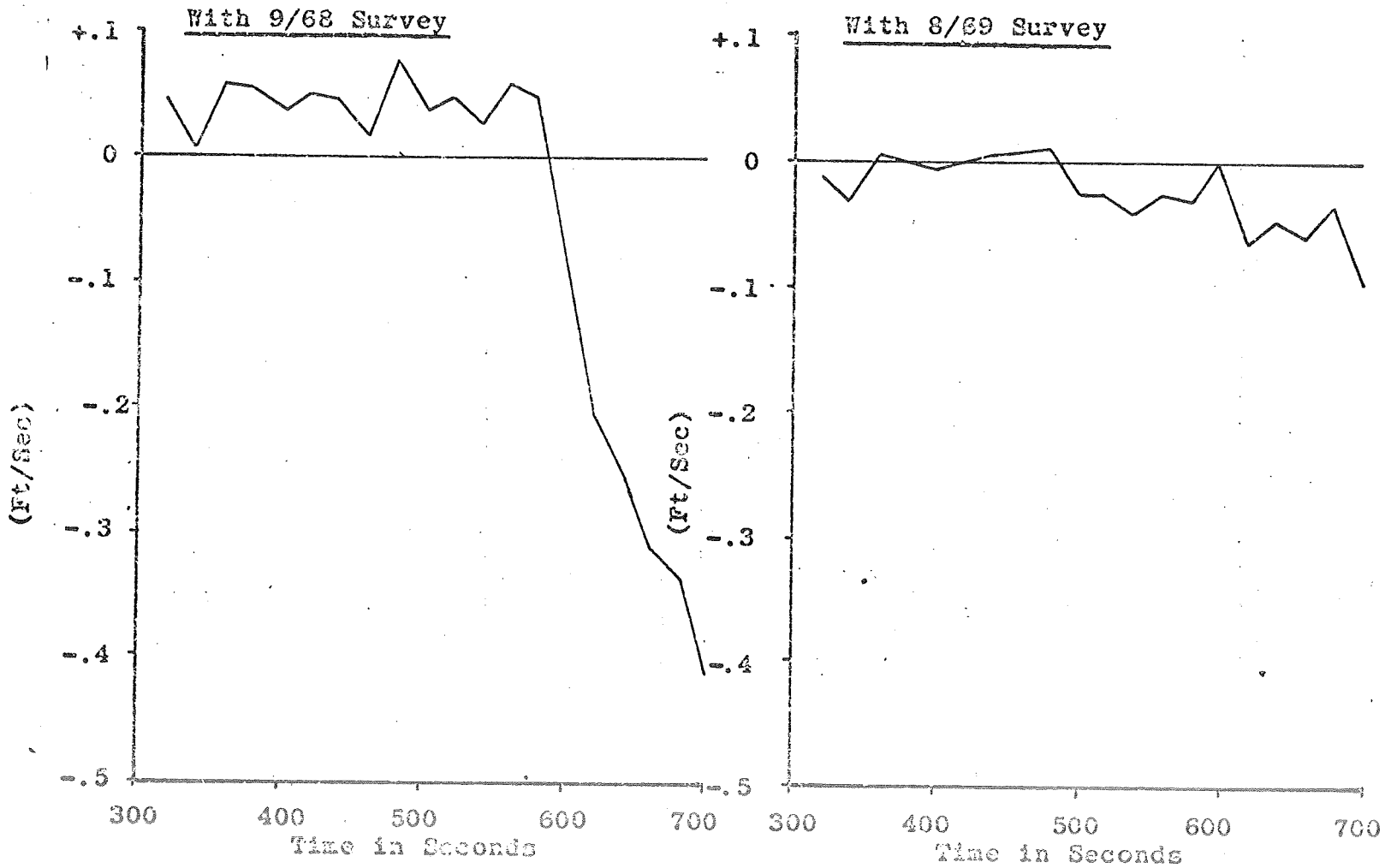

ANTIGUA RS VELOCITY RESIDUALS (MM T -1721, 300-700 Sec)

SLIDE 11

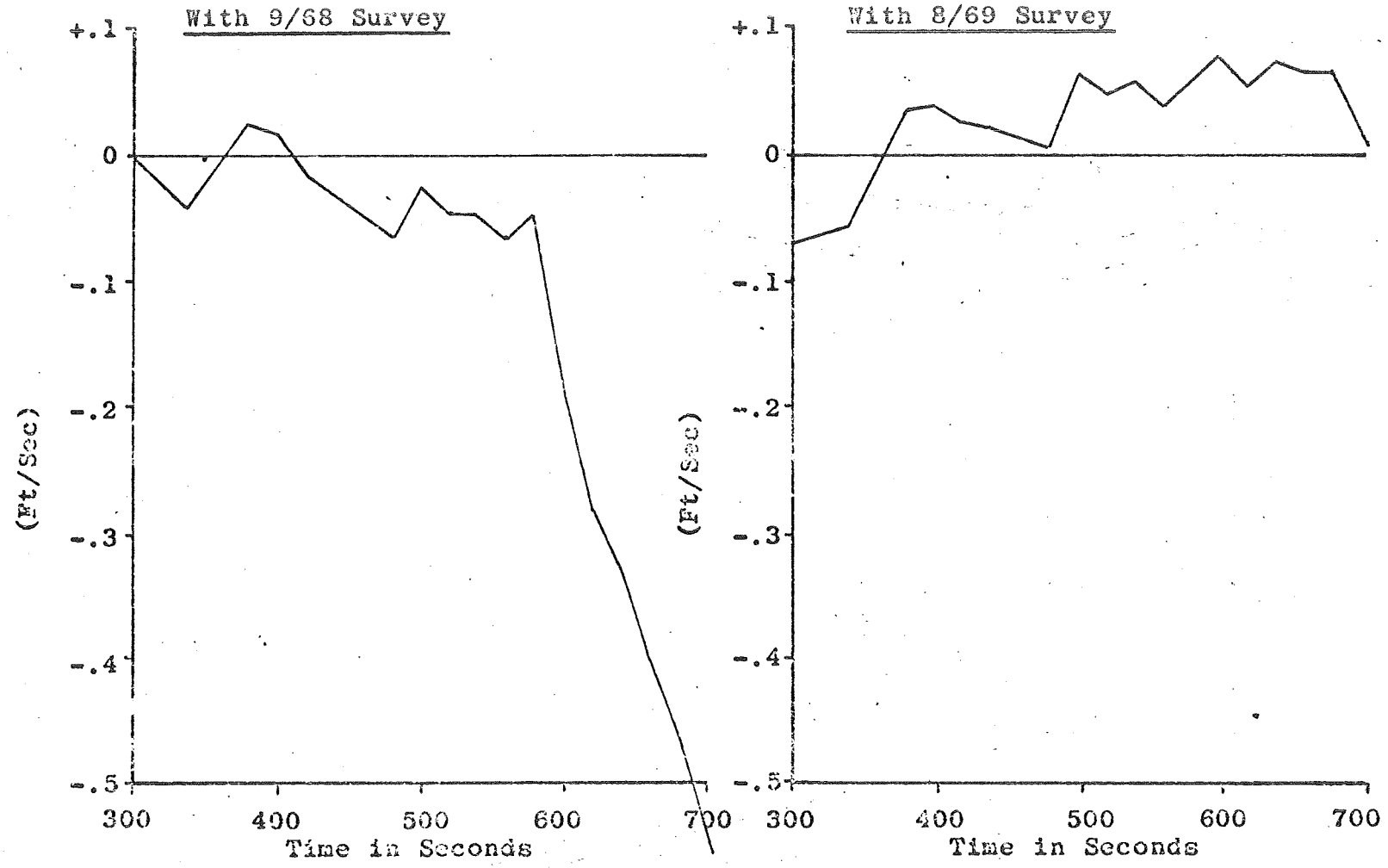

TRINIDAD RS VELOCITY RESIDUALS (MM T-1721, 300-700 Sec)

SLIDE 12

MEAN VALUES

FOUR SUBSEQUENT TESTS

FEET

		Mean Value	Uncertainty As of 8/69
Grand Turk	X	-2	7
	Y	0	5
	Z	6	7
Antigua	X	6	12
	Y	-3	9
	Z	-8	11
Bermuda	X	48	11
	Y	5	10
	Z	2	11
Trinidad	X	-13	20
	Y	22	22
	Z	2	15

SLIDE 13

SUMMARY

(1) Major problems found

(2) Internally consistent

(3) Generally consistent with other results

(4) Relatively fast results

ACOUSTIC DATA REDUCTION AND CALIBRATION FOR THE GEOS-II C-BAND RADAR MARINE GEODESY EXPERIMENT IN THE BAHAMAS

by

A. G. Mourad, A. T. Hopper, D. M. Fubara, and G. T. Ruck

Battelle Memorial Institute
Columbus Laboratories

INTRODUCTION

In late 1969, Battelle was involved in a NASA experiment in the Bahamas the overall objective of which was to determine the feasibility of using C-band radar for ship positioning and for establishing marine geodetic control points. It was the first such experiment initiated by NASA and was aimed ultimately at the practical application of existing satellite and space technology for better understanding of the earth, particularly the complex ocean environment. Battelle's initial role was to handle that portion of the experiment requiring acoustic techniques.

Results obtained, using the Apollo ship Vanguard and the GEOS-II satellite, were excellent, despite existance of some gaps in the data obtained and the fact that general-purpose acoustic system components were used. For example, standard errors of about 0.24 arc second and three meters were obtained in determining the latitudes and longitudes, and depth of the three ocean-bottom transponders respectively.

Figure 1 shows the location of the experiment and indicates, generally, how the ship position was determined relative to ocean-bottom-mounted acoustic transponders during observed passes of the GEOS-II satellite. The new acoustic procedures which were developed, referred to here as Transponder Location by Surface Positioning (TLSP), permit use of any type of accurate surface-ship-positioning data available; they involve measurement of acoustic slant ranges from the ship to any number of underwater acoustic transponders or hydrophones and consideration of the velocity of sound. TLSP can utilize all available acoustic data and lends itself to a weighted least-squares determination of transponder coordinates.

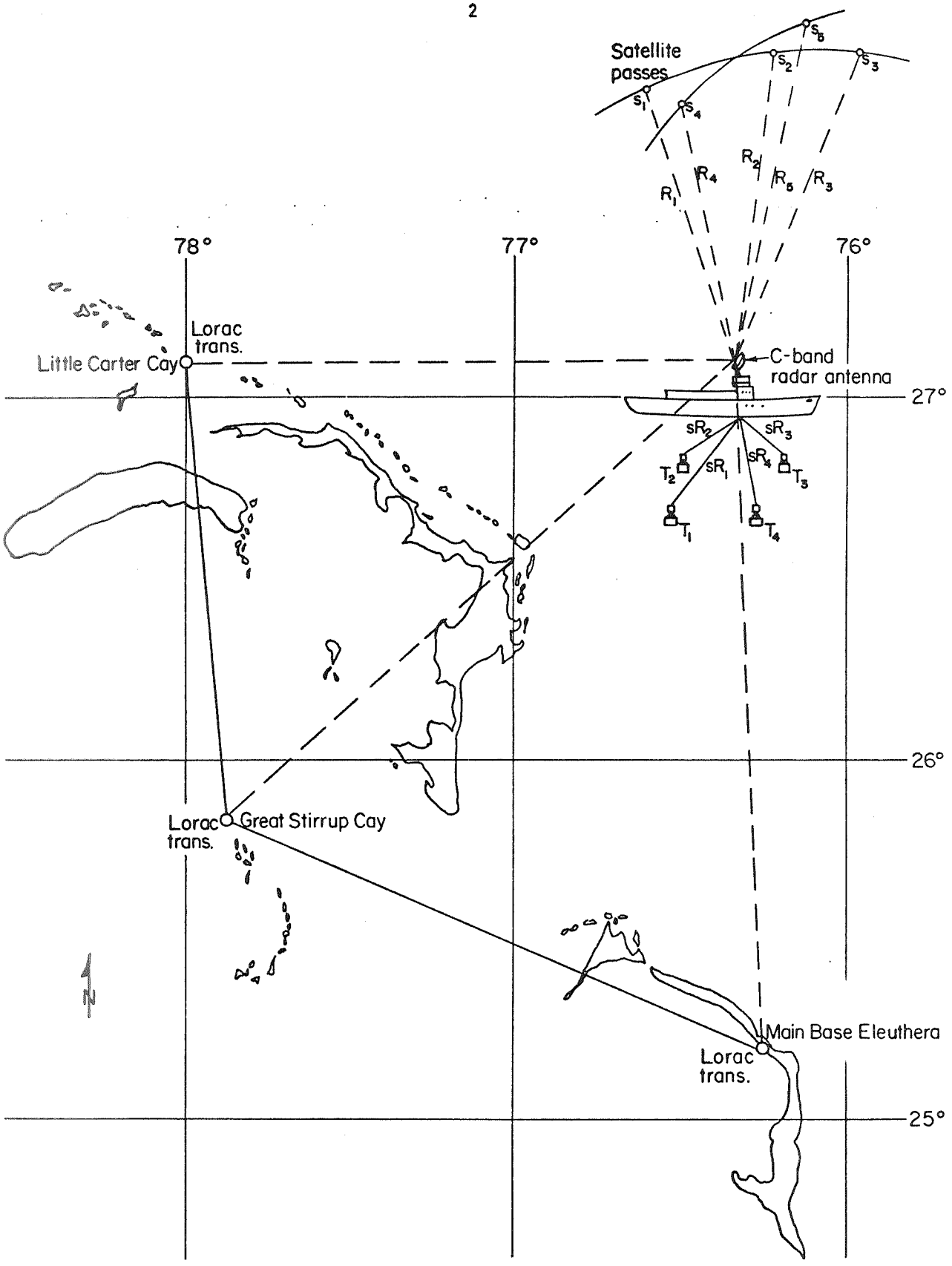

FIGURE 1. LOCATION OF C-BAND RADAR MARINE GEODESY EXPERIMENT

The feasibility of establishing marine geodetic control points on the ocean floor using bottom-mounted acoustic transponders had previously been demonstrated in November, 1968, by the Battelle/Industry Group experiment in the Pacific Ocean[6]. A standard point error of ± 15 to ± 20 m was obtained in determining the coordinates of the control point that was established about 120 miles west of Los Angeles using a LORAC airborne DME line-crossing technique. Although the airborne DME system is capable of providing fairly high geodetic accuracy at sea, it is range-limited (up to a few hundred miles). Therefore, the use of satellite systems is attractive because of the world-wide coverage possible by their use.

Present indications are that if high-accuracy in marine geodetic measurement can be achieved, many difficult problems will be well on the way to solution. Such problems include, for example, determining ocean circulation, establishing reference points for ocean tidal measurements, determining ocean-floor spreading, providing "ground truth" for calibration of satellite altimetry and evaluating shipboard positioning systems, making accurate gravity measurements, determining geoidal heights, and making deflection-of-the-vertical measurements.

The use of C-band radar for marine measurements is desirable for two reasons: (1) C-band radar can be operated in a ranging mode (measure distances from ship to satellites) which provides a particular advantage in that errors in ship velocity are not as critical as they are with the Doppler satellite techniques (the only satellite system operational at sea) and (2) several ships already have C-band radar systems on board.

GENERAL DESCRIPTION OF THE EXPERIMENT

Figure 1 shows the general location of the experiment conducted in the Bahamas. This location was chosen: (1) because of its proximity to the test area for the Vanguard (the experiment was a task added to the primary Vanguard mission) and (2) because of the availability of the four underwater acoustic transponders previously established by the U. S. Navy Compass Island ship in about 16,000 feet of water. The four transponders formed a quadrangle having about 3.5 mile sides. However, during the experiment it was possible to collect data from only three of them.

The experiment involved six major elements: (1) the Apollo ship "Vanguard" and its instrumentation systems, (2) the GEOS-II satellite, (3) three underwater acoustic transponders, (4) a C-band radar land-based tracking network, (5) a LORAC surface positioning network, and (6) the Navy Transit satellites. The ship instrumentation systems used include: (1) the FPS-16 C-band radar, (2) the SRN-9 Doppler satellite navigation receiver, (3) the Inertial/Star Tracker System (INS), a LORAC receiver, (4) the Bathymetric Navigation System (BNS), and (5) timing and computer systems.

Basically, simultaneous measurements were made of (1) C-band radar ranges (between the ship and the GEOS-II satellite), (2) acoustic ranges (between ship and three underwater acoustic transponders, (3) surface LORAC positions (between ship and three land LORAC transmitters, and (4) the Inertial/Star Tracker coordinates.

The ship was positioned continuously over the triad formed by the three ocean-bottom-mounted acoustic transponders during the GEOS-II and Doppler satellite passes. Acoustic data were collected during 5 of 7 GEOS-II passes, 22 of 32 Doppler satellite passes, and 11 acoustic calibration runs.

DESCRIPTION OF ACOUSTIC SYSTEM USED

The acoustic system used consisted of two major components: (1) the three ocean-bottom-mounted acoustic transponders and (2) the shipboard Bathymetric Navigation System (BNS). The BNS system on board the Vanguard is capable of interrogating ocean-bottom-mounted transponders, receiving their replies, and recording the acoustic slant ranges to the transponders. This capability of the BNS was utilized in this experiment. Operation of the BNS is as follows[1, 2]. The BNS transmits an interrogation signal with a frequency of 16.0 KHz ± 50 Hz and a pulse width of 15 ± 1 milliseconds (ms) to the transponders. The leading edge of the interrogation signal activates a digital counter which starts counting the pulses from an 800-pps clock. The reply signal from a transponder is applied to a signal processing unit which recognizes the center of the returned pulse and stops the counter. The time interval measured by the counter represents the range from the BNS transducer to the acoustic transponder (in yards, an acoustic velocity of 4800 ft/sec is assumed) plus several fixed delays. To

correct the time interval and obtain the true range, the BNS subtracts 175 ms (8 ms for transponder-turn-around time, 160 ms for BNS signal-processing time, and 7 ms for signal-recognition time) from the measured time interval.

ACOUSTIC TECHNIQUES FOR DETERMINING GEOMETRY OF TRANSPONDERS

Two techniques have been developed for determining the coordinates and orientation of the ocean-bottom transponders. These are:

(1) Acoustic line-crossing technique

(2) Ocean-surface positioning technique.

The basic line-crossing technique involves the measurements of: (1) the ship's heading, (2) the acoustic slant ranges or the two-way travel times of an acoustic signal from a ship to two adjoining ocean-bottom transponders, and (3) the velocity of sound[6]. The ship, allowed to travel at a constant speed and heading, crosses the lines joining the transponders and records the points of closest approach (PCA) to each of the transponders and the acoustic slant ranges versus time during the crossings. The sum of two slant ranges is minimum when the ship is in the vertical plane containing the two transponders. The minimum sums can be obtained by least-squares curve fitting or graphically by plotting the horizontal ranges against time. From the ship's heading and course, and minimum distances, forward and backward azimuth, the relative coordinates of the transponders are determined. The technique is sensitive to ship heading and must depend on good data, particularly during the PCA's. Battelle's experience in the Pacific, as well as in the Bahamas, indicates that adverse operational conditions and/or equipment malfunction can occur, thus limiting the value of using such techniques.

The ocean-surface positioning technique, known as transponder location by surface positioning (TLSP), involves the use of a computer code incorporating any available accurate surface-ship coordinates (e.g., LORAC, SINS, DECCA), acoustic slant ranges from the ship to the transponders, and velocity-of-sound profile to determine the positions of the transponders. Basically, each transponder was independently positioned relative to a set of LORAC surface positions. The LORAC positions were given in terms of geodetic latitude and longitude. These positions were transformed to a space rectangular coordinate system X, Y, Z where

the Z-axis coincides with the polar axis of the reference ellipsoid and the X- and Y-axes are situated in the equatorial plane, perpendicular to each other, and X-axis going through the 0-meridian. The original Navy coordinates for the transponders were used as approximate coordinates (X_o, Y_o, Z_o), and an observation equation $V = AX + L$, was written for each selected LORAC position. The computed slant ranges SR_o are given by:

$$SR_o = [(x_o - x_i)^2 + (y_o - y_i)^2 + (z_o - z_i)^2]^{1/2}$$

where

$(x_i\ y_i\ z_i)$ = coordinates of ship converted from LORAC geodetic positions at times i; i = 1, ..., n where n is the total number of observations.

The adjustment was carried out with the following matrices:

X_o = approximate values of unknowns (in this case they represent the approximate transponder coordinates)

X_a = adjusted values of unknowns

$X = X_a - X_o$

SR_b = observed slant ranges as determined from the two-way acoustic travel times and velocity of sound (all slant ranges were corrected for refraction):

$L = SR_o - SR_b$

$$A = \frac{\partial SR_o}{\partial (X_o, Y_o, Z_o)}$$

The least-squares solution of the observation equations,

$$V = AX + L$$

is given by

$$X = -N^{-1}U$$

where

$N = A'PA$

$U = A'PL$

$P =$ weight matrix.

After the adjusted X, Y, Z coordinates of the transponders were obtained, their orientation was determined by computing the inverse geodetic problem. The solution gives also the variance covariance matrix and the eigenvectors and eigenvalues of this matrix which are used in the error ellipsoid computations.

ACOUSTIC TECHNIQUES FOR DETERMINING SHIP POSITIONS

Ship positions relative to ocean-bottom-mounted acoustic transponders can be determined by either of two techniques developed at Battelle[6] and for which computer codes exist.

The first technique which employs the least-squares solution for a two-dimensional computer model is based on the intersection of three circles in a plane. The Z-coordinate is held fixed at Z = 0. One transponder is used as the origin of the local coordinate system with the positive X-axis corresponding to east and the positive Y-axis corresponding to north.

An observation equation $AX + L = V$ is written and solved in matrix form. The general solution is similar to that already described. The unknowns in this case are the rectangular ship coordinates (X, Y) at times of the acoustic readings.

The second technique, which employs the three-dimensional computer code is based on the intersection of three slant ranges corrected for velocity of sound and refraction. The coordinate system is an earth-centered XYZ system as in TLSP. The general equation for the slant ranges from the ship to the transponders is given by:

$$(X - X_i)^2 + (Y - Y_i)^2 + (Z - Z_i) = SR^2 .$$

The solution of the quadratic equation results in two positions. These two positions will result in two values for X. The desired position is that corresponding to the larger X value.

Velocity-of-Sound Measurement

Actual measurement or determination of velocity of sound during the time of operation is essential for accurate reduction of acoustic data. At the time of the experiment, the Vanguard did not have a capability for making velocity-of-sound measurements. Therefore, it was necessary that existing data be utilized. Two velocity-of-sound curves were provided for the area of operation[2, 4]. Figure 2 shows the curve made by the Compass Island velocimeter during July, 1969, with a mean value of 4989 ft/sec[4] and the other curve represents the mean of five observations taken in the area during the months of August and September in different years prior to 1967 with a mean value of 4964 ft/sec[2]. These mean-velocity values were not used in the final computations. Instead, data points were read directly from the two velocity-of-sound curves into the ray-tracing program.

DISCUSSION OF RESULTS

The results of TLSP are summarized in Tables 1, 2, 3, 4, 5, and 6. Tables 1 and 2 give the adjusted geodetic coordinates of the transponders and their standard errors in both curvilinear coordinates (based on the 1960 Fischer Ellipsoid) and cartesian coordinates. The data used to obtain these coordinates included approximately 1500 acoustic ranges from the ship to the three underwater acoustic transponders taken during the acoustic calibration runs and the GEOS-II satellite passes. The ship positions consisted of LORAC surface positions and SINS positions during these runs. Several corrections were made to the raw data in an attempt to eliminate systematic errors. The corrections were for ship velocity effects on the acoustic data, antenna offset from the BNS transducer, and corrections for velocity of sound and acoustic refraction.

The least-squares solution of the observational data included weighting criteria. Table 3 shows the six different cases that were applied for determining the proper weighting criterion for the experiment data.

Table 4 shows the coordinates of the transponders and their standard errors as determined by using the two available sound velocity profiles. It also gives the transponder coordinates as were determined by the Navy.

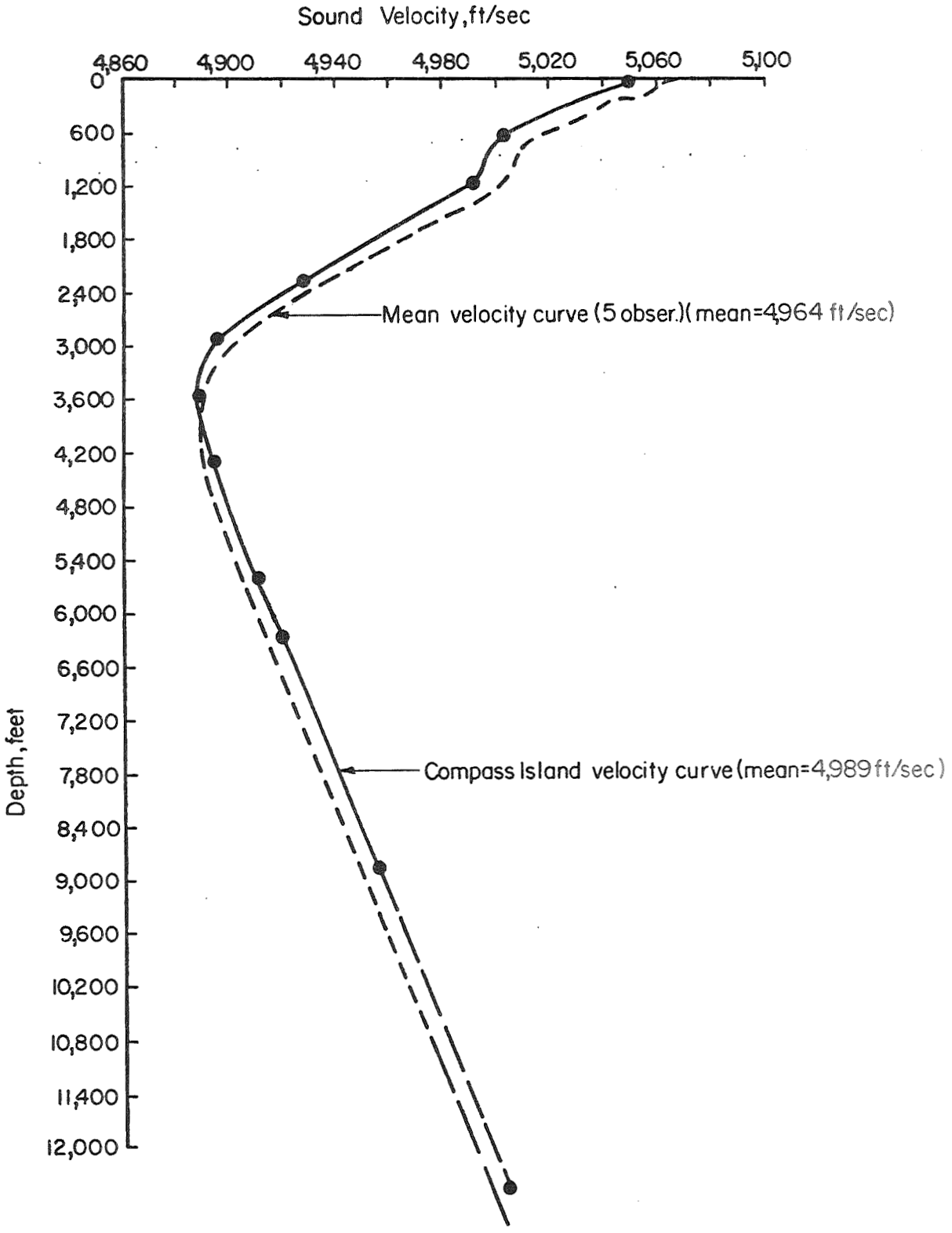

FIGURE 2. SOUND VELOCITY CURVES FOR BAHAMAS EXPERIMENT

TABLE 1. ADJUSTED GEODETIC COORDINATES (CURVILINEAR) BASED ON NAVY SOUND VELOCITY PROFILE (1960 FISCHER ELLIPSOID)

Transponder No.	Latitude - φ (North) °	'	"	Longitude - λ (West) °	'	"	Height (m)	Standard Errors σ_φ(")	σ_λ(")	σ_h(m)
2	27	8	14.75	76	23	14.60	-5018.0	0.24	0.19	3.38
3	27	8	22.05	76	20	03.73	-5016.5	0.23	0.19	2.65
4	27	5	44.92	76	21	35.51	-5016.1	0.19	0.20	2.99

TABLE 2. ADJUSTED GEODETIC COORDINATES (CARTESIAN) BASED ON NAVY SOUND VELOCITY PROFILE

Transponder No.	X (m)	Y (m)	Z (m)	Standard Errors σ_x(m)	σ_y(m)	σ_z(m)
2	1,335,766.98	-5,516,086.75	2,889,502.18	4.74	3.32	7.76
3	1,340,846.95	-5,514,749.83	2,889,702.74	5.46	1.96	7.07
4	1,338,912.43	-5,517,486.64	2,885,401.47	5.56	5.07	4.37

TABLE 3. CRITERIA FOR WEIGHTING OBSERVATIONS

Weighting Criterion	Standard Errors of Adjusted Parameters in Meters σ_x	σ_y	σ_z	Variance Factor Ratio	Expected Limits for Confidence Interval (95%) of Variance Factor Ratio[8,9]			Remarks
P_1=1 (equal)	7.91	8.97	6.50	5.59	0.77	to	1.25	Variance factor ratio outside expected limits. Criterion rejected.
$P_2=f_2(K_1,\theta)$	6.39	2.23	8.17	1.16	0.77	to	1.25	2nd best criterion judged on the confidence ellipsoid for adjusted parameters
$P_3=f_3(HR)$	8.07	2.87	10.53	1.17	0.77	to	1.25	3rd best criterion judged on the confidence ellipsoid for the adjusted parameters
$P_4=f_4(SR,\theta)$	5.46	1.96	7.07	1.00	0.77	to	1.25	Criterion adopted for all other adjustments. Best confidence ellipsoid for adjusted parameters.
$P_5=f_5(K_2,SR)$	6.81	2.39	8.83	4.85	0.77	to	1.25	Variance factor ratio outside expected limits Criterion not acceptable.
$P_6=f_6(K_3,SR)$	6.84	2.40	8.89	1.94	0.77	to	1.25	Variance factor ratio outside expected limits Criterion not acceptable but better than P_5.

TABLE 4. TRANSPONDER COORDINATES AS DETERMINED BY USING DIFFERENT SOUND VELOCITY PROFILES (1960 FISCHER ELLIPSOID)

Transponder Number		Navy Determination	TLSP Determinations Using Navy Sound Velocity Profile	Std. Error	TLSP Determinations Using Average Sound Velocity Profile	Std. Error
2	φ	27 08' 16.32"	27 08' 14.75"	0.24"	27 08' 14.43"	0.24"
	λ	76 23' 16.56"	76 23' 14.60"	0.19"	76 23' 13.93"	0.19"
	h*	-4966.7 m	-5018.0 m	3.38 m	-4998.3 m	3.38 m
3	φ	27 08' 21.54"	27 08' 22.05"	0.23"	27 08' 21.21"	0.24"
	λ	76 20' 03.42"	76 20' 03.73"	0.19"	76 20' 04.13"	0.21"
	h*	-5023.4 m	-5016.6 m	2.76 m	-4998.7 m	2.89 m
4	φ	27 05' 44.16"	27 05' 44.92"	0.19"	27 05' 45.45"	0.19"
	λ	76 21' 38.28"	76 21' 35.51"	0.20"	76 21' 35.44"	0.20"
	h*	-4977.6 m	-5016.6	2.99 m	-4995.2 m	2.98 m

* A geoidal undulation of 60 m (i.e., geoid is 60 m below the ellipsoid) was assumed.

Although the standard errors for each transponder did not change much, influence of sound velocity variations on the coordinates was more noticeable, particularly in the depth determination. This influence on the depth was of the order of 18 to 21 m for the three transponders. Furthermore, the transponder ellipsoidal depths as determined by TLSP are about the same for all three transponders while they were different in the Navy determination.

Table 5 shows clearly these differences in the three transponder depths (ocean surface to bottom) as determined by TLSP and the Navy. The largest difference between TLSP, using Navy velocity, and the Navy determination is about 51 m in Transponder 2. Transponder 3 has the smallest difference of 7 m.

Table 6 presents the results of the error ellipsoid computations for all three transponders. The largest errors are associated with the depth values for Transponder 2 and 3. Both these transponders did not have sufficient ship-track data over them. Transponder 4 has one ship track data over it, which is indicated perhaps in the small error component in the depth axis. In general the geometry of the error ellipsoids indicate that better results could be obtained if data all around the transponders were taken rather than the one-sided data used here.

Preliminary reduction of the acoustic data taken during the calibration runs revealed many obviously erroneous data at the "critical points", such as at the times of PCA's and line-crossings. Therefore, only four "best" runs (Numbers 8, 9, 10, and 3A) were selected and reduced. Figure 3 shows a plot of the acoustic calibration runs as determined by surface LORAC positions. The results are summarized in Table 7 and Table 8. Because of the inaccuracy of the data in line crossing determinations, it was necessary to develop the TLSP technique.

Table 9 presents primarily the results of the distance and azimuth determinations by the TLSP and line crossing techniques. In addition, the distances between the transponders and their forward and backward azimuths were also computed from the Navy given coordinates.

Table 10 summarizes the results of the angles between the three transponders from TLSP, line crossing techniques, and the Navy computed values.

Once the final coordinates were determined for the three ocean bottom transponders, the relative ship positions during the GEOS passes are then determined by using program TRISPR. The results of the ship positions during GEOS

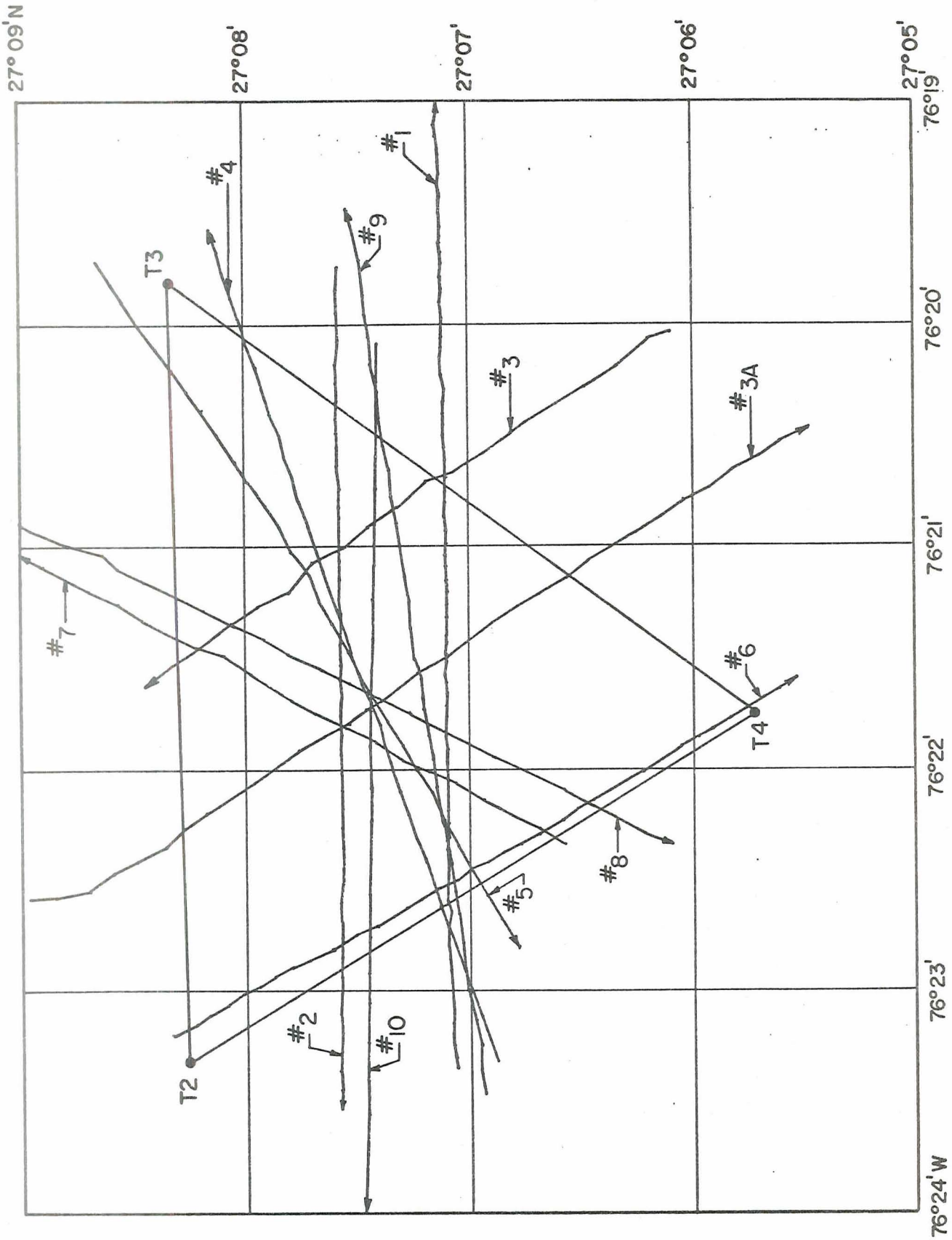

FIGURE 3. LORAC SHIP TRACKS DURING ACOUSTIC CALIBRATION RUNS

TABLE 5. TRANSPONDER DEPTHS

Transponder Number	Navy Determination	Battelle Determinations from TLSP Using Sound Velocity Profiles by Navy	Average
2	4906.7 m	4958.0	4938.3
3	4963.4 m	4956.6	4938.7
4	4917.6 m	4956.6	4935.2

TABLE 6. PARAMETERS OF CONFIDENCE ELLIPSOID FOR THE ADJUSTED COORDINATES AT 95% CONFIDENCE LEVEL* (8)

Transponder Number	Semi-axis in Meters	Axes Orientation Angles with Respect to the Positive Directions of the Geodetic Coordinate Axes X	Y	Z
2	15.30	37° 12'	123° 56'	103° 28'
	3.51	54° 27'	35° 38'	87° 42'
	22.44	80° 23'	99° 37'	13° 40'
3	15.05	15° 46'	85° 24'	105° 02'
	3.70	91° 32'	11° 47'	78° 19'
	20.72	74° 18'	100° 49'	19° 13'
4	15.13	27° 32'	116° 16'	82° 16'
	18.47	64° 30'	46° 55'	126° 10'
	3.34	80° 14'	54° 28'	52° 44'

* This is not the conventional standard error ellipsoid (whose confidence level is 20%) but a confidence ellipsoid scaled such that the probability that the point being determined lies within it is 95%. (8)

TABLE 7. TRANSPONDER DISTANCES DETERMINED FROM LINE CROSSINGS

Run No.	$T_2 - T_3$ (m)	$T_2 - T_4$ (m)	$T_3 - T_4$ (m)
8	5182.2	5498.9*	-
9	-	5488.8*	5393.8*
10	5428.5	5325.0	5428.5
	(5457.4)	(5405.6)	
3A	5323.0	-	5498.6
	(5320.6)		(5519.3)
Avg.	5320.8	5437.6	5440.3
	(5315.7)	(5451)	(5443.7)

* Poor data, not graphed
( ) Distance determined from individual values at times of crossings

TABLE 8. TRANSPONDER AZIMUTHS DETERMINED FROM LINE CROSSINGS

Run No.	$T_2 - T_3$ (°)	$T_3 - T_2$ (°)	$T_2 - T_4$ (°)	$T_4 - T_2$ (°)	$T_3 - T_4$ (°)	$T_4 - T_3$ (°)
8	89	269	146	326	-	-
9	-	-	152	332	207	27
10	-	-	151	331	207	27
3A	85	265	-	-	201	21
Avg.	87	267	149.6	329.6	205	25

TABLE 9. COMPARISON OF TLSP WITH LINE-CROSSINGS AND NAVY RESULTS

Dist., in Meters Az., degrees	Lines	TLSP	Line Crossings	Navy
Dist.	T_2-T_3	5260.9 m	5315.7 m	5321.0 m
Dist.	T_2-T_4	5358.6 m	5451 m	5409.2 m
Dist.	T_3-T_4	5457.1 m	5443.7 m	5503.5 m
Az.	T_2-T_3	87° 32' 17.06"	87° 00' 00"	88° 15' 27.07"
Az.	T_3-T_2	267° 33' 44.12"	267° 00' 00"	268° 16' 55.17"
Az.	T_2-T_4	149° 22' 29.55"	149° 36' 00"	149° 57' 56.30"
Az.	T_4-T_2	329° 23' 14.72"	329° 36' 00"	329° 58' 41.09"
Az.	T_3-T_4	207° 36' 02.26"	205° 00' 00"	208° 20' 51.76"
Az.	T_4-T_3	27° 35' 20.43"	25° 00' 00"	28° 20' 08.52"

TABLE 10. COMPARISON OF TRANSPONDER ANGLES

Angle	TLSP			Line Crossing			Navy		
	°	'	"	°	'	"	°	'	"
α_2	61	50	12.49	62	36	00	61	42	29.23
α_3	59	57	41.86	62	00	00	59	56	03.41
α_4	58	12	05.71	54	24	00	58	21	27.43

passes are shown graphically in Figure 4 at one-minute interval. Figure 5 shows the same tracks as determined by the LORAC surface ship positions.

It is significant to note that the ellipsoidal height, h, of the ship (initially assumed to be-60 meters) was recovered accurately in the computed acoustic time history of the ship motion. The maximum variation in the computed heights was about 9 m. The mean value was 60.05 m with a standard deviation of ± 1.65 m. These results indicate the confidence in the adjusted coordinates of the transponders and their derived depths. The fact that the computed ship positions were derived from only three intersecting ranges (no redundancy) but corrected ray paths indicate the reliability of both TLSP and the acoustic ray tracing programs.

SUMMARY OF RESULTS AND CONCLUSIONS

An improved technique for determining the geometry and orientation of underwater acoustic transponders has been completed, and analysis of data obtained during the Bahamas experiment indicates that the technique will make possible more accurate measurements at sea than other techniques previously known available.

The results of TLSP adjusted geodetic coordinates in both curvilinear and cartesian coordinates are shown in Tables 1 and 2. Analysis of TLSP results revealed that standard errors of less than 0.24 arc seconds were obtained in the determination of the latitudes and longitudes for all three transponders. Moreover, the standard error of depth determination was about 3 meters at depths of about 5000 meters. Such remarkable accuracy, particularly in depth determination will make it possible to establish vertical reference datum and provide, for example, "ground truth" for future satellite altimetry measurements.

About 1500 observation equations were used with nine unknowns (transponder coordinates) in a least-squares solution to determine the transponder coordinates and orientation. Corrections applied to the data include velocity of sound and refraction corrections, antenna offset correction between the LORAC antenna and the BNS transducer and correction for ship speed. In addition, from a thorough investigation of several possible weighting criteria coupled with statistical tests, proper weights were applied to the observation in the least-

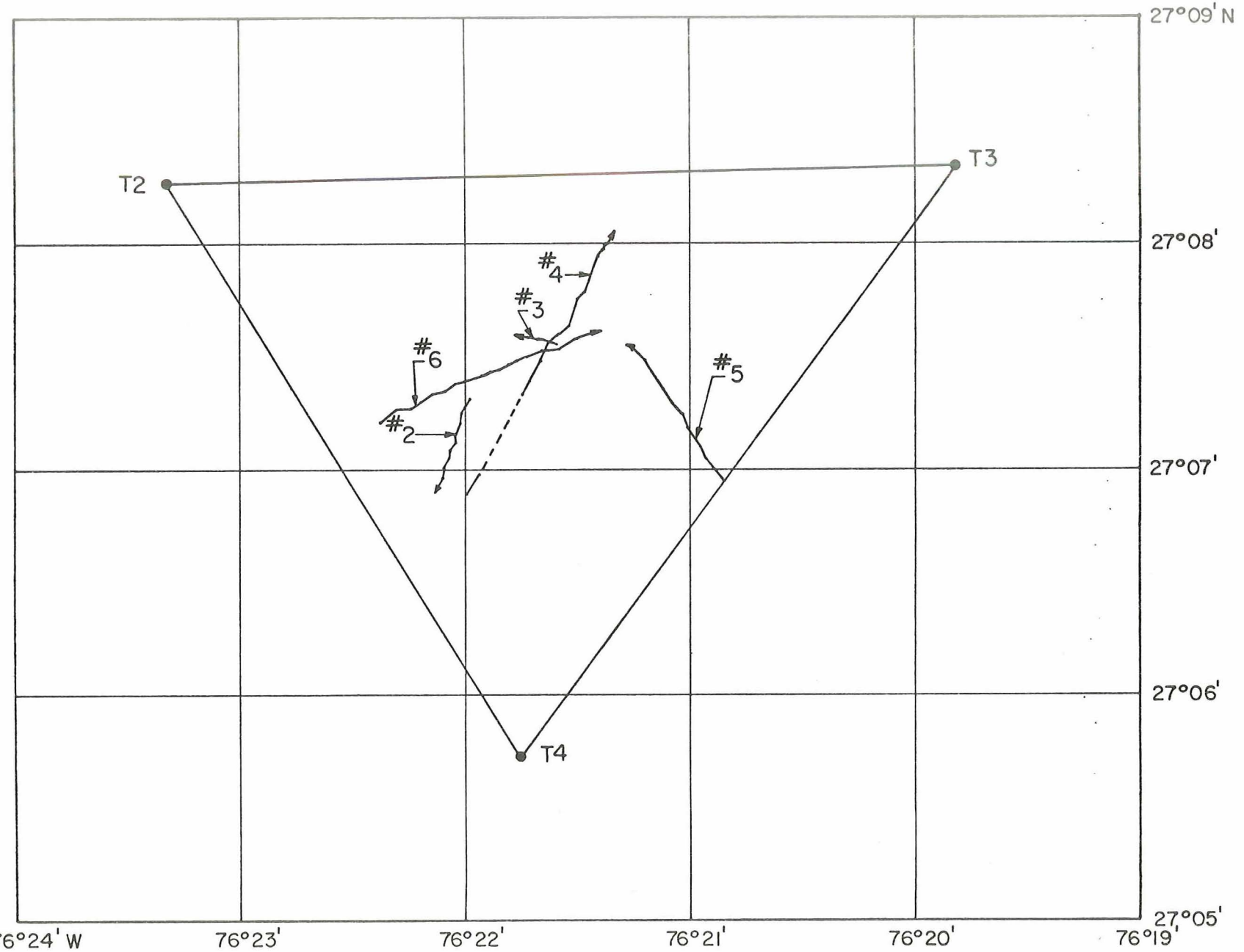

FIGURE 4. ACOUSTIC SHIP TRACKS DURING GEOS PASSES

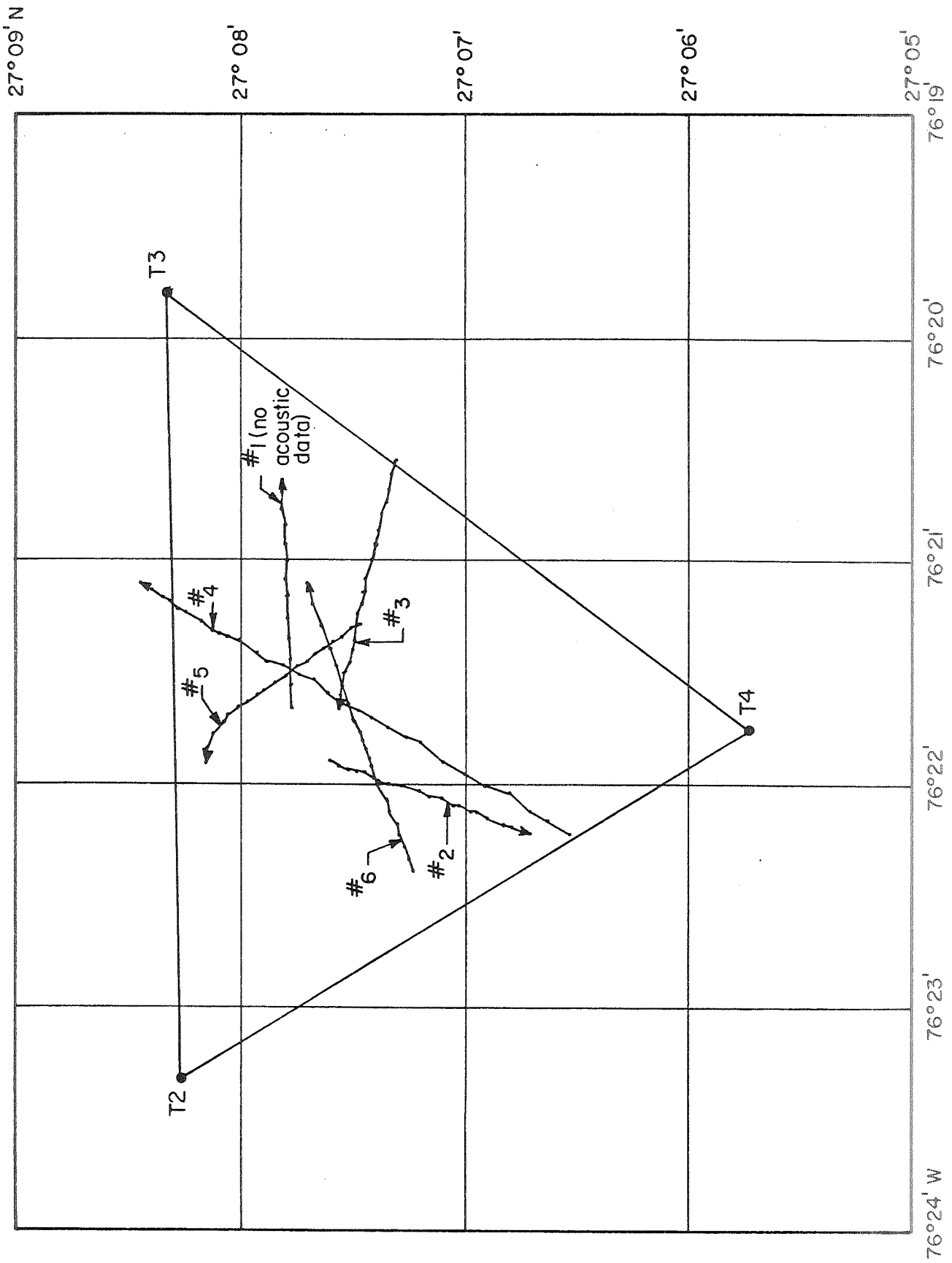

FIGURE 5. LORAC SHIP TRACKS DURING GEOS PASSES

squares solution[8, 9]. Two velocity-of-sound curves were used. The results indicate sensitivity of the TLSP technique to the velocity of sound curves used. Velocity of sound effects were most noticeable in depth determination. Results proved to be sensitive to ship speed, and antenna offset correction made a negligible effect on the precision estimates of the adjusted coordinates. As expected, the increased number of observations improved the precision of the adjusted coordinates of the transponders.

The line-crossing technique was applied to the data first but preliminary data reduction revealed there were many obviously erroneous data recorded at the points of closest approach (PCA's) and at the times of line crossing. Although the line-crossing technique is relatively simple with respect to data reduction, it is operationally time consuming. Moreover, it is apparent that the technique is sensitive to ship heading and course, and its effectiveness depends on the obtaining of reliable and accurate data, particularly during PCA's.

The time-history of ship positions with respect to the adjusted transponder coordinates as determined by TLSP proved the accuracy and reliability of the TLSP and the ray tracing programs. The ellipsoidal heights of the ship positions with respect to the transponders were recovered with standard deviation of ± 1.65 m.

On the basis of the results of this experiment and results of an earlier, similar experiment, several conclusions can be drawn and a number of recommendations can be made. The results achieved to data show how the newly developed techniques for data reduction and analysis can improve the accuracy and potential use of data, even when they are not as precise as desired. Furthermore, all past investigations have involved the use of off-the-shelf equipment designed for general-purpose use and not specifically for geodetic programs. Indications are that with appropriate limited modification of present equipment, the potential for achieving high accuracy at sea is substantial and that eventually investigating difficult problems such as ocean spreading will be quite possible. Accordingly, the following steps are recommended:

(1) Develop an operational test area suitable for conducting controlled-condition experiments for testing hardware and newly developed techniques

(2) Modify and improve present hardware designs, particularly those for underwater acoustic transponders and shipboard receiving equipment.

ACKNOWLEDGMENT

The results of investigations reported in this paper have been supported by NASA, Wallops Station under Contract No. NAS6-1733. The efforts of Mr. Ray Stanley (Technical Monitor) and Mr. John Alvey (Test Manager on USNS Vanguard during the experiment) are greatly appreciated.

REFERENCES

(1) Alvey, J. D., "The Apollo Instrumentation Ship Navigation System Capabilities and Limitations", Goddard Space Flight Center, Greenbelt, Maryland, May 21, 1967.

(2) Crump, E., NASA/GSFC, "Information on Velocity of Sound and Bathymetric Navigation System", Personal Communications, January, 1970.

(3) Heiskanen, W., and H. Moritz, "Physical Geodesy", W. H. Freeman and Company, San Francisco, 364, 1967.

(4) Leonards, R., Naval Strategic Systems Navigation Facility, "Information on Velocity of Sound", Personal Communications, December 6, 1969.

(5) Mourad, A. G., N. A. Frazier, J. H. Holdahl, F. W. Someroski, and A. T. Hopper, "Satellite Applications to Marine Geodesy", Report Prepared for NASA/OSSA Under Contract No. NASr-100 (11), August, 1968, Published by NASA, CR-1253, January 1969.

(6) Mourad, A. G., J. H. Holdahl, and N. A. Frazier, "Preliminary Results of the Establishment of a Marine Geodetic Control Point in the Pacific Ocean", Proceedings of the 2nd Marine Geodesy Symposium, Marine Technology Society, 1970. Also published in Bulletin Geodesique of the International Association of Geodesy, No. 96, June, 1970.

(7) Cramer, H., "Mathematical Methods of Statistics", Princeton University Press, 575, 1946.

(8) Fubara, D. M. J., "Three-Dimensional Geodesy Applied to Terrestrial Networks", Ph.D. Dissertation, U. N. B., Fredericton, 223, 1969.

(9) Hamilton, W. C., "Statistics in Physical Science", The Ronald Press Company, New York, 230, 1964.

(10) Linnik, Yu V., "Method of Least Squares and Principles of the Theory of Observations, Pergamon Press, The Macmillan Company, New York, Translated from Russian by R. C. Elandt, 360, 1961.

NEAR REAL TIME
RADAR CALIBRATION

N. Bush

Pan Am/RCA Engineering Planning and Analysis
Pan American World Airways, ASD

June 1970

Presented at the GEOS-II Review Conference at Goddard Space Center
22- 24 June 1970

I. INTRODUCTION

One of the continuing projects at AFETR is the maintaining and understanding of instrumentation accuracy. This is accomplished both by hardware modifications and by software analysis. The specific aspect that this report is concerned with is the calibration information that can be obtained for the C-band radar by collecting and analyzing radar data from satellites with C-band beacons (software analysis).

AFETR's interest in instrumentation calibration utilizing satellites was first proposed in 1957. A satellite calibration project was approved in 1960 under AFETR Project 8938. When all formal satellite projects were transferred to ESD by Headquarters AFSC in 1962, the new calibration task was ESD Project 5930, Task 5930.03. Under this project, an AFETR calibration satellite was formulated [1] and was unsuccessful in achieving orbit on 13 July 1966. Instrumentation calibration utilizing satellites was continued by use of the Agena 10 and 11 as well as the NASA GEOS-B (See Reference [2]). This particular study was accomplished utilizing data obtained from GEOS B.*

There are many aspects to radar calibration. Idealistically, we would like to obtain a permanent set of calibration coefficients that would always be applied to the radar data and whose values would change very slowly. In this way, the permanent set of calibration values would only have to be updated periodically. However, a more realistic situation is that some of the important calibration values are only constant over short periods of time and, therefore, need to be re-evaluated on a timely basis. For example, the azimuth (A) and elevation (E) zero set biases may remain constant over a few weeks or in some instances may only remain constant for one or two days. In a multiple radar solution, the A and E zero set biases would not be important since range (R) basically determines the solution and A and E can be easily self-calibrated. However, for a single radar

* See references [4] and [5].

solution, A and E are very important and cannot be easily self-calibrated. Therefore, the calibration of A and E zero set biases constitute a significant contribution to improving the accuracy of single radar solutions.

II. ANALYSIS

In order to obtain a good calibration of A and E biases it is necessary to exercise the radar over a range of A and E values. That is, a dynamic calibration is certainly more valuable than a static calibration. The target board static calibrations are useful for obtaining the gross A and E biases, but a dynamic calibration is needed for the fine grain correction needed to obtain the ultimate accuracy. Therefore, a satellite with a C-band beacon can be invaluable for obtaining good dynamic angle calibrations for the radar system.

ETR is in the unique position of being able to immediately process radar data on the CDC-3600 at Cape Kennedy due to the real time data transmission link between the MIPIR radars and the computer. It is, therefore, possible to immediately obtain timely angle calibration values from a multiple radar satellite calibration pass to be applied to radars when they are tracking a different vehicle. The CDC-3600 computer program, which is capable of producing an orbital fit for many radars, is the GPTP program (See reference [10]). If the same processing is done post flight where the radar data is carefully edited and corrected, then the NITE program [3] (run on the IBM 7094) is utilized. A comparison of the main features between GPTP and NITE is shown in Table 1.

The purpose of this report is to evaluate the usefulness of the GPTP program in producing good near real time calibration values. The criteria is based on a comparison of these values with the post flight reduction done on the NITE program, which is assumed to be the most accurate data processing technique for obtaining angle calibration values. The set of data used for these comparisons were obtained utilizing GEOS B in March 1968 and May 1968. A detailed description of the ETR Radar Calibration using GEOS B is given in reference [11].

For the March 1968 experiment, radar data were collected and analyzed over five GEOS B revs of data: 801, 807, 808, 813, 814. The radar coverages is shown in Table 2 and specified details of data processing can be found in references [6] and [7]. The comparison between GPTP and

TABLE 1
COMPARISON OF GPTP AND NITE SOLUTIONS

ITEM	GPTP	NITE
Site Corrections	Complete Model for MIPIR Zero Set for FPS-16	Same
Input	A, E, R Teletype Data	Radar and Camera Data
Input Sample Rate	1 Point/10 Seconds - MIPIR 1 Point/6 Seconds - FPS-16	Up to 10 pps
Automatic Editing	Yes	No
Geopotential Model	65 Terms	200 Terms (NWL8D)
Radar Error Model	14 Zero Sets	Extensive Error Model
Survey Adjustments	None	Up to 60 per Interval
Residual Output Rate	Same as Data Input Rate	Same as Data Input Rate
Error Analysis	Zero Set Error Analysis	Modeled and Unmodeled Error Analysis Including Geopotential
Completion Time	1/2 to One Day	Two Weeks to Two Months

TABLE 2

NITE SOLUTIONS

Arc	Revs	RADARS										
		Cape 1.16	Mer. Isl. 19.18	PAFB 0. 18	GBI 3. 18	Wallops Isl.	GTK 7. 18	ANT 91.18	BDA 67.18	ASC 12.16 12.18	Carnav.	White Sands
1	801	X	X	X			X					
2	807		X	X			X	X	X		X	
	808	X	X	X							X	
3	813		X	X			X	X	X			
	814	X	X	X								X
4	1672									X		
	1673					X	X	X				
	1674			X	X							
5	1685									X		
	1686	X				X	X	X	X			
	1687	X		X		X	X					
6	1698									X		
	1699			X	X		X	X				
	1700	X		X	X		X					

TABLE 3

GPTP VS NITE FOR MARCH 1968 DATA

(Angles in Milliradians)

REV		0.18 GPTP	0.18 NITE	19.18 GPTP	19.18 NITE	7.18 GPTP	7.18 NITE
801	A	.053	.050	.000	.004	.071	.017
	E	.194	.252	-.197	-.202	.091	.130
807	A	-.027	-.034	-.015	.034	.005	-.005
	E	.164	.142	-.300	-.310	.124	.137
808	A	.097	.097	.025	.018		
	E	.182	.230	-.046	-.051		
813	A	-.105	-.121	.086	.086	-.057	-.105
	E	-.055	-.055	-.119	-.100	.174	.136
814	A	-.061	-.077	.063	.024		
	E	-.033	-.024	-.144	-.151		

NITE for A and E angle biases only are given in Table 3 for radars 0.18, 19.18 and 7.18. The omitted comparisons were either due to obvious hardware problems or data not collected for that particular revolution.

The specific details of this March experiment were documented in a Secret report [7]. The results presented in this report constitute the unclassified part of the report. From Table 3, it is seen that there is an excellent agreement between the GPTP and NITE solutions for angle biases where the great majority of the azimuth bias differences are $<.04$ mr. As noted in [7], there was some hardware discussion concerning reasons why some of the zero set levels changed. For example, for radar 0.18 there was a malfunctioning parametric amplifier over revs 801-808 and there was a possibility of a mislevel error. With the exception of the 0.18 bias levels, which changed significantly probably due to a hardware problem, the other bias levels for 19.18 and 7.18 appear fairly stable, at least in the sign of the correction. There seems to be a fair amount of consistency between revs 801 and 807 and between revs 808 to 814 for radar 19.18. It appears that angle bias results may be stable for one-half to one day.

Another GEOS B experiment was run in May 1968 (see references [8], [9]) where we also obtained comparison computer runs on GPTP and NITE. In this particular comparison, the zero set biases were assumed to be constant from revs 1672 through 1700, or over a period of two days. The radar coverage for these revs is given in Table 2. Both the GPTP and NITE programs were run under the constraint of constant biases. Table 4 shows the results of the May 1968 comparison.

TABLE 4 - GPTP vs NITE FOR MAY 1968 DATA
Includes Revs 1672, 1673, 1674, 1685, 1686, 1687, 1698, 1699 and 1700.
(Angles in Milliradians)

Angle Bias	0.18		3.18		7.18		91.18		12.18	
	GPTP	NITE	GPTP	NITE	GPTP	NITE	GPTP	NITE	GPTP	NITE
A	-.030	-.049	.124	.111	.047	-.006	.000	-.003	.160	.098
E	-.178	-.177	.391	.397	-.106	-.156	-.219	-.132	-.350	-.390

As in the March 1968 experiment (Table 1), there is good agreement between the GPTP and NITE angle zero set biases. The differences between the NITE and GPTP angle biases are mostly $<.04$ mr with the exception of 91.18 elevation difference of .09 mr and 12.18 azimuth difference of .06 mr. Although these differences are larger than those found in Table 1, they are still small enough in order to utilize the GPTP results as meaningful. The main reason for the additional variation is probably due to the fact that the biases were assumed to be constant over two days. It seems to be apparent that more consistent results can be obtained if we restrict our bias evaluation to less than two days. An analogy would be if we performed the standard radar pre-calibration two days before the radar was to be used. Obviously, for those tests that would require good angle calibrations, the dynamic satellite calibration should be done as close as possible to the time the radar will be used for observing test data. More explicit information concerning the May 1968 experiment can be found in Reference [9].

Summing up, it can be stated from the data comparisons shown in Tables 3 and 4 that the angle calibrations from the GPTP program are usable in a near real time sense to obtain improved radar test data. It is perfectly conceivable that we could obtain updated angle biases from a multiple radar GPTP solution and apply the angle bias calibrations to a single radar test - all in the same day.

ACKNOWLEDGEMENTS

The author gratefully acknowledges the contributions of RCA Systems Analysis at PAFB, Fla. for their analysis contributions to this study. In particular, I wish to thank J. A. Greene, D. R. Pfingsten, and J. F. Pinion.

REFERENCES

[1] "AFETR Plan For Use of Calibration Satellites for Calibration and Evaluation of Range Instrumentation," Pan American World Airways, RCA International Service Corp., Patrick Air Force Base, Florida, December 1965.

[2] "AFETR Instrumentation Calibration Task Plan (C-Band Pulse Radar)," Pan American World Airways, RCA International Service Corp., Patrick Air Force Base, Florida, November 1966.

[3] Parks, D. H., et al, "NITE," RCA Data Reduction Computer Program No. 615, Patrick AFB, Florida, March 1968.

[4] Bush, N.; Pfingsten, D. R.; Greene, J. A.; et al, "Mistram MRS Survey Improvement Study," AFETR TR-69-6, Pan American World Airways, RCA International Service Corp., Patrick AFB, Florida, October 1969.

[5] Bush, N., and Pfingsten, D. R., "Mistram MRS Survey Qualification Study," ETV-TM-70-47, Pan American World Airways, RCA International Service Corp., Patrick AFB, Fla., October 1969.

[6] Pinion, J. R., "GEOS-B Test Report, Test 1815, Date of Test 14, 15 March 1968," Report No. 40-1815-68-1, RCA Systems Analysis, Patrick AFB, Fla., May 1968.

[7] Pinion, J. R., "GEOS-B Satellite Test Report, Test 1815 (U)," Report No. 41-1815-68-2, RCA Systems Analysis, Patrick AFB, Florida, September 1968.

[8] Baldwin, J. L., "GEOS-B Test Report, Test 1815, Date of Test 21-23 May 1968," Report No. 40-1815-68-1A, RCA Systems Analysis, Patrick AFB, Florida, August 1968.

[9] Pinion, J. F., "GEOS-B Radar Evaluation and Calibration Test Report, Test 1815 (Experiment 2) (U), Test Date 21, 22, 23 May 1968," Report No. 40-SR-69-9, RCA Systems Analysis, Patrick AFB, Florida, April 1969.

[10] "1604/3600 Computer Operating Instructions for Model 9, Best 9.1, Fact-9, Milestone 7," (L-1569/006/00A), System Development Corp., Santa Monica, California.

[11] Pfingsten, D. R., et al, "Radar Calibration (With the Use of Satellites," ETV-TM-70-98 , Pan American World Airways, RCA International Service Corp., Patrick AFB, Florida, May 1970.

SHIP BORNE RADAR TRACKING FOR PRECISE SHIP POSITIONING

By

C.F. Martin
Wolf Research and Development Corporation
6801 Kenilworth Avenue
Riverdale, Maryland

and

W.B. Krabill
National Aeronautics and Space Administration
Wallops Station
Wallops Island, Virginia

Presented at the

GEOS II Review Meeting
Goddard Space Flight Center
Greenbelt, Maryland

June 22-24, 1970

ABSTRACT

C-band radar tracking of the GEOS-B satellite by the Vanguard Apollo tracking ship has been used, in conjunction with land-based C-band radar tracking, to obtain estimates of the ship position. For a two revolution dockside solution, a position agreeing with the surveyed position to within 17 meters was obtained. At sea radar tracks by the Vanguard were reduced using the ship inertial navigation system (SINS) data for the change in ship position after the beginning of track. Both one and two revolution solutions were used for ship positioning. In all cases, poor fits of the radar data to the orbit determined by the land-based stations gave indications of problems with the SINS data and station recoveries in error by 2 km or greater. Comparison with a LORAC position for one case also showed discrepancies on the order of 3 km.

SECTION 1.0
INTRODUCTION

The precise determination of land-based geodetic positions through the use of satellite tracking is a well established art. In general, the procedure is to use minimum variance statistical estimation techniques such that a set (or sets) of orbital parameters and sets of tracking station coordinates provide a "best fit" of the tracking measurements to the satellite orbit. The coordinates of some stations must, of course, be constrained in some manner (such as fixing latitude and longitude) in order to obtain a non-singular solution.

A similar procedure may also be used to estimate the geodetic location of a tracking instrument located on a ship. It is, however, necessary to have information about the motion of the ship during the tracking period. This information may take several forms, including: (1) inertial navigation data, (2) ranges from the ship to fixed acoustic transponders, and (3) radio fixes to land-based transmitters as via the LORAC network. The results presented in this paper use primarily the first type of information. For some of the tests discussed, some data of both of the other types does exist and will be used in data reductions yet to be completed.

With perfect knowledge of the change in ship position from one measurement point to the next, the accuracy of station position estimation can be established through the use of an error analysis simulation, or through the use of ship data when the ship is known not to be in motion. The latter technique was actually used. This has the advantage of gaining familiarity

with the use of actual data and an assessment of the errors which may exist in the ship-borne tracker.

With the ship at sea, the technique used was to calculate the change in ship position from its position at a reference time (generally at the beginning of a satellite track) using the ship inertial navigation system data. The Wallops A/Omega program, which accepts data from a moving tracker, was then used to estimate the position of the ship at the reference time in a minimum variance solution which also determined the orbital parameters. The measurement weighting used, however, was such that the orbit was determined primarily by land-based tracking stations.

SECTION 2.0
SELECTION OF DATA

Although C-band radar data almost always includes azimuth and elevation measurements, such data is of much lower accuracy than are range measurements. In an orbit determination using data from more than one radar, it is possible to utilize range measurements only, with no degradation of overall orbit accuracy. For this reason, the orbits for ship positioning were obtained using land-based radar range measurements. In most cases, data from only two land-based locations was available. However, error analyses have shown that this is not a serious limitation so long as the land-based stations are not widely separated from the ship which is being positioned.

The FPS-16 type radar on the Vanguard makes angle measurements just as its land-based counterparts do. However, since calibration and stabilization problems are greatly more difficult on the ship than on land, the angle data would be expected to be, and is, far less accurate in terms of positioning accuracy than is the range data. The estimation of a two (or three) dimensional ship position using range data alone from a single satellite pass can be done, in most cases, but is rather sensitive to errors of almost any nature. Two satellite passes provide a much greater positioning capability as should be expected simply on the basis of the extended exercise of geometry. (For GEOS-B, e.g., tracking of the satellite on successive revolutions automatically means a pass east of the ship and a pass west of the ship.) For this reason, considerable emphasis has been placed on obtaining ship positions using two passes of satellite track.

The only data which has thus far been available for obtaining ship movement, relative to some fixed position or time, has been from the ship inertial navigation system. In the data reductions, it was assumed that the SINS position might contain an error at the reference time, but that the error remained constant throughout the one or two satellite passes. It was recognized in advance that this was only an approximation, and perhaps a poor one. The analysis reported in this paper had as one of its objectives to determine the degree of validity of this approximation.

It should be noted that the data reductions herein reported were made using "raw" C-band range data from the ship, with the reduction performed in a moving tracker program. Computer programs on board the ship are designed to provide C-band data referenced to a fixed point. This data, generally called low-speed data, contains, in addition to the SINS errors, the effects of angle biases and any radar range biases which may exist. Since this transformation introduces large errors from the biases alone, it was decided to use the radar data in its raw form so that radar errors themselves, if they exist, could be more clearly identified.

One such error source known to exist in the C-band data is a range bias. Far stronger position recoveries would be possible if the radar data were sufficiently well calibrated for its bias to be negligible. Unfortunately, calibration procedures used to date have not satisfied this requirement. For all data reductions performed to date, it has been found necessary to require the data reduction process to estimate an independent radar bias on each pass.

SECTION 3.0
DOCKSIDE TESTS

Using two GEOS-B tracks by the Vanguard C-band radar with the ship in Port Canaveral, it has been possible to check out the radar and data handling and reduction processes under near ideal conditions. Lack of motion by the ship removed the complications of the moving tracker. And the position of the tracker was tied to a well surveyed point. Position recovery under these conditions should give an indication of the accuracy that should be expected when the ship motion is perfectly accounted for.

Table 1 shows the radar position recovered when tracks of Revolutions 7972 and 7973 were used in conjunction with land-based tracking by Wallops and Bermuda radars. The estimated position, when compared to the survey position also shown in Table 1, shows a difference of only 17 meters. This figure should be considered a measure of the accuracy of the estimated position relative to Wallops and Bermuda.

For both radar passes, independent radar range biases were estimated along with the ship position. Biases of -67 and -17 meters were recovered, indicating both significant biases and biases which differ from pass to pass.

The ship radar and land based radar residuals (differences between the observed ranges and the calculated ranges to the fitted orbit) for Revolutions 7972 and 7973 are shown in Figures 1 and 2, respectively. The raw radar range residuals are denoted by ISTA19. The residuals denoted by ISTA66 refer to the low speed data transformed by the ship computer. The trends in these residuals are an indication that something was wrong in the transformation process. The ISTA19 residuals seem quite comparable to the land-based radar range residuals.

TABLE 1

DOCKSIDE SHIP TEST

GEOS-B REVS 7972 - 7973

NAD-27 POSITIONS

	Adjusted	Survey
Latitude	28° 24' 31.8"	28° 24' 31.4"
Longitude	279° 23' 44.1"	279° 23' 44.5"
Height	7.2 m	14.6 m

Orbit Determination by:

Wallops FPS-16

Bermuda FPQ-6

Bermuda FPS-16

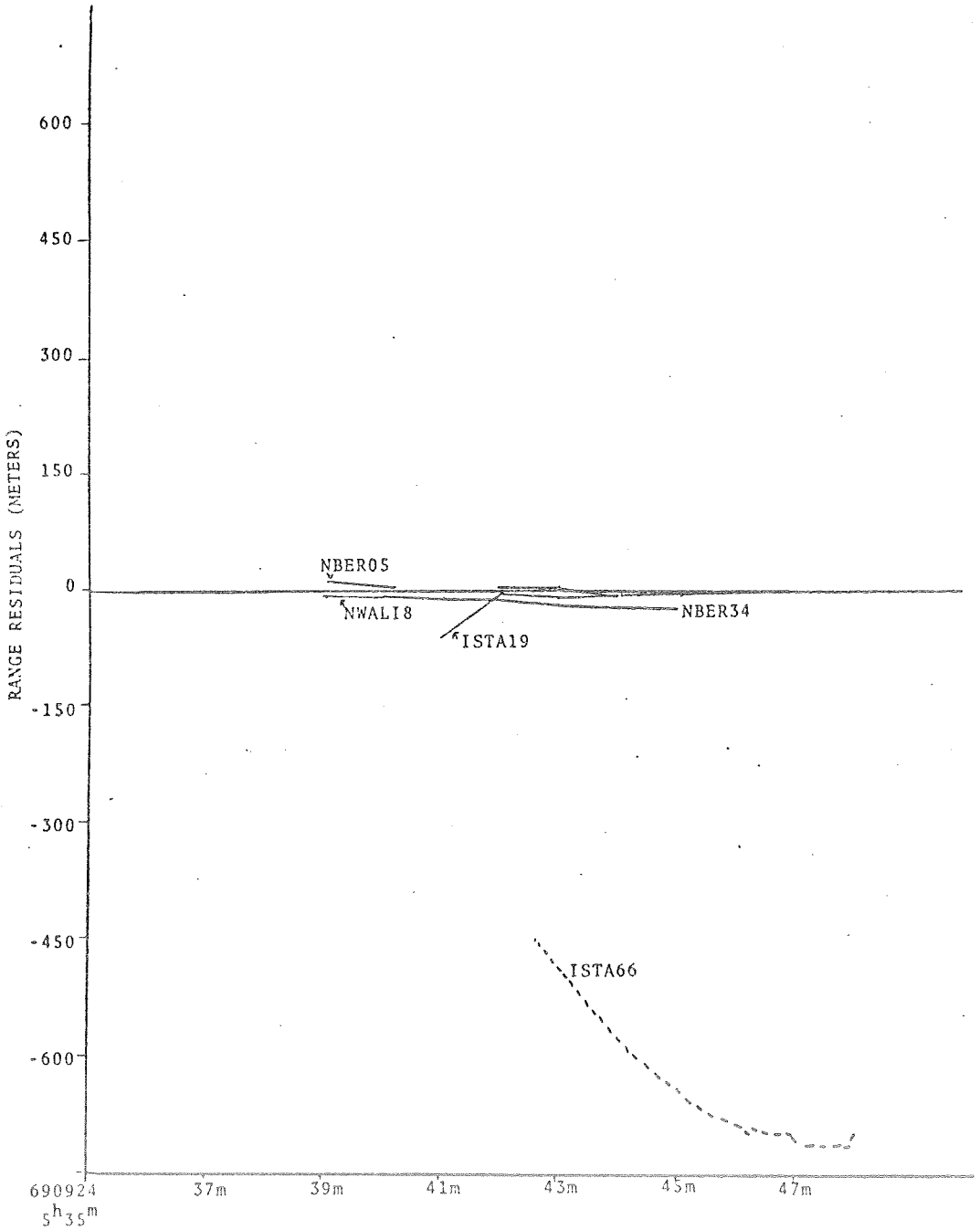

Figure 1. Residuals for GEOS-B Rev 7972

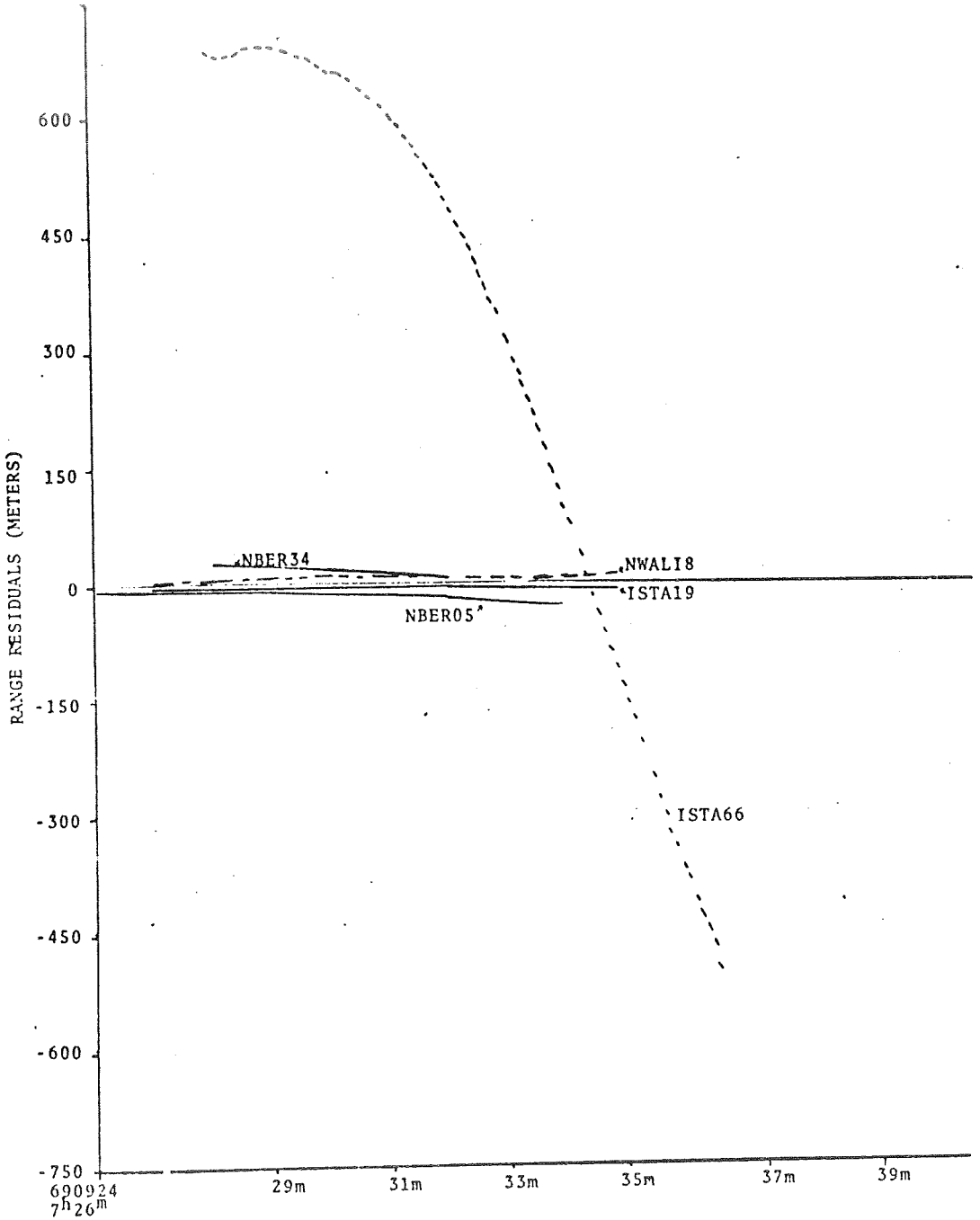

Figure 2. Residuals for GEOS-B Rev 7973

SECTION 4.0
AT SEA TESTS

At sea Vanguard tracks on three different days have been reduced, in all cases using the SINS data for relating the position of the ship during track to its position at the beginning of track. When tracks on successive revolutions were available, the initial position used was that at the beginning of the first track.

Results for the three different tests will first be given. Some analysis will then be made of the recovered ship positions and the implications of the large measurement residuals obtained for all at sea tests.

It should be noted that a height recovery was not attempted for any of the at sea tests. This constraint was used because of the limited amount of data on some passes and the necessity for recovery of range biases on all passes. In addition, the probability of height improvement did not seem very high.

4.1 ONE PASS SOLUTION

Table 2 gives the estimated ship position at the beginning of track on GEOS-B Revolution 7991. The only available comparison position is the SINS position, also listed in Table 2. Differences are approximately 440 meters in latitude and 30 meters in longitude. A reliable estimate for the accuracy of the SINS position is, however, not available.

The residuals for the ship range measurements after the ship position (and radar bias) estimation are shown in Figure 3. Residuals for the land based radars were negligibly

TABLE 2

AT SEA SHIP TEST

GEOS-B REV 7991

	Latitude	Longitude
SINS	28° 23' 22.4"	280° 15' 18.0"
Adjusted	28° 23' 36.7"	280° 15' 16.8"

Orbit Determination by:

Wallops FPQ-6

Wallops FPS-16

Bermuda FPS-16

Figure 3
Ship Range Residuals for GEOS-B REV 7991

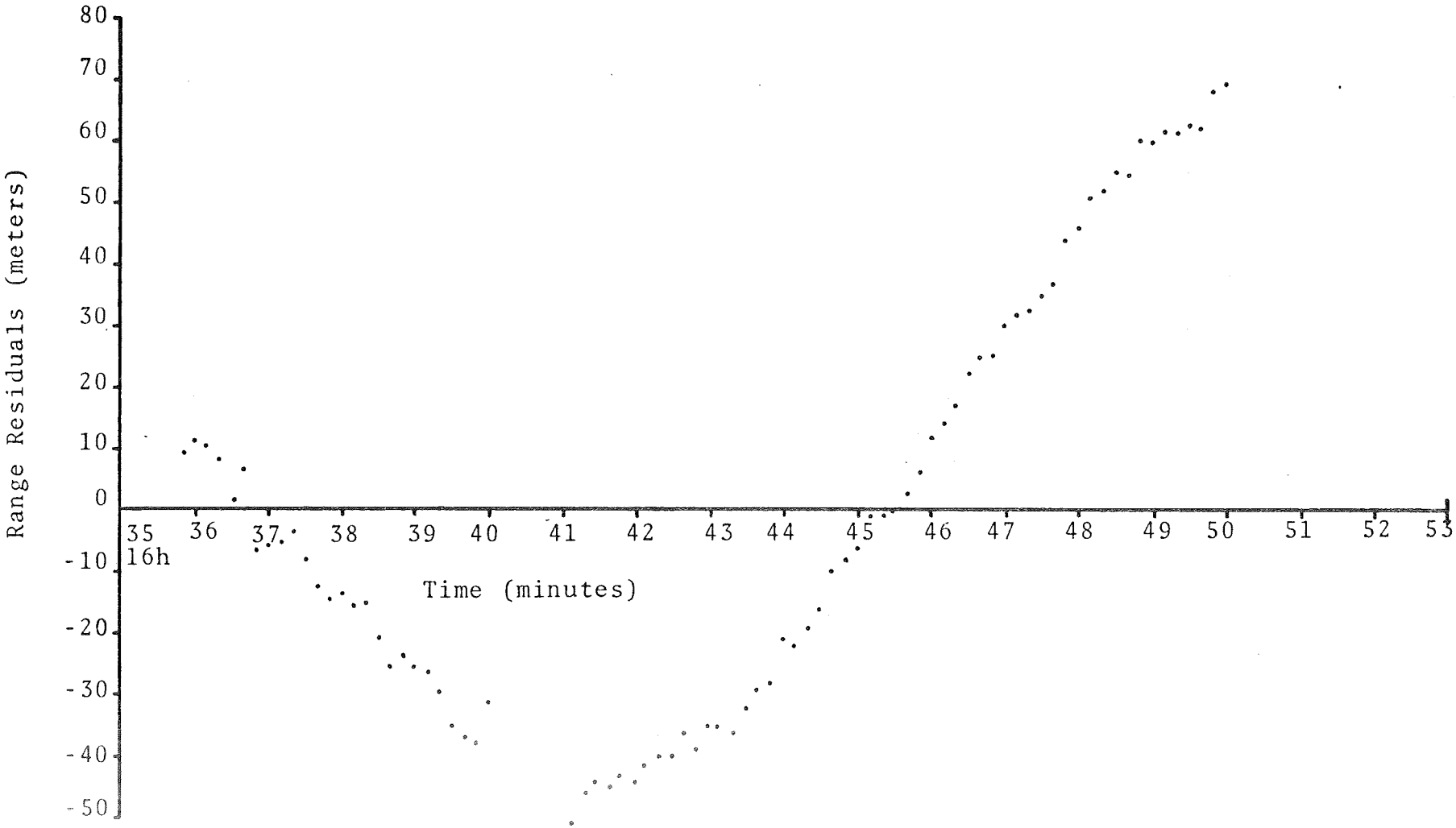

small on the scale of this figure and were consequently not plotted. The explanation for the large systematic residuals almost certainly lies in errors in the SINS relative positioning inaccuracy. A preliminary analysis of the residuals, assuming the simplest error models for a well damped SINS system, indicates that such models can do only a very poor job of explaining the actual residuals. A simple velocity error alone must be in excess of 3m/sec to give the best residual fit. This would indicate rather serious SINS problems during this pass of an unknown nature.

4.2 TWO PASS SOLUTIONS

Two sets of two pass solutions have been reduced, with the results shown in Tables 3 and 4. For one of these tests, a LORAC position is available for comparison with the estimated position and the SINS position. If the LORAC position is accepted, Table 3 says that the adjusted position is in error by about 500 m in longitude and 3000 m in latitude. These differences appear to be largely attributable to SINS errors, as discussed below.

Figure 4 shows the ship range residuals after the ship position (and range bias) estimation on Revs. 8003-8004. Figure 5 shows the corresponding residuals for Revs. 8010-8011. For both tests, land based radar range residuals are essentially negligible on the scale of the graph and for that reason are not plotted.

As might be expected, SINS systematic errors over a period of two hours do not necessarily take a very simple form and it is not possible to account easily for the residuals

TABLE 3

AT SEA SHIP TEST

GEOS-B REVS 8003 - 8004

	Latitude	Longitude
SINS	27° 7' 17.5"	283° 39' 0.6"
Adjusted	27° 9' 12.9"	283° 39' 10.9"
LORAC	27° 7' 32.0"	283° 38' 53.0"

Orbit Determination by:

Bermuda FPS-16

Antigua FPQ-6

TABLE 4

AT SEA SHIP TEST

GEOS-B REVS 8010 - 8011

	Latitude	Longitude
SINS	27° 6' 41.8"	283° 38' 10.5"
Adjusted	27° 7' 26.5"	283° 37' 38.0"

Orbit Determination by:

Wallops FPS-16

Bermuda FPS-16

shown in either Figures 4 or 5. For Figure 4, however, a fair fit to the residuals is obtained by assuming velocity errors of 0.3 m/sec S and 0.1 m/sec W. These errors correspond to position errors of about -400 m in longitude and about 1600 m in latitude. These numbers correspond to about half the observed LORAC-A/Omega differences for latitude - and in the right direction - but are in the wrong direction for improving longitude.

It may be noted that the SINS position shows less agreement in Table 3 with the estimated position than it did in Table 2, probably due mainly to the longer time span. However, the SINS velocity errors necessary to account for observed residuals are lower by about an order of magnitude.

Results for Revs. 8010-8011 appear to be somewhat worse than those for Revs. 8003-8004. The SINS and estimated positions of Table 4 show closer agreement, but the residuals shown in Figure 5 are larger. Most of the data taken fro this test is on Revolution 8011. Reduction of this pass by itself (and land based data) shows residuals of the same magnitude and shape as was found for Rev. 7991, giving again indications of rather poor SINS performance. Accordingly, further analysis of this test was postponed until additional data is available. When available, acoustic transponder data will be combined with the radar data to obtain an improved set of ship positions.

4.3 AT SEA DATA ANALYSIS

The results of much of the analysis of the sea test data have been given above. In general, the large residuals obtained for the ship radar are simply not explicable

Figure 4

Ship Range Residuals for GEOS-B REVS 8003 & 8004

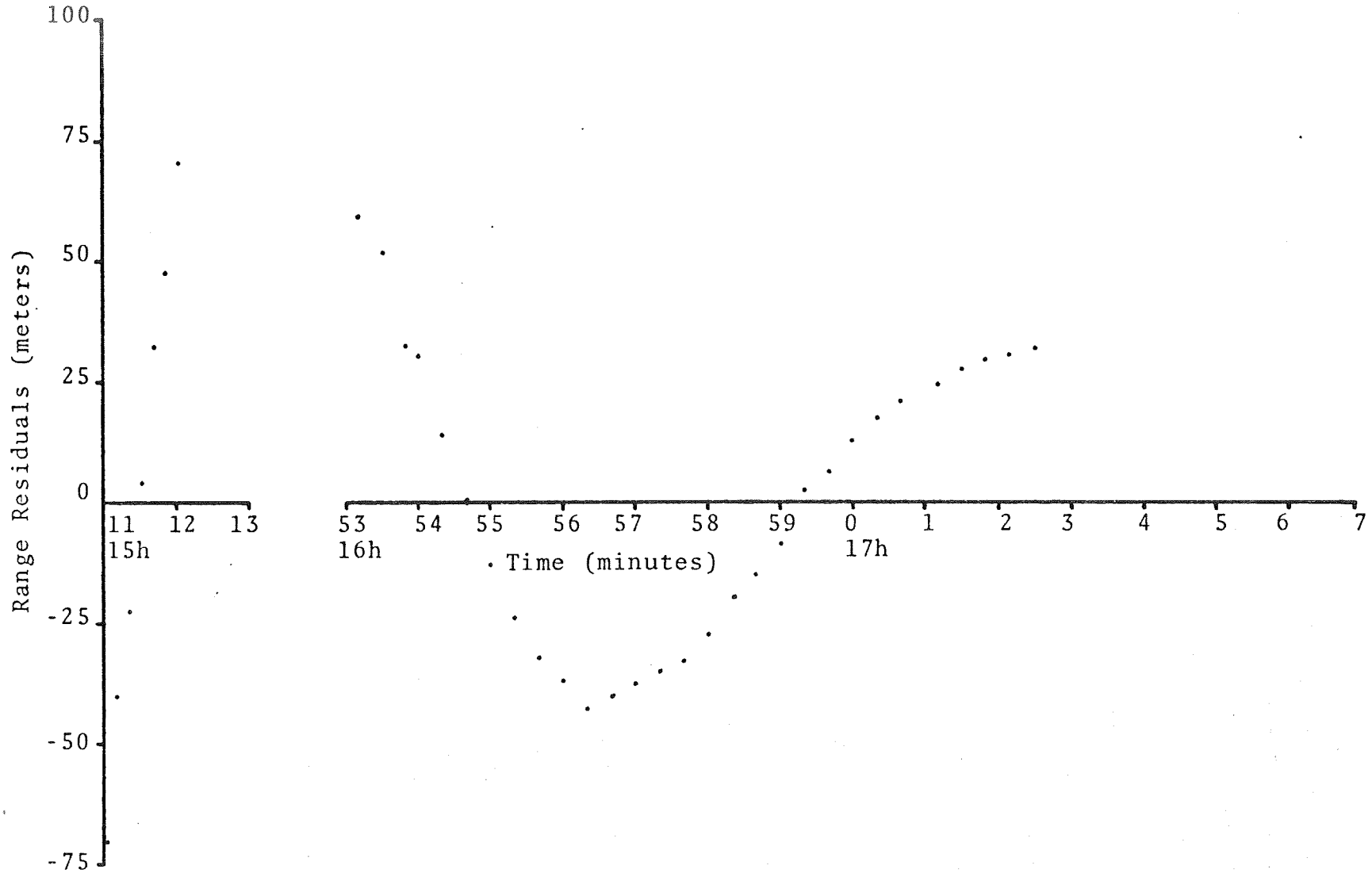

Figure 5

Ship Range Residuals for GEOS-B REVS 8010 & 8011

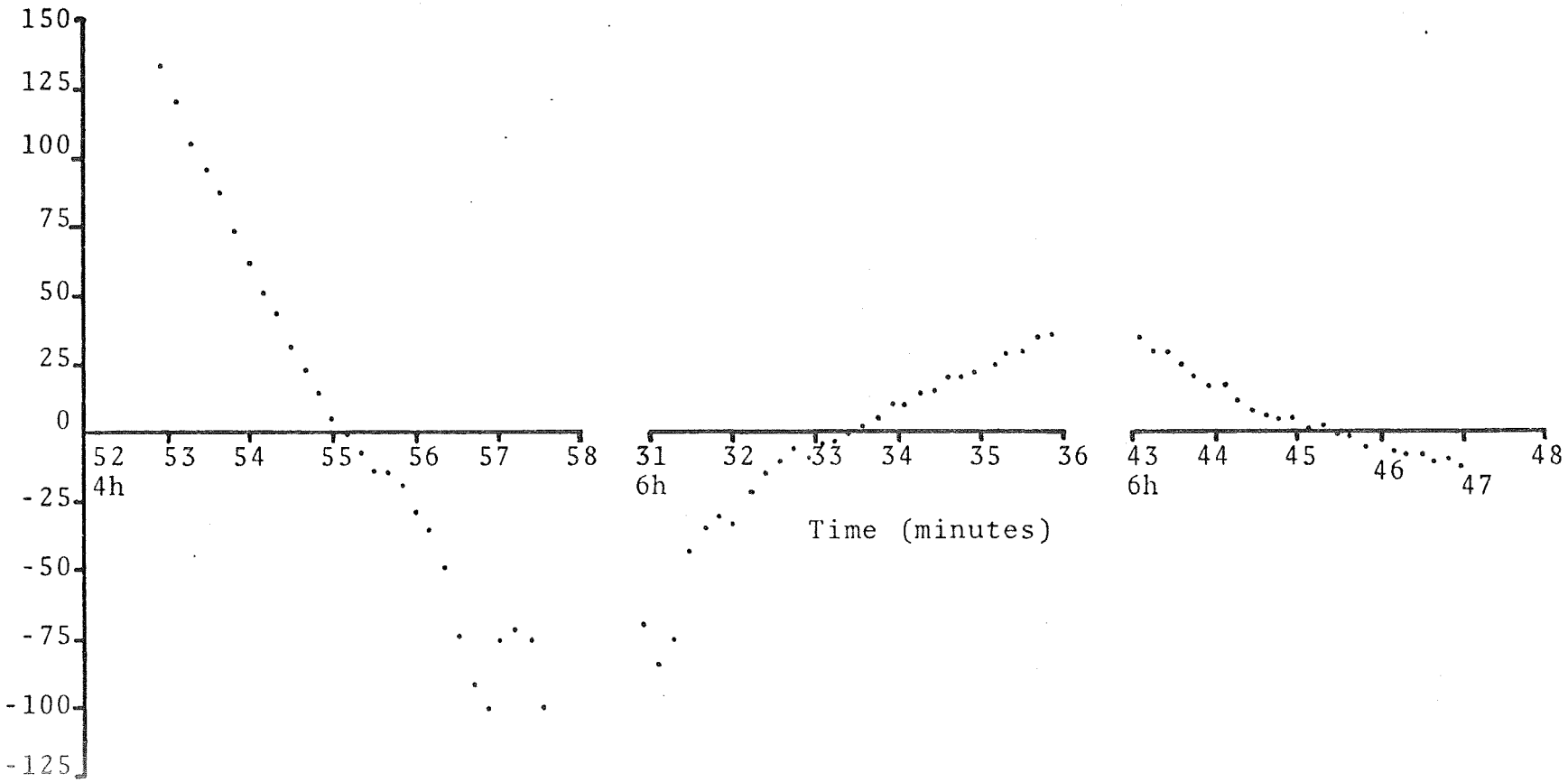

on any basis other than errors in the SINS data used for the ship motion history. Several of the simpler SINS error model forms have been modeled in a simulation program to see their effects on the recovered ship position and on the measurement residuals. With a very limited amount of data, as was the case for all tests, it is impossible to solve for a large number of error model coefficients. This difficulty is due to the fact that a number of the error model terms have similar forms over the periods for which data is available. In such a situation, one or two parameters may be chosen to effectively absorb the error in all parameters. In all the analysis made to date, no more than two components of velocity error have been useful in accounting for observed residuals.

The large errors in the estimated ship positions can, as has been emphasized, be attributed to large SINS errors, with no accounting made in the data reduction for such errors. Some improvement can be made, in most cases, by the solution for one or two selected parameters. As has been noted, however, the magnitude of SINS errors appears to differ greatly from day to day. This suggests that the data might be potentially much better than it generally is.

The velocity errors which have been quoted as accounting for observed residuals should not be interpreted as being actual velocity errors, particularly for the two revolution solutions. The velocity error best accounting for the 8003-8004 residuals was stated to be 0.33/197°. The speed and heading of the ship was completely changed between Revolutions 8003 and 8004, with some expected perturbations on the SINS system. The velocity errors would then be expected to be different on the two passes.

SECTION 5.0
CONCLUSIONS

The results presented in the preceding sections have shown that C-band radar data from the Vanguard is potentially useful for accurate geodetic positioning provided the relative ship movement can be accurately accounted for. The results obtained and the implications for further analysis may be summarized as follows:

1. A two satellite pass position estimation accuracy on the order of 15 meters is possible using a ship C-band radar when relative ship position between data points is known from other sources.

2. Ship position estimation using SINS data for relative ship motion gives position errors which may exceed 3 km. (One single pass result, GEOS-B revolution 8004, gave answers which residual analysis indicated should be accurate to 500 meters.)

3. Apparent SINS errors observed are much greater than quoted SINS errors.

4. Modeling of SINS errors over a one pass period appears possible, with the solution for speed and heading errors.

5. The crucial item in ship positioning is an independent source of relative position. The use of acoustic transponders for this purpose should be one perfectly adequate solution.